CRREL Report 98-7

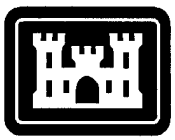

US Army Corps of Engineers®
Cold Regions Research & Engineering Laboratory

Cold Regions Research &

Investigations of Plastic Composite Materials for Highway Safety Structures

Piyush K. Dutta

August 1998

Prepared for
FEDERAL HIGHWAY ADMINISTRATION

PREFACE

This report was prepared by Dr. Piyush K. Dutta, Materials Research Engineer, Applied Research Division, Research and Engineering Directorate, U.S. Army Cold Regions Research and Engineering Laboratory (CRREL), Hanover, New Hampshire.

Funding for this research was provided by the Federal Highway Administration, U.S. Department of Transportation, McLean, Virginia, under contract number DTFH61-9-Y-00035, Charles McDevitt, Contracting Officer's Technical Representative.

The author thanks John Bouzoun, Barry Coutermarsh, and Richard Lampo for technically reviewing the manuscript of this report.

The information provided in this report constitutes a condensation of literature search, studies, and results of some experiments. The report gives a basic overview and assessment of different concepts and technologies of using polymer composites in structures generally used for highway safety. The United States Government assumes no liability for its contents or the use thereof. This report does not constitute a standard, specification, recommendation, or regulation. The United States Government does not endorse products or manufacturers. Trade and manufacturer's names appear herein only because they are considered essential to the objective of this document.

CONTENTS

ILLUSTRATIONS

Figure

Figure Page

TABLES

Table Page

ACRONYMS

AASHTO	American Association of State Highway and Transportation Officials
ACI	American Concrete Institute
ASTM	American Society of Testing and Materials
BCT	Breakaway cable terminal
COTR	Contracting Officer's Technical Representative
CPC	Crushable plastic cushion
CRREL	Cold Regions Research and Engineering Laboratory
CSM	Cross stitched mat
DF	Douglas fir
FHWA	Federal Highway Administration
FRP	Fiber reinforced plastic
FOIL	Federal Outdoor Impact Laboratory
GFRP	Glass fiber reinforced plastic
HDPE	High density polyethylene
MEKP	Methyl ethyl ketone peroxide
MTS	MTS Company
MRI	Magnetic resonance imagery
NCHRP	National Cooperative Highway Research Program
PET	Polyethylene terephthalate
RPC	Recycled plastic composite
RTM	Resin transfer molding
SI	Standard International Units
SCRIMP	Seeman Composite Resin Infusion Molding Process
SMC	Sheet molding compounds
TFHRC	Turner-Fairbank Highway Research Center
USDOT	United States Department of Transportation
UV	Ultraviolet

NOMENCLATURE

a	acceleration
α	thermal expansion coefficient
b	beam width
β	coefficient of moisture swelling
d	beam depth
δ	deflection
ε	normal strain
E	Young's modulus
E_f	flexural modulus
g	acceleration due to gravity
G	shear modulus
h	half thickness of beam
I	moment of inertia
L	length or span
m	mass
M	moment
ν	Poisson's ratio
p	creep parameter
P	load
q	creep parameter
S	flexural strength
σ	normal stress
t	time
T	temperature
U	energy
v	velocity
W	weight
x,y,z	axial directions

Investigations of Plastic Composite Materials for Highway Safety Structures

PIYUSH K. DUTTA

CHAPTER 1: INTRODUCTION

This report describes the results of a study performed to evaluate a series of concepts using various composite materials for highway safety structures. The structural systems for which these materials were studied consisted of a highway barrier W-beam guardrail, its posts and blockouts, sign posts, concrete reinforcing rebars, breakaway couplers, and crushable cushions for roadside sign or utility posts. The composite material systems included fiber reinforced plastics (FRP) in laminated and bar forms, and the commercially available recycled and reconstituted structural plastics.

FRP composites are a relatively new class of materials and are perceived to have excellent durability. They are commercially available, and their varieties range from short-glass-fiber-reinforced thermoplastics for injection molding to about 70% continuous-carbon-fiber-reinforced advance composites. These are the materials of choice for aircraft structural components, auto body panels, appliances, and a plethora of other industrial, civil engineering construction, and consumer products (Ballinger 1991, Busel 1995, Rizkalla and Abdelrahman 1995, Karbhari 1995, English 1987, GangaRao 1995). Although not always as strong or rigid as metals, plastics and composites offer unique design flexibility and the ability to put the strength exactly where it is needed.

The application of plastics and composites to roadside safety hardware systems is considered attractive for a variety of reasons, including corrosion resistance, reduced maintenance, improved crashworthiness, and safety. Each year about 5% of the 36 million small sign supports on our Nation's roadsides must be replaced due to off-the-road accidents or vandalism. Some county engineers spend as much as 15% of their annual maintenance budgets to replace small sign supports. Corrosion-proof composites appear to be a viable material for such structures. Also, the nonconductive property of composites makes them relatively safe during accidental contact with live power lines. Because of the lack of any large-volume market, the growth of production technology for composite materials has been rather slow in the U.S. The application of composites on high-volume roadside safety hardware items could create a market that would support large-scale production, lower production costs, and make composite materials available for other highway applications.

Moreover, plastics and composites hardware development technology can address the crucial national issue of recycling reclaimed plastic materials. This process can lead to a further reduction of cost, making reinforced plastic composites an alternative to timber and steel whenever possible.

In this investigation, to achieve the objective of evaluating the use of composite materials for roadside safety hardware, literature on composites design requirements, material properties, and composite manufacturing processes was reviewed. A prototype guardrail (W-beam) was designed, and a 91.5-m (300-ft) length of this design was fabricated to match or slightly overperform the tensile strength and stiffness of the AASHTO M180

Class A Type 2 corrugated sheet steel guardrail beams. Samples of these prototypes were then laboratory tested. This study tested commercially available recycled plastic composite (RPC), a timber-like product, for its mechanical properties, to investigate the feasibility of its use as guardrail posts and blockouts, commercially available glass FRP rebars for their long-term creep behavior over a wide temperature range, and design concepts of FRP breakaway couplers and crushable plastic cushions (CPC) for roadside signs and utility posts. This report describes the results of these investigations.

Before the feasibility of using FRP in any structure for highway construction is considered, it is essential to understand the basic properties of the FRP composite materials available in the market. Composite properties reported in literature were reviewed before the start of the experimental work in this project. These properties and the reference literature are cited in Appendix A. Chapter 2 of this report specifically discusses the general properties of composites. The design, development, and testing of each element of this investigation are discussed in subsequent chapters. Chapter 3 deals with the design and development of the FRP composite W-beam. Chapter 4 discusses the mechanical tests performed on the RPC. A study of the creep properties of FRP rebars is documented in Chapter 5. Chapters 6 and 7 summarize the concepts of the FRP breakaway coupler and the crushable plastic cushion, respectively. Chapter 8 gives conclusions and general remarks on the use of FRP composites for highway safety structures.

CHAPTER 2: BACKGROUND

Roadside safety hardware (barriers, crash cushions, signs and light supports, etc.) must perform important safety functions to the errant, out-of-control vehicles, and yet must have low installation and maintenance costs. Metals (steel and aluminum) and concrete have been the most common materials for these structures. However, over the past three decades, the engineering use of fiber reinforced plastics (FRP) composites has proliferated, and FHWA has been actively examining these materials for various highway uses, including the roadside safety structures. The Agency has supported important studies of the impact behavior of the FRP composites produced in the pultruded form (Svenson et al. 1993), investigated the durability of FRP rebars for concrete (Anderson et al. 1994), and sponsored a bold new initiative in design developments for all-composite vehicular bridges (Seible 1996). A summarized version of the current research effort of this report and the program goals of the applications of FRP and RPC in highway safety structures has been reported earlier (Dutta and McDevitt 1994, McDevitt and Dutta 1993).

To the general engineering community, FRP is a complex and unfamiliar engineering structural material. It is perceived by many as an aerospace material and, therefore, would be expensive to produce, design with, and use. The sections of this chapter are therefore devoted to describing this material, referred to either as FRP composite or FRP.

Fiber reinforced polymer (FRP) composites

In polymer composites, high elastic modulus fibers are incorporated into a lower elastic modulus matrix to achieve structural reinforcement. Most common fibers are E-glass, carbon or graphite, and aramids (Kevlar). Typically the elastic modulus and strength of these fibers are a magnitude higher than those properties of the polymer matrix in which the fibers are embedded. The essential quality of a good composite is that the bond between the fiber and the matrix is well established and is continuous both around the fiber and along its length. Thus, a good composite's performance essentially depends on the interfacial bond quality. When a load is applied in the direction of the fiber orientation of the composite, the load is shared both by the fiber and the polymer matrix. The ratio of this load distribution depends on the relative elastic modulus of the fiber and the matrix (Chamis 1974). However, the elastic modulus of the polymer matrix is significantly influenced by the temperature. At lower temperature, the modulus of elasticity increases considerably, and thus the load distribution between the fibers and the matrix changes. In its simplest form, the polymer composite material can be visualized as a bundle of solid rods held together with a glue, filling up all the void space around the fibers (see Fig. 1). However, in the microscopic scale, these solid rods have a diameter varying in the range of 5 microns for carbon fibers, to about 20 microns for glass fibers (one micron = 1 μm). It is interesting to note how these fibers are packed together. Figure 2a shows a square array packing when the fibers lie on top of each other. Under this packing condition, the void volume is greater than the void volume in the hexagonal array of packing shown in Figure 2b. The

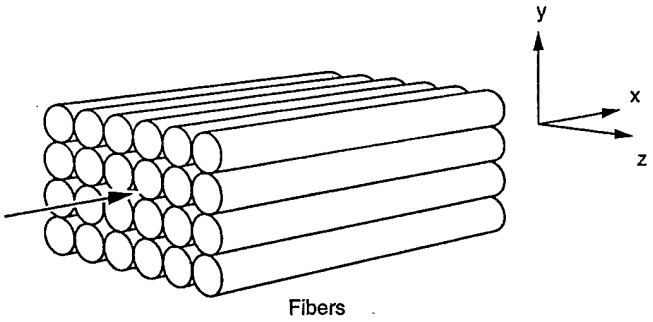

Figure 1. Representation of fiber composites as a bundle of solid rods.

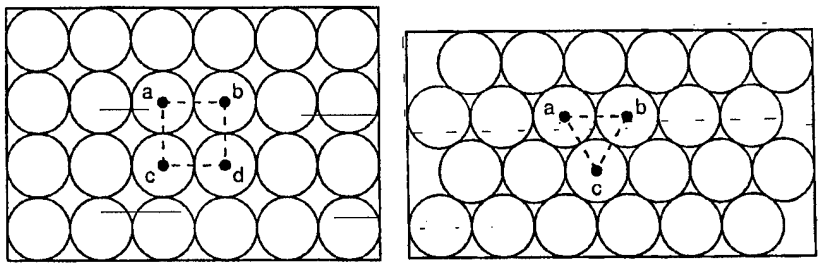

a. Square array (fiber volume fraction: 78.5%).

b. Hexagonal array (fiber volume fraction: 90.7%).

Figure 2. General arrangements (packing) of fibers.

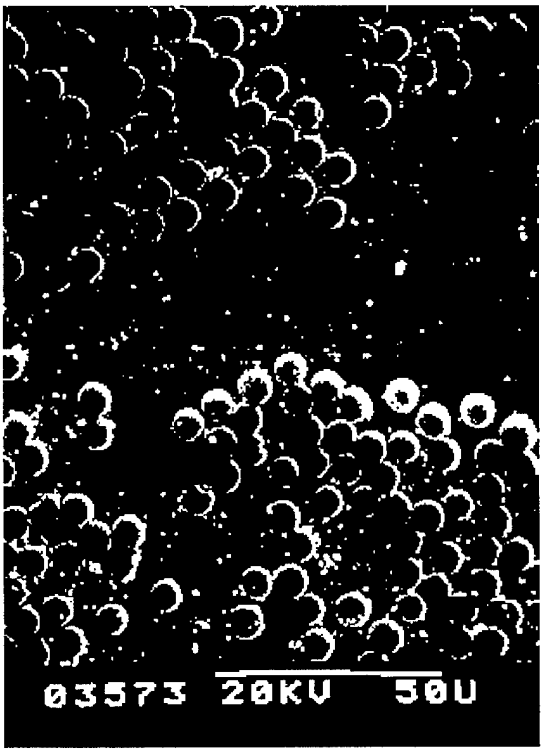

Figure 3. Photomicrograph of a polymer composite.

theoretical volume fraction of fibers under the square array is 78.5% and under the hexagonal array is 90.7%. In reality, however, the packing condition is quite arbitrary, and large spaces in between fibers are common, as shown by the micrograph of a composite in Figure 3. In most composites the fiber volume varies from 55 to 65%.

Figure 1 shows that the orientation of the fibers controls the overall behavior of the composite, and it is necessary to refer to these orientations and other directional properties with some designated axes, say 1, 2, and 3. For example, in Figure 1, we can designate $x = 1$, $y = 2$, and $z = 3$. Thus, if we have to refer to a tensile or compressive stress σ in the x direction, we refer to it as σ_{11}; similarly, for the y direction we have σ_{22}, and the z direction is σ_{33}. Other elastic parameters, such as strains, ε, modulii (E for Young's modulus, and G for the shear modulus), or Poisson's ratios, ν, as well as the thermal and moisture absorption coefficients (α and β, respectively), are also referred to their directionality with appropriate subscripts.

Unidirectional composites

The bundle of rods shown in Figure 1 can be assumed to represent a model of the unidirectional composites. The unidirectional composites

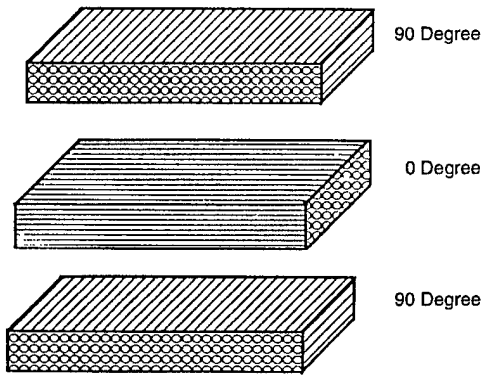

Figure 4. Schematic representation of a fiber composite lamina.

could be either a flat arrangement of unidirectional fibers, which are called a lamina, or structural shapes like rods, bars, or beams, which are usually produced by continuous manufacturing processes using roving of the fibers. Figure 4 gives an example of three laminas, in each one of which the fibers are oriented in a specific direction. The glass-fiber-reinforced plastic bar which we have considered for creep tests under this study is also a unidirectional composite manufactured in the form of a rod from glass fiber roving. The polymer for the matrix of these composites is usually polyester or vinyl ester (the latter has slightly higher fracture toughness, flexural strength, and chemical resistance, but a somewhat higher cost).

Laminated composites

The manufacturing of laminated composites starts with the incorporation of a large number of fibers into a thin layer of matrix called a ply. The thickness of the ply usually ranges from 0.1 to 1 mm (0.004–0.04 in.). As said before, a laminate containing only unidirectional fibers is called a lamina. For a laminate containing unidirectional fibers, the material has the highest strength and modulus in the longitudinal direction of the fibers. However, in the transverse direction, its strength and modulus are very low. Therefore, a varied amount of fibers in different directions (Fig. 5), as well as the use of different types of fibers, can be used to control the properties in different directions. Generally, continuous fibers or mats of the reinforcing fibers in bidirectional orientations are used to form the laminate. Sophisticated laminate theories and computer-aided design methods are available to produce optimum properties of the desired laminates. The FRP W-beam design developed under this program was a laminate design, as will be discussed later.

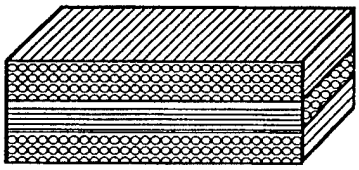

Figure 5. Schematic representation of a fiber composite laminate.

Manufacturing processes

FRP composites are created by combining primarily two materials, one serving as the reinforcement and the other as the matrix. Because composites present such immense opportunities for tailoring the material to the specific requirements of structures, the processes available are multiple and varied. They include molding, compression molding, pultrusion, filament winding, resin transfer molding, and the recently developed Seeman Composite Resin Infusion Molding Process (SCRIMP). The key ingredient in selecting a successful production process is the cost effectiveness, which depends largely on high rates of production and uniformity of quality.

The early manufacturing methods included the slow and labor-intensive hand-layup technique, which slowly gave way to the methods that can support mass production rates. With the introduction of automation, well-controlled resin curing techniques, new fiber forms, and high-resolution quality control tools, the manufacturing technology of FRP composites is advancing at a rapid pace.

The bag molding process, which is common in the aerospace industry, requires a "prepeg," which contains fibers impregnated with resin in a partially cured state. The prepeg plies are laid up in the desired fiber orientation angle, as well as in the desired sequence. The entire assembly is then cured in a preheated autoclave. While the bag molding process is relatively simple, it cannot handle parts of complex geometry. For parts of complex geometry, the compression molding process is more suited. It involves transferring sheet molding compounds (SMC) into finished products in relatively short periods of time. In this process, precut amounts of SMC plies are placed as a charge on to the bottom half of a preheated mold cavity, and the top half of the mold is then lowered on the charge, applying pressure on it and squeezing out the excess resin. With the applied heat, the charge assembly is cured.

Pultrusion is a continuous molding process. It produces long, straight structural members of constant cross-sectional area by using continuous strand fiber roving. For improving transverse strength, mats or woven roving are added at or near the outer surface. The ratio of continuous roving to mat determines the mechanical properties. The use of polyester or vinyl ester resins is common in the pultrusion process. The process involves pulling the continuous strand roving and mats from one end of the line into a liquid resin bath where strands are thoroughly wetted. Then the fiber resin stream is pulled first through a series of preformers and then through a long, preheated die, in which final shaping, compacting, and curing take place.

In a filament winding process, a band of resin-impregnated roving (monofilaments) is wrapped around a rotating mandrel and cured, to produce axisymmetric hollow components.

SCRIMP, which is similar in concept to resin transfer molding (RMT), is common in the plastics industry. SCRIMP requires only one tool side and a simple vacuum bag. Before the resin is infused, all air voids are first eliminated and the resin is infused in a controlled fashion. The resin wets out the reinforcing fibers and eliminates any voids. The major advantage of this process is that the manufacture of very large parts in a high-quality fashion can be accomplished without large investments.

Durability of FRP composites

The durability of FRP composites has been researched in depth by many authors (Monaghan and Brinson 1994, Hahn and Kim 1978, Dewimille and Burnsell 1983), and their results have been briefly reviewed recently (Dutta 1995a, 1995b). The mechanisms that control the durability include chemical or physical changes of the polymer matrix, the loss of adhesion or debonding at the fiber/matrix interface, and the reduction of fiber strength and modulus. Environment plays a crucial role in changing the properties of polymer matrix composites. By environment we mean both the ambient environment and the loading environment, because both can affect the durability of the composites. Considering the ambient environment, we find that both matrix and fibers may be affected by moisture, temperature, sunlight (UV radiation), ozone, and the presence of degrading chemicals like salts or alkalis. Repeated excursions to very high and low temperatures (freeze-thaw cycling) may also introduce some changes. Under a mechanical loading environment, as in steel, repeated loading may introduce

fatigue in composites. Sustained load over a period of time may cause the material to creep.

It is important, however, to note that because of the relative newness of these materials, there is a considerable gap in the definitive durability data of polymeric composites. Systematic investigations to predict the life of most commonly acceptable fiber composites in the civil engineering construction environment are rare, and in many cases, the data available are not relevant to practical applications.

Extreme changes in the temperature of composite materials result in several important effects (Dutta 1994, Lord and Dutta 1988). Most materials expand when the temperature rises. In fiber-reinforced polymer matrix composites, the coefficient of thermal expansion of the matrix is usually an order of magnitude greater than that of the fibers. A decrease in temperature, due either to cooling during the fabrication process or to low-temperature operating conditions, will cause the matrix to shrink. Contraction of the matrix is resisted by relatively stiff fibers through fiber-matrix interface bonding, setting up residual stresses within the material microstructure. However, except for a severely cold environment, the induced residual stresses are not of much concern. Most resin matrix materials become stronger and stiffer, but brittle, as they are cooled. These changes can influence the modes of failure.

Unless an FRP composite contains a significant percentage of interconnected voids that are filled with water, the freeze-thaw effects on the strength, within the normal range of temperature (+30°C to –20°C), (+86°F to –4°F), are insignificant. Commercially available glass fiber composites usually contain about 0.4% voids, which does not allow any appreciable frozen moisture to cause any serious damage.

The effect of ultraviolet (UV) light on polymeric compounds is well known (Larsson 1988). On prolonged exposure to sunlight, the matrix may harden and discolor. The problem is generally overcome by adding a UV-resistant coating to the composites. Of major concern is the degradation of reinforcing polymeric fiber such as aramid. However, the effect is a self-screening type—that means only the skin of the composite structure is affected. So, in thicker composites, the degradation effect is minimal on structural properties.

Creep behavior

Creep is the increase in strain with time at a constant stress level. Creep occurs because of a combination of elastic deformation and viscous flow. When the stress is removed after a period of time, the elastic deformation is immediately recovered, but the deformation caused by the viscous flow recovers slowly to an asymptotic value, called the recovery strain.

In FRP composites, the creep strain depends on the stress level and temperature and is a function of the distribution of stress between the fiber and the matrix. In general, highly cross-linked thermosetting polymers exhibit lower creep rates than thermoplastic polymer composites. With the exception of aramid fibers, commercial reinforcing fibers such as glass and carbon do not creep appreciably at normal loads (Mallick 1988).

Fatigue properties

The fatigue property of a structural material represents its response to cyclic loading. Repeated cyclic loading usually changes the strength properties of metallic materials. The FRP composites, on the other hand, are generally well known for their excellent fatigue behavior. One of the major problems of predicting the fatigue failure limit of FRP composites is the complexity in assessing the modes of failure (Lorenzo and Hahn 1986). A unique feature of a fiber composite material in fatigue testing is that it exhibits a gradual softening with increased cycling. Thus, tests are sometimes done not to a failure represented by the separation of the specimen, but to a predetermined limit of specimen stiffness or residual strength.

Fire hazards and flammability

Although the use of FRP composites in structural construction is increasing at a rapid pace, at present the coverage of these materials in construction and building codes is not extensive. Usually the construction authorities, early in the selection process, establish the fire resistive requirements of the selected composites that may have to be verified by fire tests. Where fire hazard exists, the fire hazard characteristics (such as the intended use of the structure to be designed, potential ignition sources, potential mode of flame and smoke spread, and the means for detection, suppression and extinguishment) are identified and the requirements determined. The specific standards for plastics in a model building code have been summarized by Heger (1981). A review of industry literature on FRP composites shows that flammability properties are usually specified by the manufacturers.

Industrial applications of FRP composites

There has been a rapid growth in the use of FRP materials in civil engineering applications during the last several years. When this project was conceived several years ago, the trend of progressive replacement of carbon steel and aluminum as structural materials in many applications was obvious. Today the composite industry produces more than 1.5 billion kg (3.3 billion lb) of composites in a wide array of products (Busel 1995). The potential of composites in construction applications, including repair and rehabilitation of civil infrastructure, has been fully understood. The use of composites has recently been widely demonstrated in building systems, marine/waterfront structures, repair and rehabilitation, corrosion reduction, and structural alternatives for utilities (Busel 1995).

The recent trend in the increasing use of FRP composites has been spurred by the need to overcome the effects of corrosion on traditional materials, such as steel rebars. The use of resin impregnated fiberglass, carbon fiber, or aramid rods has been studied extensively both within the U.S. and abroad (Meier and Kaiser 1991, Kim and Meier 1991, Rizkalla and Abdelrahman 1995). Notable successes of these applications have been reported. Lately, "all-composite" bridge structures have been designed and built at several places.

Differences between FRP and traditional materials

Most traditional construction materials are homogeneous and isotropic, which means they have the same properties in all directions. As stated before, composites are made of fibers embedded in a matrix and commonly placed in layers to form laminates. The fibers may be oriented in different directions in different layers. This gives the laminate different properties in different directions, rendering it anisotropic. Commonly used fibers are glass, carbon, and aramid. Commonly used matrices are polyester, vinyl ester, epoxy, or phenolic.

A comparison of various composites vs. structural steel is presented in Table 1. Many composites are in fact stronger than structural steel, but their weight could be only a fraction of that of steel. Their modulus of elasticity is also lower than steel. Also, as mentioned before, composites do not usually exhibit yield, and they break at a strain much lower than steel. Creep is practically negligible for FRP composites, although Kevlar composites may show noticeable creep over long time periods. Composites are also well known for their fatigue resistance. Fiberglass composites, which are a common choice for general applications in structures because of its relatively low cost, do not have a fatigue limit comparable to steel. The impact resistance of composites is difficult to define and cannot be compared well with conventional materials, as the failure mechanism in composites is complex and totally different from steel, as discussed before. Carbon composites may have a negative thermal expansion coefficient; in general, the thermal expansion coefficients are primarily controlled by the fiber architecture (layering) of the composite.

Disadvantages of composites as structural construction materials

At the present time, the primary obstacle to the wide application of composites is higher material cost. Moreover, the fabrication techniques do not follow any well-established civil engineering or construction practice; rather, they are constantly evolving. The anisotropy of the material properties, often leading to unfamiliar analysis techniques for civil engineers, has added to the problem. In general, the lower values of Young's

Table 1. Representative properties of FRP composites.

Characteristics	*Materials*						
Matrix	Epoxy	Polyester	Vinyl ester	Vinyl ester	Phenolic	Epoxy	Steel
Reinforcement	Graphite	Graphite	Glass roving	Chopped glass	Glass fiber	Kevlar	
Fiber vol. fraction (%)	62	62	75	28	62	62	
Tensile strength (psi)	278,000	220,000	55,000	13,000	44,000	72,000	50,000
Elongation (%)	1.4	1.1	0.8				12
Flexural strength (psi)	254,000	272,000	111,000	28,000	66,000	58,000	40,000
Flexural modulus ($\times 10^6$ psi)	17.1	17.7	3.8	1.6	3.5	3.3	30

SI conversion factor: 1 psi = 6.89 kPa

modulus for glass fiber composites cause a major design problem if deflections are to be limited. At higher temperatures, the properties of most composites degrade. Some degradation of properties at lower temperatures has been reported (Dutta 1992). The fire resistance capacity and the toxicity of the smoke of most composites remain practically unknown. The test methods to define the properties of composites are still evolving, and material standards as well as design and analysis codes are lacking.

Recycled plastic composites (RPC)

Because of growing concerns about pollution of the environment and decreasing capacity of the sanitary landfill sites, the recycling of plastics started gaining momentum in the U.S. in the mid-1980s. At this time, there is considerable emphasis by the FHWA on the use of recycled materials for highway construction. Section 1038 of public law 102-240, the "Intermodal Surface Transportation Efficiency Act," enacted by Congress on 18 December 1991, directs the U.S. Environmental Protection Agency and the U.S. Department of Transportation, in cooperation with the states, to conduct studies on the use of recycled materials in highway construction (Bloomquist et al. 1993). Recycled polyethylene terephthalate (PET) bottles have been considered as a cheap source material for polymer concrete and polymer mortar. Recycled PET has also been tested as a secondary reinforcement in concrete (Auchey and Dutta 1996). During the last several years, a large number of recycled plastics, both with reinforcements and without, have appeared in the market. Many of them have been fabricated in the shapes of structural components, such as rods and bars of various cross sections and diameters. Their mechanical and physical properties have been investigated (Cao et al. 1991). Some of these materials contain large voids in the interior because of the unescaped air during the manufacturing. Cao et al. observed that for these materials the core area is the weakest region because of these voids. The voids appeared to be elliptical with the major axis oriented in the longitudinal direction. Thus, the properties differed across the cross section of the materials. Initially, the application of these structural materials was restricted to noncritical load-bearing structures, such as park benches, picnic tables, fences, fence posts, curbs, parking blocks, etc. In 1990 a composite form of recycled plastics, in which an admixture of sawdust or wood-waste fibers were blended, was identified by the U.S. Navy as a pilot project to determine the feasibility of creating a "recycling loop" for shipboard-generated plastic wastes. Recycling the shipboard-generated plastic wastes was found to be successful in producing the so-called "plastic lumber" without a lot of internal voids, but the sections had a relatively coarse grain due to the size of the sawdust particles (Middleton et al. 1991). In the present study, this RPC was investigated for application in highway structures, and the results are discussed briefly in Chapter 4.

Fracture behavior and energy absorption characteristics of FRP composites

The energy absorption mechanism of ductile metals, steel or aluminum largely results from plastic deformation. In contrast, the fracture of composites involves a large number of different microcracking processes, which depend on the properties of the fibers and resins and on the geometrical arrangement of the fibers. Experience has shown that although the fiber-reinforced-composite tubes or rods can fail in a brittle manner when loaded in compression, a progressive crushing failure can still be produced by appropriately triggering microcracking (Hull 1983). The actual fracture mode is strongly dependent on the fiber arrangements. The microcracking processes can lead to extensive breakdown of the material and the absorption of large amounts of energy. In-depth studies of polymer composites by Hull showed that when a composite fails, the fracture energies are absorbed by matrix cracking, fiber breaking, fiber-matrix debonding, frictional work following debonding, and fiber pullout. He observed that in composites, the specific absorption energies are significantly larger than those observed in the collapse of ductile metallic tubes. The energy absorption property is a significant consideration in the design of guardrails in highway barriers.

General requirements of roadside safety hardware

A discussion of specific roadside safety elements and their requirements are not within the purview of this report. However, the proper design of roadside hardware is important to the safe operation of highways. Although most drivers operate their vehicles safely within the roadway, statistics show that a certain percentage of drivers in any stream of traffic is likely to leave the road unintentionally (Tutt and Nixon 1970).

In general, the roadside terrain should be such that it can be safely traveled by an out-of-control vehicle for a distance sufficient to bring the vehicle under control.

The safety aspects of the roadside environment deal primarily with the interaction of the vehicle with impact attenuation devices, such as guardrails, bridge rails, median barriers, utility poles, sign posts, and embankment slopes. Their design, construction, and maintenance are a major responsibility of highway engineers. Conventional construction materials for these devices include steel, concrete, aluminum, and wood. Fiber-reinforced plastics are a recent addition, and this report will deal with this material in detail in the following chapters. The selection of materials for these safety elements must be judicious, taking into consideration the modes of failure, impact resistance, energy absorption, stiffness, durability, and, of course, cost.

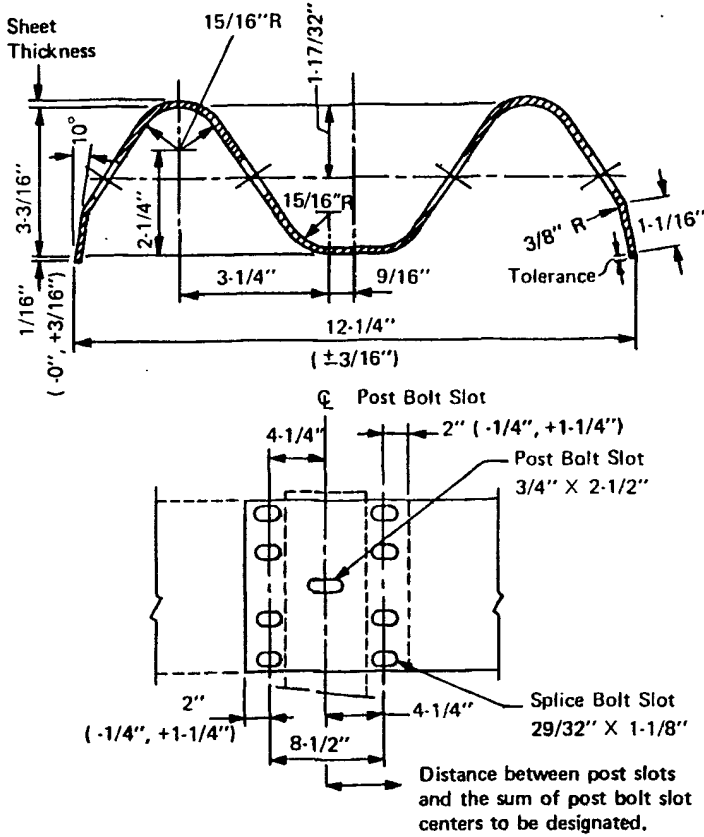

SPECIFICATIONS

Corrugated sheet steel beams shall conform to the current requirements of A.A.S.H.T.O. M180, Class A, Type 2.*

Dimensional tolerances not shown or implied are intended to be those consistent with the proper functioning of the part, including its appearance, and accepted manufacturing practices.

INTENDED USE

This corrugated sheet steel beam is used as a rail element in standard barrier designs G2, G4, MB2, MB4, MB4B, and BCT.

Note: Typical designations are RE-3[2@6'-3"=12'-6"]-73 and RE-3[4@6'-3"=25'-0"]-73.

* If another class or type is required this should be indicated by a modified part number. For example, if corrosion resistant steel is required show thusly: RE-3[2@6'-3"=12'-6" Class A, Type 4]-73.

W BEAM

HM-TF-13 STANDARD	RE-3	DESIGNATE POST SLOT CENTERS & SUM OF CENTERS	-73

Figure 6. Standard W-beam design.

CHAPTER 3: FRP W-BEAM GUARDRAIL

Guardrails are common and are critically important elements of highway safety systems. Every year about 2,165 km (1,345 mi) of guardrails are constructed on Federal projects (McDevitt and Dutta 1993). The existing W-beam design shown in Figure 6 is specified under the "Standard Specification for Corrugated Sheet Steel Beams for Highway Guard Rail, AASHTO Designation: M180-84." The beam consists of open hearth sheet steel with the following mechanical properties:

Yield point,
minimum: 344.5 MPa (50,000 psi)
Tensile strength,
minimum: 482.3 MPa (70,000 psi)
Elongation,
minimum: 12%

Figure 7. Three-point bending test of standard AASHTO W-beam—Class A.

Tests are done per the ASTM A525 procedure. Depending on the type of beam, the thickness varies from 2.67 mm (0.105 in.) to 2.82 mm (0.111 in.) for Class A beams, and 3.43 mm (0.135 in.) to 3.58 mm (0.141 in.) for Class B beams.

Initial tests

Under the current investigation, the W-beam material considered was the fiber-reinforced plastic (FRP) composite. Initial tests were the three-point flexural bending tests on two 1.22-m (4-ft) long pieces, MW-1 and MW-2, of AASHTO Class A W-beam design, with a loading span of 609.6 mm (24 in.) (Fig. 7). The load-deflection and energy absorption characteristics are shown in Figures 8a and b for MW-1 and MW-2, respectively. The loading and the two support points were provided by 50.8-mm- (2-in.-) diam. hardened steel rods. Loading was applied by a screw-driven testing machine. The midpoint deflection and the load were measured manually. The beams started yielding at about 60.08 kN (13,500 lbf) load. The yielding happened primarily at the loading contact point of the beam to the rod, as shown in Figure 9.

To understand the comparative behavior of an FRP beam under similar tests, we tested a commercially available FRP W-beam (manufactured for some special applications) with a thickness of 3.81 mm (0.15 in.) (Fig. 10). As for the steel

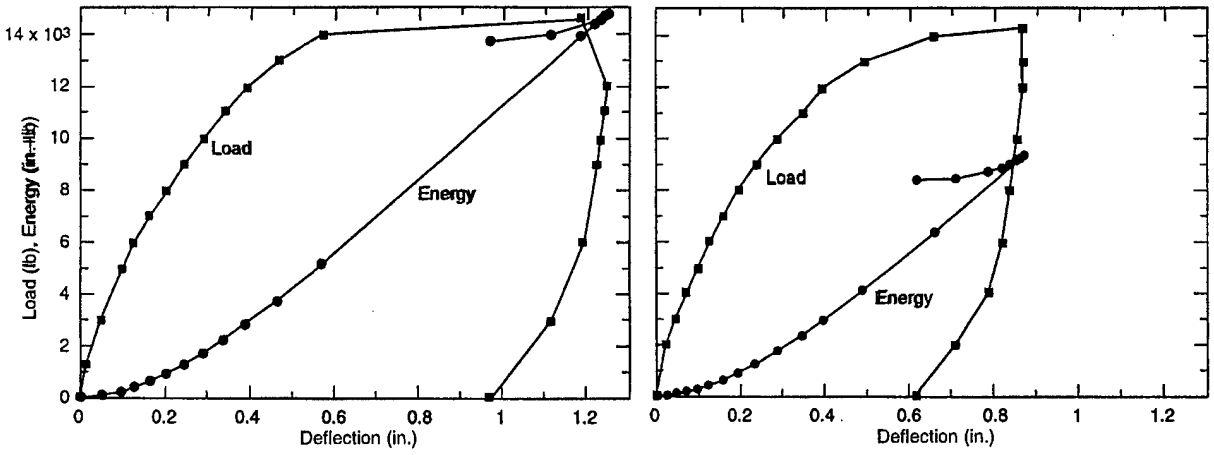

a. MW-1. *b. MW-2.*

Figure 8. Load deflection characteristic of AASHTO W-beam under three-point flexure test.

Figure 9. Tested (left) and untested (right) AASHTO W-beams. Note the local "yielding" as the energy absorption mechanism in these beams.

Figure 10. Commercially available pultruded FRP section of W-configuration, used for initial test (layup unknown).

W-beam, loading was applied in a three-point bending test configuration (Fig. 11) and load-deflection characteristics were recorded (Fig. 12). Note that the beam rebounded after the load was removed. Energy was absorbed by a fracture that developed at the loading point. The area between

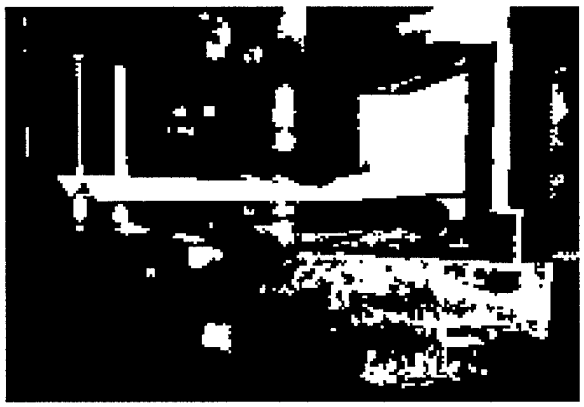

Figure 11. Testing of commercial FRP beam W-configuration.

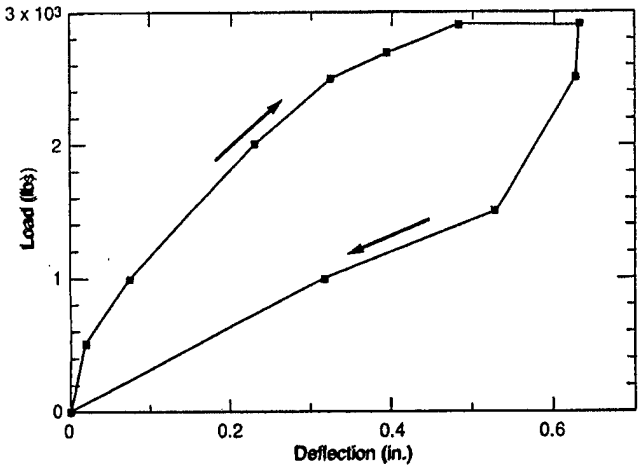

Figure 12. Test results of commercial FRP beam of W-configuration.

the loading and unloading curve gives the energy absorbed in the fracture process.

The key to developing a large amount of energy absorption is to design the composite W-beam with constituents arranged in such a manner that progressive crushing occurs. The crash would be expected to move at approximately a constant load equal to the residual load and also at the velocity dictated by the deceleration rate of the errant vehicle. The aim here is to achieve extensive microfracturing of the matrix and partial failure of the fibers by breakage and pullout, so that sufficient residual load is sustained to guide the errant vehicle back to its previous course.

FRP W-beam design approach

The initial tests showed that the FRP composites will have a low stiffness and will be highly resilient, despite brittle fracture. Before a composite W-beam was designed, a detailed review of the

Figure 13. Breakaway cable terminal (BCT).

Figure 14. BCT speared on a 817.2-kg (1800-lb) car.

material properties of candidate composite materials was conducted. We also decided that the proposed test prototype W-beam should have tension and flexure strength properties comparable to those of the existing Class A steel W-beams. Laminates would be designed and fabricated with strength, modulus, and other mechanical and durability characteristics similar to FRP materials currently available in the market.

We aimed at making the flexural stiffness of one set of specimens match the AASHTO Class A steel W-beam, and some additional beams at a lower stiffness. The turned-down guardrail terminal, also known as Texas Twist, was developed in the late 1960s because the ends of W-beam rails were observed to spear into cars in end-on impacts. Currently, about 250,000 turned-down Texas Twist terminals are used in this country (McDevitt and Dutta 1993). The twisted versions differ in detail, but all have a W-beam rail that is twisted through 90°, turned down to the ground, and bolted to a recessed concrete block, as shown in Figure 13. Turned-down terminals have been very popular because they have a lower initial cost than any other terminal. However, crash tests have shown that the turned-down W-beam forms a ramp that can launch cars (Hinch et al. 1984). The turned-down steel W-beam is too stiff for 825-kg (1,800-lb) cars to push it to the ground and pass over it. Consequently, the Federal Highway Administration has banned the use of turned-down terminals on strong-post guardrails on Federally-funded, high-speed, high-volume roads (Willett and Bennett 1990). Turned-down terminals are still used on low-speed, low-volume facilities, and on weak-post guardrail systems.

The breakaway cable terminal (BCT) was developed in the 1970s. It solved the spearing problem without creating a launching problem and became widely used. However, full-scale tests have shown that the BCT can spear or overturn 825-kg (1,800-lb) cars in end-on impacts, as shown in Figure 14, because the steel W-beam rail is too stiff (Kimball et al. 1982). A substitute for the steel W-beam rail, made of a composite material that is not as stiff as steel, was therefore also considered for developing a retrofit design for the BCT.

The 12.7-mm- (0.5-in.-) thick composite W-beam design was intended to be a one-for-one substitute for a steel W-beam. This design is shown in Figure 15. It was to have the same tensile capacity in the longitudinal direction and the same lateral stiffness as a steel W-beam. Producing these W-beam sections by the pultrusion process could result in significantly lower production costs, but would require heavy capital outlay for tooling. It was therefore decided to manufacture the prototypes by another available low-cost manufacturing technique.

Design analysis

An engineering analysis was conducted based on the performance of the beam. The key design equation for limiting beam deflection takes the form

$$\delta = f(P)/(EI) \qquad (1)$$

which shows that the deflection δ is dependent on the product EI, the flexural stiffness. The numerator $f(P)$ is a function of the applied load, depending on the beam geometry and supporting conditions. Among the common engineering materials, E is 206.7 GPa (30 million psi) for steel and 68.9 GPa (10 million psi) for aluminum. The values for polymeric materials range from 172.25 MPa (25,000 psi) (polyurethane) to about 20.67

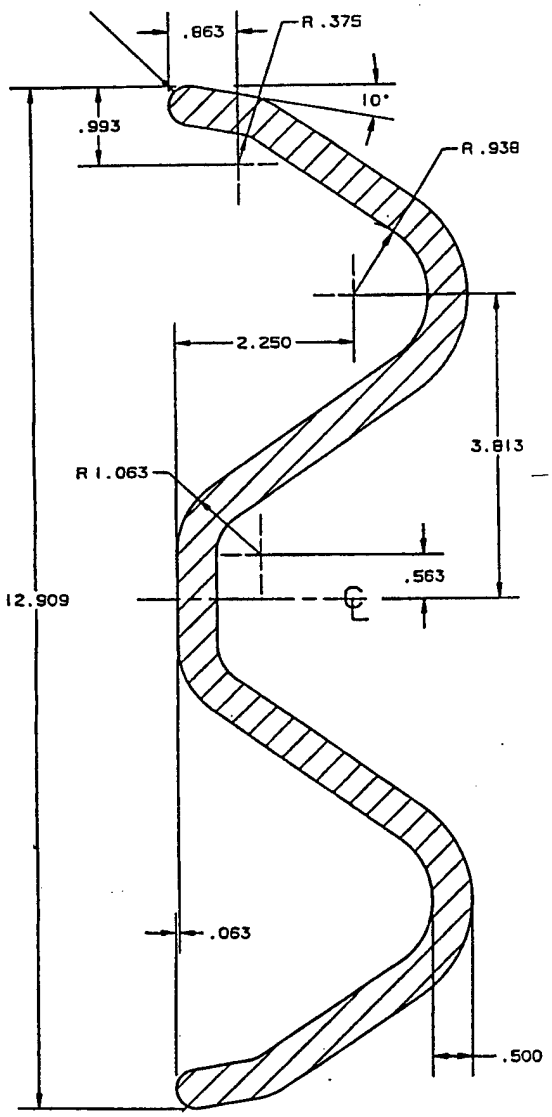

Dimensional tolerance: ± 0.01 in.
Length of each section: 16 ft
No. of sections req'd: 10
Material: Fiberglass/polymer composite
Tensile strength > 70,000 psi
Young's modulus > 3,000,000 psi

Figure 15. W-beam design, 12.7 mm (0.5 in.) thick, using FRP composite.

GPa (3 million psi) for glass-reinforced polyester composites, and about 137.8 GPa (20 million psi) for graphite epoxy composites. Thus, unless the value of I is increased under the same loading conditions, the deflection δ for the polymeric material will become unacceptably high. Low-modulus plastics or composites can compete with high-modulus steel only if the I value can be changed by the proper design of the shape. In designing composite beams, shape and thickness would be optimized for the required flexibility. Initial sensitivity studies also showed that prototype FRP W-beams could be fabricated to have approximately one-third, one-half, two-thirds, and the full stiffness of a 12-gauge steel W-beam. By changing the profile and, if necessary, the cross section, these variations in stiffness could be achieved.

The design analysis for the composite beams also considered preventing permanent bending caused by holding the piece at each end. Assuming the beam is simply supported at each end and is loaded by its own weight, the maximum moment occurs in the center of the beam:

$$M_{max} = wL^2/8 \qquad (2)$$

where w = weight
L = length
M = moment

The maximum bending moment that the element can handle is related to the yield stress σ and the rail geometry, as follows:

$$M_{max} = (\sigma\, I/h) \quad (3)$$

where σ = yield stress
I = moment of inertia
$2h$ = thickness

Equating eq 2 and 3 and solving for eq 1 yields

$$L = [\,(8/w)(\sigma\, I/h)\,]^{0.5} \quad (4)$$

From eq 4 it is obvious that longer beams can be used if the I value can be increased by design.

Test specimen fabrication

Materials considered for fabrication of the composite W-beam included both thermoplastic and thermoset composites, including graphite-reinforced plastics, aramid-reinforced plastics, and fiberglass-reinforced epoxy, polyester, and vinyl ester. Because of cost considerations and ease of fabrication, only glass-fiber-reinforced polyester composite was chosen for specimen fabrication.

The costs of different fabrication processes, including sheet molding, pultrusion and thermoforming, were examined. Since we needed a long, constant cross-section product, the pultrusion process was the most feasible option. To manufacture the specimens, it was necessary to solicit the cooperation of the pultrusion manufacturers to design suitable dies and molds. Several pultrusion and molding companies were contacted and designs were reviewed with them. Because of the high cost of manufacturing the dies and tooling, the pultrusion process was abandoned. Instead, a vacuum bag technique using a mold made of existing steel W-beams was used. It was also decided that pigments and coatings would be provided on the FRP W-beams to give them a weathered zinc-coated look. The layup was also to be developed by the vendor, using the laminated theory and their own design protocol, to achieve the goals of tensile strength (482.3 MPa, 70,000 psi) and stiffness (E = 20.67 GPa, 3 million psi).

For obtaining the highest strength in composite laminates, the aim is always to maximize the reinforcing glass fibers and minimize the matrix material. Before putting them into the W-beam mold, all glass fiber fabrics were carefully impregnated with a measured amount of resin, which helped to ensure uniform "wet-out" of the reinforcement and eliminate almost all delaminations in the fabrication processes. The impregnated reinforcements are called "prepegs." The materials required for the fabrication process are shown in Table 2.

The glass fiber prepegs were then cut to length in both the longitudinal and transverse directions. There was no splicing of the reinforcement, so as to effect continuous strand reinforcement, thereby maximizing strengths in both the warp and weft directions. A surfacing veil consisting of a 170.1-g (6-oz) C-glass mat was first laid down. This was followed by a single layer of 510.3-g (18-oz) bidirectional, stitched E-glass. Thereafter, different layers of S-2 glass prepegs and E-glass fabric prepegs were applied to build the thickness and strength. The final two layers consisted of the bidirectional stitched E-glass and the surface veil of the C-glass mat.

The number of layers and their orientations were experimentally determined by reiterating and running simultaneous tensile tests of the cured laminate coupons in the MTS testing machine and then fabricating the laminates. Figure 16 shows the dimensions of the coupon samples. A number of typical coupon test specimens after the test are shown in Figure 17a, and an enlarged view of the typical fracture area is shown in Figure 17b. Figure 18a gives the testing configuration of the test coupon, and Figure 18b shows a typical stress-strain curve from the tensile test of one of the initial laminate designs. Note

Table 2. Materials used for the FRP W-beam fabrication.

Resin:	MR12311 isophthalic polyester
Catalyst:	DDM 9 brand of methyl ethyl ketone peroxide (MEKP)
Glass fiber:	C-glass, E-glass, and S-2 glass

The mechanical properties of the above materials, as declared by the suppliers:

Properties	*Resin*	*E-Glass**	*S-Glass**
Tensile modulus (psi × 10^6)	0.5	4.3	6.4
Tensile strength (psi × 10^3)	10.0	105.0	123.0
Tensile modulus (psi × 10^6)	0.5	4.3	6.4
Tensile elongation (%):	2.4	—	—
Flexural strength (psi × 10^3)	18.0	142.0	100.0
Flexural modulus (psi × 10^6)	0.5	4.4	4.5
Compressive strength (psi × 10^3)	—	73.0	—
Compressive modulus (psi × 10^6)	—	3.1	—

* Reinforcement: Matrix ratio = 60:40. Data supplied by manufacturer for unidirectional laminates.
SI conversion factor: 1 psi = 6.89 kPa

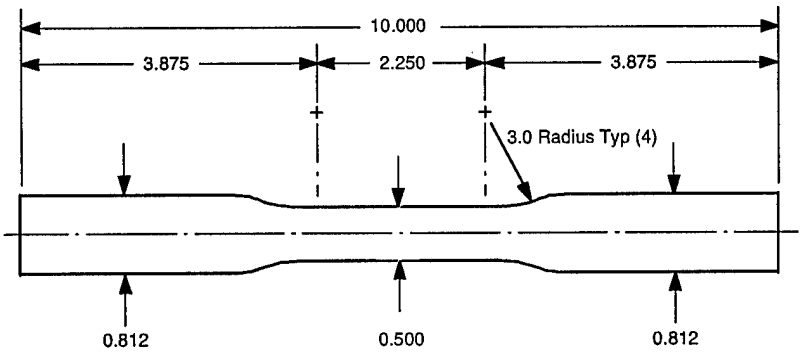

Figure 16. Dimensions of the coupon test specimens.

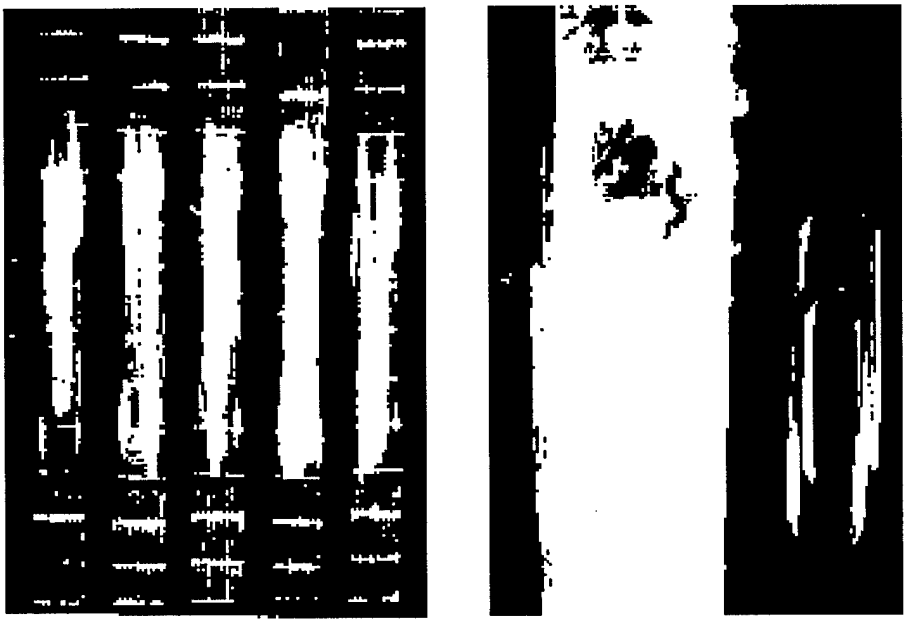

a. FRP laminate coupons after the tensile tests.

b. Enlarged view of the failed area.

Figure 17. FRP laminate coupons.

that the stress-strain curve is bilinear, which is typical for most 0°/90° laminates if the 90° fibers occur at the outer layers. The change of slope from elastic modulus E = 11.58 GPa (1.68 $\times 10^6$ psi) to a lower value of E = 6.48 GPa (0.94 $\times 10^6$ psi) indicates the first ply failure of the composite. This transition has always occurred with a slight sound during testing. Table 3 gives the sequential testing of the laminate coupons until the most optimum layup was developed.

The series of tests revealed that the layup of CRREL-5 laminate had the maximum strength, 449.6 MPa (65,255 psi). As a result, the composite W-beam manufacturing vendor was tasked to produce the W-beam with this layup. The layup was further modified slightly, for manufacturing and finishing reasons. The final layup of the 12.7 mm (0.5 in.) nominal thickness W-beam is shown in Figure 19.

The "wetted-out" laminate prepeg was then placed in the mold of the W-beam. A vacuum bag made of polyethylene sheet was then placed around the part and a vacuum created. This ensured against any inconsistencies in the prepeg layup and created a uniform homogeneous matrix. After curing, each W-beam manufactured in 6.1-m (20-ft) lengths was prepared for gel coat and subsequently painted.

A total of 15 guardrails, each 6.1 m (20 ft) long and 12.7 mm (0.5 in.) thick, was fabricated. As

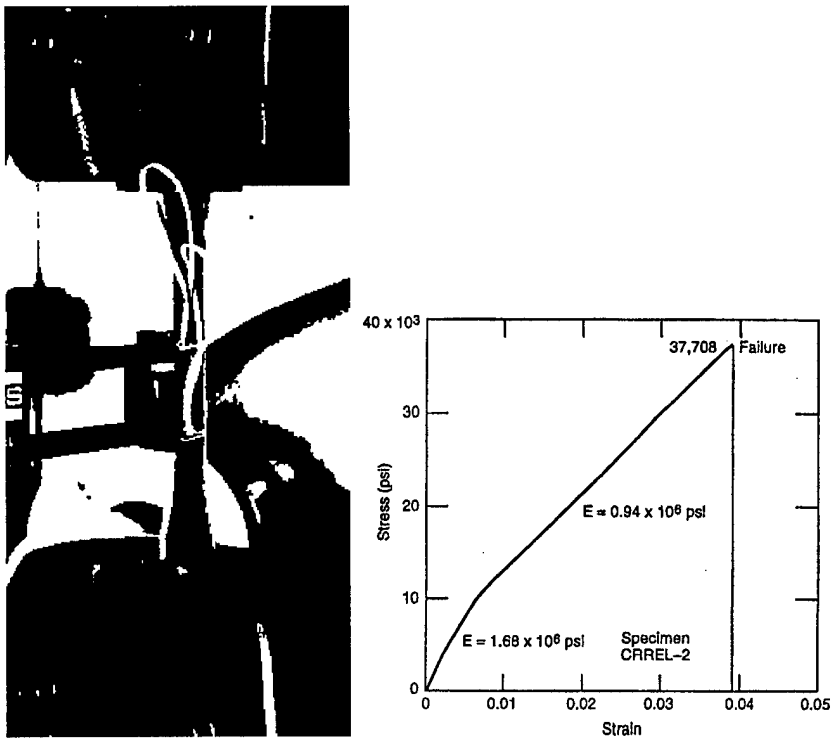

Figure 18. Typical stress–strain curve and bilinear elastic characteristic of the laminate.

Table 3. Sequential tests of tensile coupons to develop optimum layup for the FRP W-beam.

Coupon batch	*No. of coupons*	*Nominal thickness (in.)*	*Resin*	*Laminates*	*Test result tensile strength (psi)*
RL	10	0.5	Derakane 470 vinyl ester	4 lam 1.5 oz CSM 6 lam 24 oz woven 4 lam 1.5 oz CSM	30,000
CRREL-1	6	0.1875	Iso-Polyester	10 lam 6 oz woven	24,992
CRREL-2	6	0.1875	Iso-Polyester	11 lam 8 oz unstitched	37,825
CRREL-3	5	0.1875	Iso-Polyester	4 lam 9 oz woven 7 lam 8 oz unstitched	38,138
CRREL-4	5	0.3125	Iso-Polyester	11 lam 10 oz unstitched	62,232
CRREL-5	5	0.3125	Iso-Polyester	8 lam 10 oz unstitched 2 lam 9 oz S-2 woven	65,255
CRREL-6	5	0.3125	Iso-Polyester	9 lam 10 oz unstitched 2 lam 5.4 oz S-2 woven	42,773
CRREL-7	5	0.25	Iso-Polyester	9 lam 10 oz unstitched 2 lam 3.6 oz woven graphite*	55,822

* Graphite fiber was used as an exploratory test.
SI conversion factors: 1 in. = 25.4 mm, 1 oz = 28.35 g, 1 psi = 6.89 kPa.

required, their profile almost mimicked the conventional guardrail (Fig. 20). The flexural stiffness of the beams also proved to be adequate as can be seen in Figure 21 in which hardly any sagging was noticed when a beam was held at the two ends. Some lengths of 6.35-mm (0.25-in.) and 9.53-mm- (0.375-in.-) thick W-beams were also manufactured, with a reduced number of internal layers.

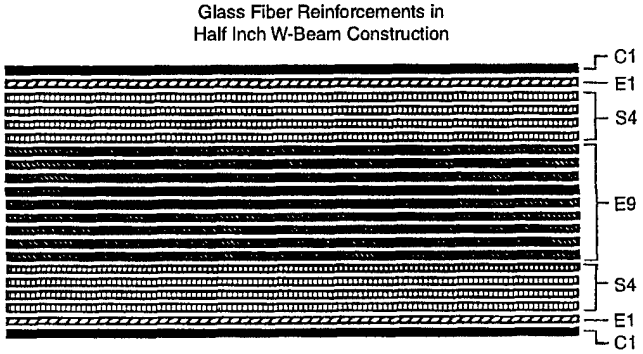

Figure 19. Layup of the final FRP W-beam construction.

Spliced bolt tension tests

Since W-beam rails have to be spliced together (and also connected to end shoes), tension tests were conducted to evaluate the strength and performance of the bolted splice joints. There was concern that the reinforced plastic might fail in bearing at the bolts.

The configuration of the 19.05-mm (0.75-in.) bolt pull-out test is shown in Figure 22a. For these tests from the flat portions of the 12.7-mm- (0.5-in.-) thick W-beams eight rectangular test coupons (Fig. 23) of 304.8 × 63.5 mm (12 in. × 2.5 in.) size were cut and machined. At 38.1 mm (1.5 in.) from the edge at each end, 19.05-mm- (0.75-in.-) diam. holes were drilled to accommodate the 19.05-mm (0.75-in.) bolts of tensioning D-links connected to 25.4-mm- (1.0-in.-) diam. eye-bolts. The loads were applied in tension to the eye-bolts by a servohydraulically operated testing machine with a cross-head speed of 2.54 mm (0.1 in.) per minute (Fig. 22b). The test results are summarized in Table 4.

The load-displacement curves from the above tests, superimposed on each other, are shown in Figure 24. A failed specimen showing the failure cracks, one longitudinal and one transverse, is shown in Figure 25.

Considering the nominal area of the W-beam for the 12.7 × 63.5 mm (0.5 × 2.5 in.) section as 806.5 mm^2 (1.25 sq. in.), the nominal stress on the beam at which the bolt failure occurred is approximately 57.435 MPa (8,336 psi). This is only about 14% of the desired maximum tensile strength of the FRP W-beam. This is a distinct disadvantage, and future work would be needed to adequately reinforce the bolt holes in the FRP W-beams.

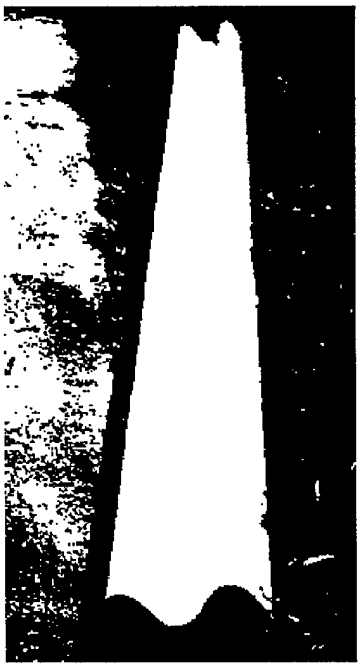

Figure 20. FRP W-beam as produced from the design.

Figure 21. Prototype 6.1-m (20-ft) long W-beam held at two ends that did not sag under its own weight.

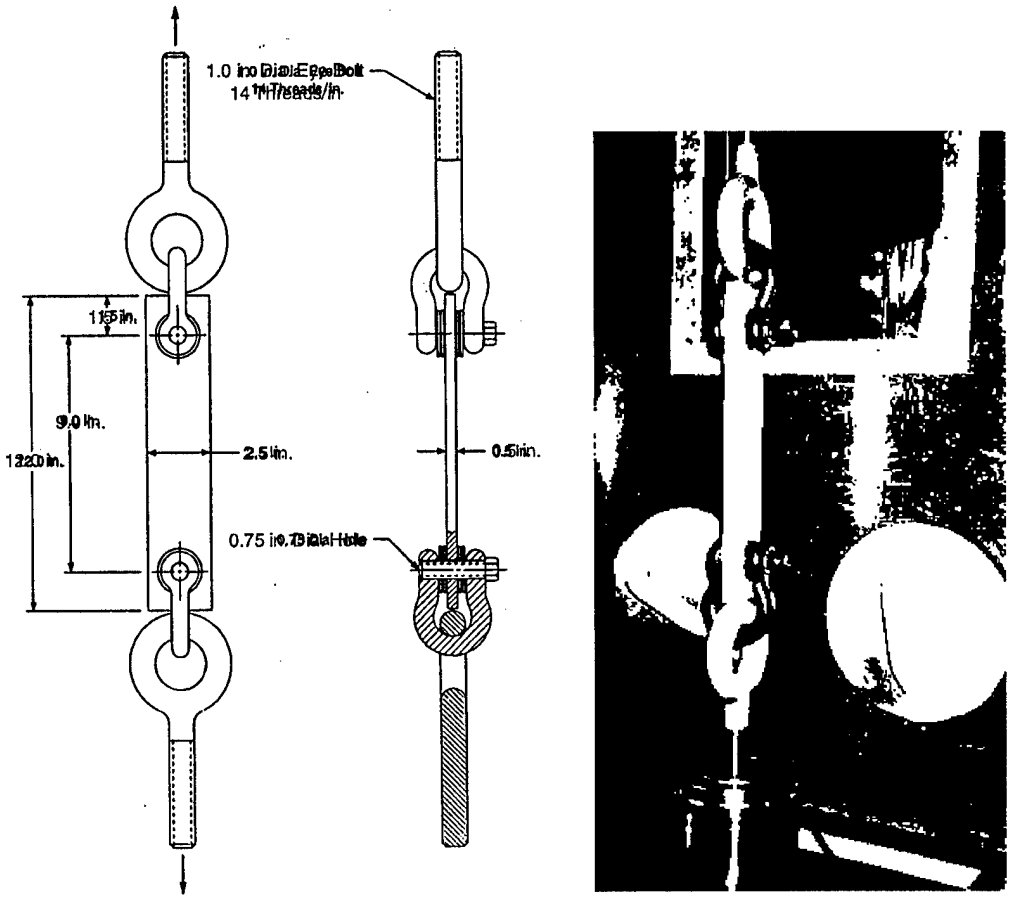

a. Bolt pull-out test configuration.

b. Bolt pull-out test for the 12.7-mm (0.5-in.) thick W-beam FRP.

Figure 22. Bolt pull-out test.

Table 4. Results of bolt pullout tests of the 12.7-mm (0.5-in.) thick FRP W-beam.

Specimen no.	*Failure load (lbf)*	*Nature of failure*
W-1	10,300	Longitudinal cracks downward from bottom hole
W-2	10,300	One longitudinal and one transverse crack
W-3	10,500	Two transverse cracks from bottom hole
W-4	10,575	Two transverse cracks from bottom hole
W-5	9,620	One longitudinal crack from top hole
W-6	11,025	Two cracks, one longitudinal, one transverse
W-7	10,300	Two cracks from the top hole
W-8	10,740	Two cracks from the top hole
	Average = 10,420	
	Std. dev. = 384	

SI conversion factor : 1 lbf = 4.45 N

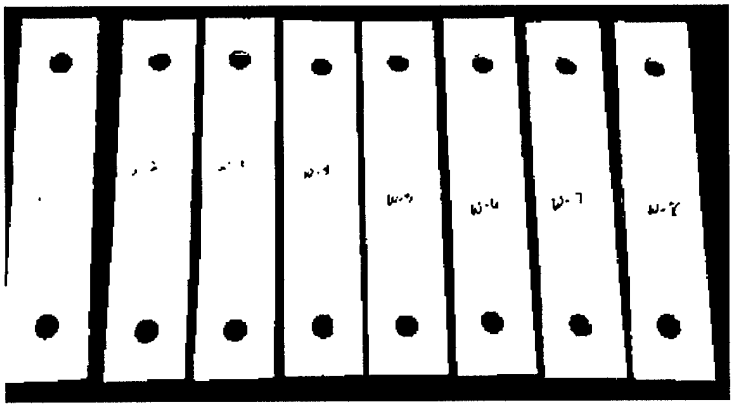

Figure 23. FRP W-beam test coupons for 19.05-mm (0.75-in.) bolt pull-out tests.

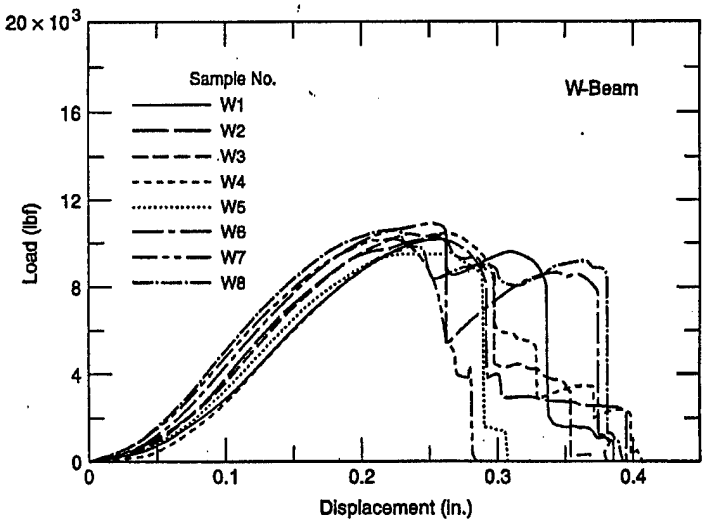

Figure 24. Load-displacement curves from the bolt pull-out test.

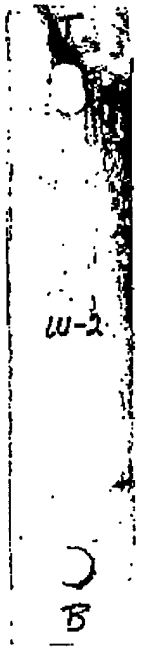

Figure 25. Failed specimen from the bolt pull-out test.

Flexural tests

As in the initial tests, flexural tests were conducted on all three composite beams shown in Figure 26. Four samples (designated as sample 1 through 4) were prepared from the 12.7-mm- (0.5-in.-) thick beam and one each from the 9.53 mm (0.375 in.) (sample 5) and 6.35 mm (0.25 in.) (sample 6) beams. The three-point test configuration is shown in Figure 27. The load was applied using the screw testing machine, as in the initial tests. The loads and deflections were recorded manually. The 12.7-mm (0.5-in.) samples 1 through 3 were loaded to failure, when fracture occurred at the point of contact with the loading bar. Sample 4, however, was loaded cyclically, first to 66.75 kN (15,000 lbf), then unloaded to 1.11 kN (250 lbf), reloaded to 84,55 kN (19,000 lbf), unloaded to 1.11 kN (250 lbf), and finally loaded to 100.13 kN (22,500 lbf), when it severely cracked but continued to deflect to 43.18 mm (1.7 in.).

During loading, low-level cracking noise was heard in each of the four samples. The load

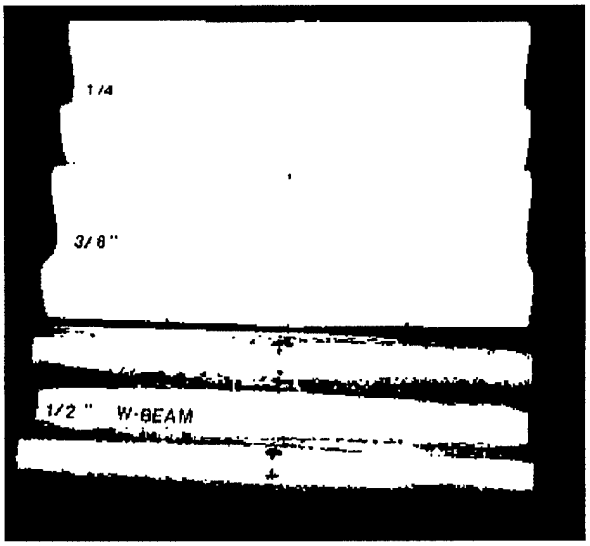

Figure 26. Three FRP W-beam samples for three-point flexure tests.

Figure 27. Three-point flexural test configuration for the FRP W-beam samples.

deflection characteristics for the four samples plotted in Figure 28 clearly show large hysteresis, indicating energy absorption by internal cracking. However, the beams maintained considerable flexural stiffness after cracking, and they bounced back to their linear shape after the load was removed. In fact, the samples shown in Figure 26 were all fractured in the test, but the cracks practically closed on removal of the load. Figure 29 summarizes the load deflection data from all samples. Failure strengths and stiffnesses of the 6.35-mm (0.25-in.), and 9.53-mm (0.375-in. beams were considerably lower than those of the 12.7-mm- (0.5-in.-) thick beams, and the thinner beams obviously deflected much more for a given load.

Table 5 is a summary of the critical data from these tests along with the data initially obtained for the steel W-beam. Table 5 clearly shows that the 12.7-mm (0.5-in.) W-beam exceeds the performance of the steel W-beam in yield strength by about 42%, but its flexural stiffness (EI) is only 34% of that of steel. It also weighs approximately 87% of the steel beam. If a lower stiffness is acceptable, the 12.7-mm (0.5-in.) W-beam can be a candidate for a one-to-one replacement of the steel W-beam. The 9.53-mm (0.375-in.) and 6.35-mm (0.25-in.) W-beams obviously have much lower flexural stiffnesses, but they also have about 86% and 43%, respectively, of the strength of the steel beam. Their weights are also only 68% and 47%, respectively, of the steel beam.

Cold weather exposure test

Although this exploratory development of an FRP W-beam guardrail was far from viable and acceptable as a proper guardrail for highways,

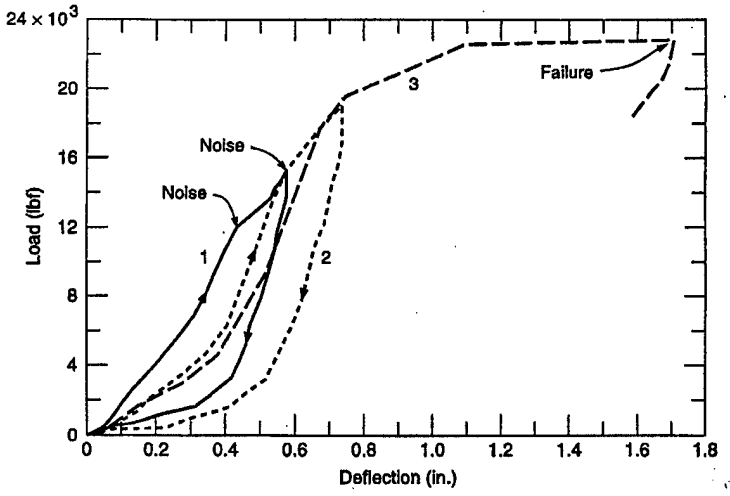

Figure 28. Load-deflection characteristics from cyclic loading of 12.7-mm (0.5-in.) thick W-beam.

Table 5. Comparison of steel and FRP W-beams of different thicknesses.

Material	Nominal size (in.)	Nominal section ($in.^2$)	Weight per ft (lbf)	Nominal tensile strength ($psi \times 10^3$)	Nominal Young's modulus ($psi \times 10^6$)	Moment of inertia (I) ($in.^4 \times 10^4$)	Flexural stiffness (EI) ($lbf\,in.^2 \times 10^{10}$)	Flexural yield load (lbf)
FRP	0.5	9.58	6.09	60.0	2.0	11.8	23.6	20.0
FRP	0.375	7.56	4.81	60.0	2.0	8.8	17.6	12.0
FRP	0.25	5.25	3.34	60.0	2.0	5.6	11.2	6.0
Steel	0.111	2.12	7.12	60.0	30.0	2.3	69.3	14.0

SI conversion factors: 1 in. = 25.4 mm, 1 $in.^2$ = 645.2 mm^2, 1 lbf = 4.45 N, 1 psi = 6.89 kPa.

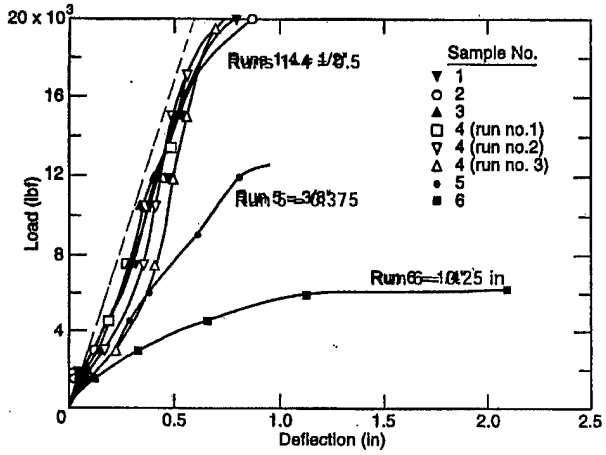

Figure 29. Results from the load-deflection tests of the FRP W-beams.

Figure 31. End-on-end epoxy glued joint.

Figure 30. CRREL's pilot installation of the 12.7-mm-(0. 5-in.-) thick FRP W-beam.

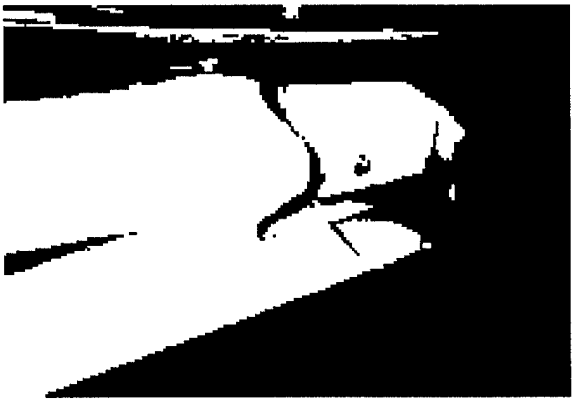

Figure 32. Splicing by cut-out piece of W-beam.

within the CRREL campus, a site was available for a pilot installation of this rail using nonstandard wooden posts (Fig. 30). This would provide an opportunity for observing any degradation of this material due to the cold and long-term weather exposure of New Hampshire, under a controlled and noncritical traffic environment. In July 1992, a length of approximately 35 m (120 ft) of these rails was installed, end-on-end was epoxy glued (Fig. 31), and back spliced with a shorter piece of W-beam cut-out which was fastened with nuts and bolts (Fig. 32). Until the demolition of the installation in the spring of 1996, no major blistering or any other signs of material

degradation was noticed. However, in the winters, the installation suffered severe snow accumulation and was subjected to snow plowing (Fig. 33); as a result, immediately after the first winter, the surface veil coating was observed to be removed at several places (Fig. 34).

Figure 33. The FRP W-beam installation exposed to heavy snow accumulation and plowing.

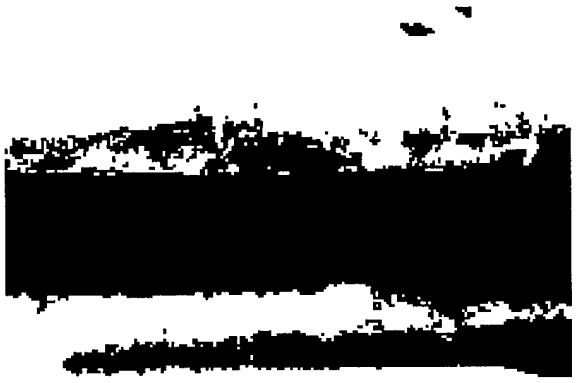

Figure 34. Snow plow abrasion damage to the FRP beam.

Impact test

An impact test of the 6.35-mm (0.25-in.) and 9.53-mm (0.375-in.) W-beam materials, designated as CR2 and CR3, respectively, was conducted by Svenson (1993) at the Turner-Fairbank Highway Research Center of the FHWA in conjunction with their intensive studies of "Impact Behavior of Composites." The results of the impact testing of a number of commercially available pultruded composites conducted using an MTS (Model 850.02A-01) vertical drop weight testing machine were reported at the 1993 Annual Conference of the Composites Institute, and readers are encouraged to read the article to review the detailed procedures of the test. The tests were conducted by dropping a striking cylinder head perpendicular to the specimen's broad surface at the center of a simply supported span. Load (P), energy (E), and velocity (v) were measured from the acceleration history of the impact. For the striker weight w, and acceleration a, these parameters were given by

$$P = ma \tag{5}$$

$$v = g \int a\, dt \tag{6}$$

and

$$E = \int Pv\, dt. \tag{7}$$

To compare test results, such as load and energy, from different specimens, the authors used a normalizing procedure using the maximum elastic bending stress equation:

$$\sigma = (2PLh)/(4I) \tag{8}$$

where σ = maximum bending stress
P = load
L = length of the specimen

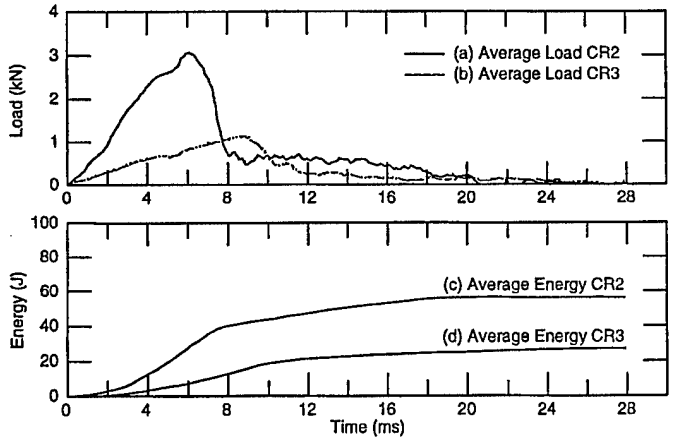

Figure 35. Average load-time history of (a) 6.35-mm- (0.25-in.-) thick CR2 and (b) 9.53-mm- (0.375-in.-) thick CR3 specimens under impact test. Average energy absorbed in (c) 6.35-mm- (0.25-in.-) thick CR2 and (d) 9.53-mm- (0.375-in.-) thick CR3 specimens under impact test.

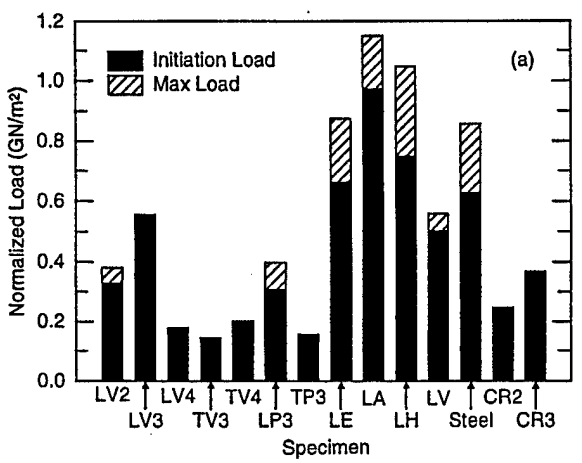

a. Comparison of normalized loads for the W-beam composites with other composites.

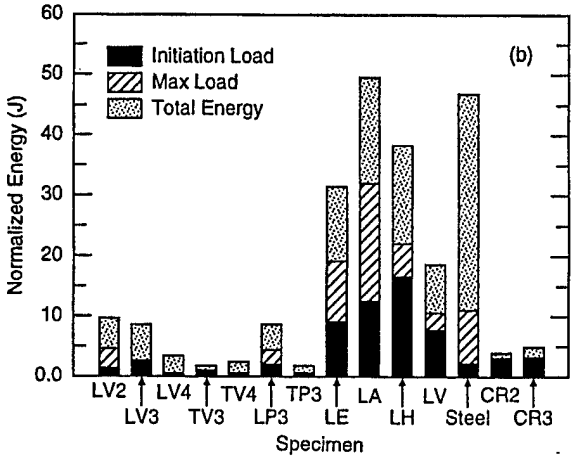

b. Comparison of normalized energy for the W-beam composites with other composites.

Figure 36. Comparison of normalized loads and energy for the W-beam composites with other composites.

h = half thickness
I = moment of inertia of the cross-sectional area.

The geometric portion of this relationship ($Lh/4I$) was used to normalize the load when specimens of different sizes were used in the test, including those obtained from the FRP W-beam. The average load–time history of the five CR2 specimens is shown in Figure 35a; the results for CR3 specimens are shown in Figure 35b. The corresponding energies are shown in Figures 35c and d, respectively. The results produced by Svenson* for comparison with other pultruded composites tested earlier by Svenson et al. (1993) are shown in Figure 36a for a normalized load, and Figure 36b for normalized energy. Figure 36b clearly reveals that the FRP W-beam rail composites fabricated for the current investigation absorbed very little energy compared to many other commercially available pultruded composites, especially when they contain a large amount of longitudinally oriented fibers. It is interesting to note, however, that both CR2 and CR3, which are only 6.35 mm (0.25 in.) and 9.53 mm (0.375 in.) thick, respectively, absorb higher amounts of energy (see cross hatching in Fig. 36b) before the initiation of yielding or fracture than does the steel, indicating that not much energy is absorbed by the composites at the post-yielding or fracture phase. This phenomenon is expected, because steel is much more ductile than FRP, as was evident from the initial test results given in Figures 8a and b for the quasi-static test condition. It is also interesting to note, from the results in Figure 36b, that suitable fiber architecture in pultruded composites can maximize the energy absorption. Unfortunately, under this series of tests no results were available for the 12.7-mm (0.5-in.) thick W-beam FRP materials, which are more relevant for the one-to-one replacement of the steel W-beam.

Discussion

The FRP beams for the above exploratory tests were fabricated in W-beam profiles using the design approaches of composite structures available to commercial vendors of small batch productions. The bidirectional reinforcements of stitched E-glass and S-2 glass mats in 21 layers (12.7-mm- [0.5-in.-] thick profile) were placed in a matrix of isophthalic polyester in a sequence such that in both the longitudinal and transverse directions, the strengths were above 413.4 MPa (60,000 psi), which is slightly more than the strength of the conventional steel W-beam. Under the applied load, the material failed in tension through interlaminar shear failure and fiber fracture before complete separation (Fig. 17). Thus, the stress-strain characteristic (Fig. 18b) shows quite a brittle behavior. This spectacular brittle behavior is primarily because no shear-load-bearing 45° oriented fibers were present. Replace

* A.L. Svenson, L.W. Hargrave, and L.C. Bank, personal communication, 1996.

ment of any 0° or 90° fiber layer with a 45° layer within the given thickness would have reduced the tensile strength from the desirable 413.4 MPa (60,000 psi). The energy absorbed by this material in tensile fracture is due almost entirely to the microfracture process. In flexural loading the FRP W-beam produced much more deflection before failure than the 2.82-mm- (0.111-in.-) thick steel beam. Despite the local catastrophic failure at the crest, the FRP W-beam regained its shape after removal of the load, while the postyield deformation of the steel beam was sustained. Thus, in installations of the FRP W-beam, the replacement could be delayed or deferred for some time without impairing the performance of the guardrail system seriously, but in case of the steel W-beam immediate replacement is necessary for maintaining the safety of the system.

Laboratory tests in both slow, flexural loading on the corrugated surface of the FRP W-beam and drop testing of weight on the plane surface of the FRP beams show a dramatic difference in the energy absorption characteristics between the steel and the FRP composites. Upon impact, the W-beam made of ductile metals deforms plastically, involving crystalline slip or molecular sliding, which are thermally activated processes. In contrast, in FRP composites made from fibers and resins that are brittle, the energy is absorbed by a large number of different microcracking processes, which are controlled by the properties of the fibers and resins and the geometrical arrangement of the fibers. In fact, the specific absorption energies are probably significantly larger in many fiber-reinforced polymer composites than those observed in ductile metals or plastics.

The key to developing a large amount of energy absorption is to design the composite W-beam with constituents arranged in such a manner that progressive crushing occurs. The crush would be expected to move at approximately a constant load equal to the residual load and also at the same velocity dictated by the deceleration rate of the errant vehicle. The aim is to achieve extensive microfracturing of the matrix and partial failure of the fibers by breakage and pull-out, so that sufficient residual load is sustained to guide the errant vehicle to its previous course.

CHAPTER 4: RECYCLED PLASTIC COMPOSITE GUARDRAIL POSTS

Commercial production of synthetic lumber from recycled plastics has been reported both in the U.S. and abroad. Many of these recycled plastics are mixed with other ingredients, forming composites, and are being marketed as structural materials. The thrust of the research presented here is a study of the mechanical characteristics of one such recycled plastic composite (RPC), which appears to have the potential for application as the guardrail posts and blockouts.

Guardrail system designs rely primarily on the soil bearing capacity to yield to impact, but the posts provide enough restraining force to redirect errant vehicles. Typical wooden posts made from Douglas fir, hemlock, etc., have a rupture strength (equivalent to the stress at which the fibers will fail in tension under bending load) that varies from 41.34 MPa to 82.68 MPa (6000 to 12,000 psi) and a modulus of elasticity of from 8.96 GPa to 13.78 GPa (1.3×10^6 to 2×10^6 psi). To develop enough restraining force to redirect errant vehicles, the impact response characteristics of an RPC post system would need to be in the same range as those of a wooden post.

There are two attractive features that favor consideration of recycled plastic composites (RPC) for highway structures. Both these features relate to the overall improvement of the quality of our environment. First, as landfill space becomes increasingly scarce, the satisfactory disposal of solid waste is becoming a critical issue. By the turn of the century, an estimated 37 billion kg (80 billion lb) of thermoplastic waste will be discarded into the solid waste stream (Miller and Johnson 1989), and because plastic wastes occupy more volume than other solid wastes, it is estimated that thermoplastic solid waste will occupy about 80% of the available space. As a result, the recycling of plastics is gaining momentum and the uses of re-formed plastics are proliferating. A potentially large volume application of recycled plastics in guardrail applications will help the national plastic waste recycling effort. Second, existing creosote treated wooden guardrail posts are not favored by many environmentalists, because of the potential danger of groundwater contamination by leached creosote. Such dangers will be minimized if the substitution of wooden posts and blockouts by RPC becomes possible. In addition, the availability of lumber throughout the world is greatly diminishing as a result of a significant international effort to preserve the rain forests. An alternative material like RPC for guardrails will reduce the demand on the pressure-treated lumber supply.

Initial survey and material identification

When this study was initiated, a survey of the U.S. marketplace showed that recycled, mixed plastics were being used for noncritical load-bearing applications such as park benches, picnic tables, fences, curbs, parking blocks, etc. However, it was noticed that a large percentage of this "plastic lumber" contained cavities (Fig. 37) in the central region of the cross section. The

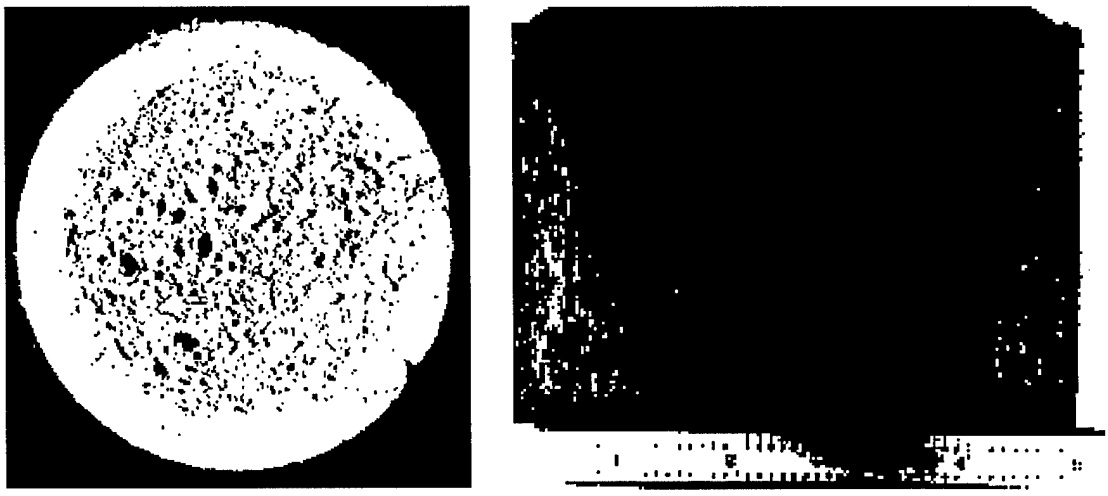

a. Manufacturer A. *b. Manufacturer B.*

Figure 37. Commercial plastic lumber containing cavities in the core area of the section.

presence of such cavities was considered undesirable for a systematic study, because it was suspected that their presence would result in extreme variation in mechanical properties across the specimen and between samples, and any water penetrating into those cavities could degrade the material subsequent to freezing at subzero temperatures. Subsequently, an RPC material that resembled wood in texture and was void-free in appearance was selected for the detailed study. The material was supplied by a manufacturer that was also working with the U.S. Navy on a pilot program for converting shipboard plastics into RPC (Middleton et al. 1991). Middleton et al. described that the manufacturer's innovative processing technology of blending 50% sawdust to plastic waste produced a material free of the air cavities and voids often found in other recycled plastic lumber. They noted that unlike most other manufacturing processes that produced recycled plastic lumber in batches, this technology allowed continuous extrusion. Another important advantage of this material was that it could be recycled by reprocessing through the plant.

The technical information bulletin on the product (Rivenite 1990) provided with the first batch of samples claimed the following attributes. The product is manufactured through a proprietary patented process of grinding, blending, heat and final extrusion. Available in a variety of profiles and sizes, the material could be sawed and generally machined. It could be nailed, screwed, painted, and stained, like wood. It resists ultraviolet damage normally experienced with similar products. It absorbs limited moisture, which does not alter its performance. It resists insect infestation and does not decay in salt or acidic water. It is nontoxic but flammable, in the same manner as pressure-treated lumber. Its applications as a structural support, framing member, or column where structural loads are to be carried were not recommended.

Initial tests

The purpose of the initial tests was to understand the basic response and failure mechanism of the material in simple compression.

The first batch of materials for the initial test was supplied by the manufacturer in two groups: the first group included six specimens of nominal 88.9 × 88.9-mm- (3.5 × 3.5-in.-) square cross section and 152.4-mm- (6-in.-) length. These specimens were designated PW1 through PW6. The second group consisted of only three cylindrical specimens of nominal 91.44-mm (3.6-in.) diam. and 152.4-mm (6-in.) length. These were designated as PWR1 through PWR3. The specimens were tested at room temperature by applying compression load in a screw driven machine at approximately 2.54 mm (0.1 in.) per minute cross-head displacement rate. Because of the expected large deformation, no attempt was made to strain gauge the specimens. Instead, displacements corresponding to the applied load were recorded manually by dial gauge. The loads at each instance were read from the load-display dial of the testing machine (Riely). Table 6 gives the results of the test from both batches.

The data in Table 6 show that although the variation of failure load between specimens was not significant, the strain to failure gave highly variable results. These results are shown graphically in Figure 38a for the square specimens and Figure 38b for the cylindrical specimens.

The reasons for the highly variable failure strains were investigated and the problem was traced to the inclusion of relatively large pieces of wood chips in the material matrix (see Fig. 39)

Table 6. Compression test data of the initial batch of RPC samples at room temperature.

a. Specimens of square cross section

Specimen no.	*Length (in.)*	*Width (in.)*	*Failure load (lbf)*	*Deformation (in.)*	*Compr. strength (psi)*	*Failure strain (%)*
PW1	5.91	3.688	24,500	0.7838	1801	13.27
PW2	5.88	3.688	23,600	0.4968	1735	8.45
PW3	5.94	3.688	24,050	0.6949	1768	11.70
PW4	5.94	3.688	24,200	0.5739	1779	9.67
PW5	5.88	3.688	24,400	0.6033	1794	10.27
PW6	5.88	3.688	24,275	0.8180	1785	13.92
Average					1777	11.21
Std. dev.					21.5	1.95

b. Specimens of circular cross section

PWR1	5.97	3.594	21,400	0.8852	2109	14.83
PWR2	5.97	3.594	21,500	1.5180	2119	25.43
PWR3	5.91	3.563	21,500	0.8414	2156	14.25
Average					2129	18.17
Std. dev.					20.33	5.14

SI conversion factors: 1 in. = 25.4 mm, 1 lbf = 4.45 N, 1 psi = 6.89 kPa.

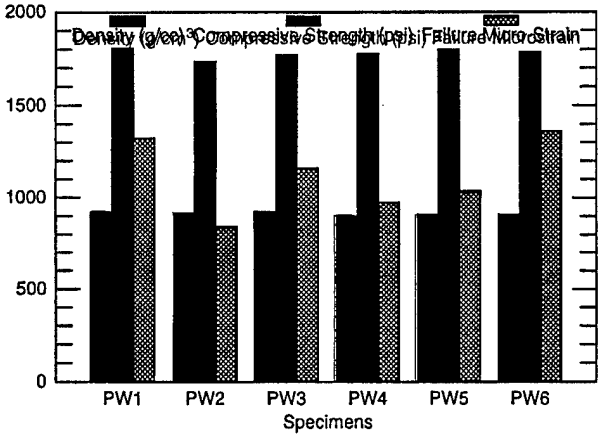

a. Square bars.

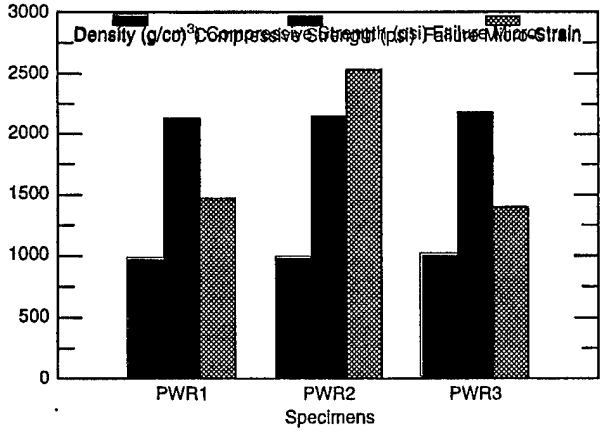

b. Round bars.

Figure 38. Compression test results of the initial RPC specimens.

in some specimens. These longitudinal wood chips were oriented primarily in the direction of loading. Besides causing local stress concentration and the nucleation of cracks, these chips influenced the deformation characteristics significantly. To obtain consistent data in the tests, it was essential that the test material be homogeneous. Thus, the manufacturer was urged to improve the consistency and granularity of the material. As a result, the manufacturer developed technology to process the sawdust to a finer mesh size [less than 1.3 mm (0.05 in.)] and virtually eliminated contamination with any large wood pieces. This made the size distribution of the sawdust more consistent with that of the ground plastics. The resultant material proved to have cross sections with more uniform grain distribution (Fig. 40), although inclusions of small specks (about 1 mm) of unmelted high-density polyethylene (HDPE) (Fig. 41) were occasionally evident in the micrographs of the matrix.

Figure 39. Some initial RPC specimens tested for compression (note the inclusion of wood chip in the second specimen).

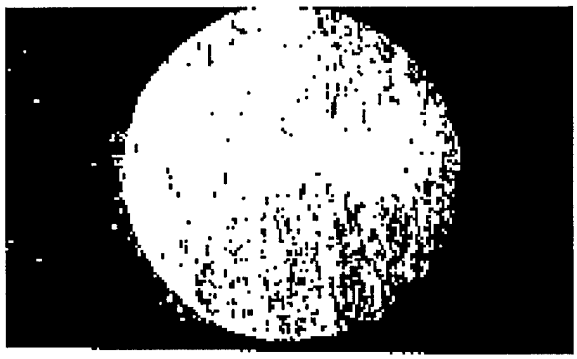

Figure 40. Section of the improved RPC specimens free of any wood chip inclusions.

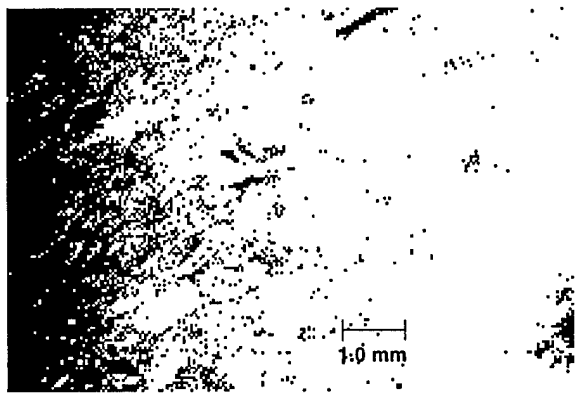

Figure 41. Micrograph of the inclusion of unmelted HDPE in the improved RPC material.

It was apparent that to use this RPC for guardrail posts and blockouts, finished beams of this material in larger cross section, 152 × 203 mm (6 × 8 in.), were required. At our request the manufacturer produced these larger sized beams, from which specimens were prepared for testing.

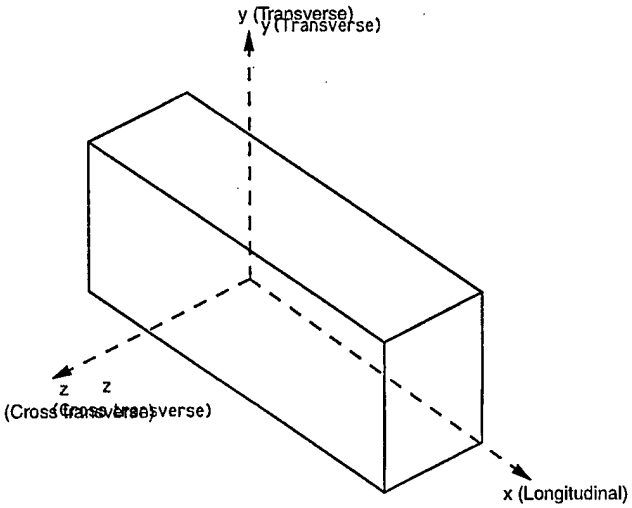

Figure 42. Axial orientations of the RPC test specimens.

two temperatures, 21°C (70°F) (room temperature) and –30°C (–22°F) (low temperature). The results shown in Table 7a show that the moisture percentage tends to increase with the smaller sized specimens. All compression tests were performed using a servohydraulic universal testing machine with an electrical data acquisition system. For low-temperature testing, the specimens were kept cooled in a coldroom for at least 24 hours before being transferred to the test chamber built on the universal testing machine, which was kept cooled by a special refrigeration system built for the purpose. Typical testing of a longitudinal beam in the test chamber is shown in Figure 43. The results from all tests are summarized in Table 7b for the room-temperature

Compression testing

Since the production process of the RPC involved a pultrusion-type manufacturing technique in which the raw materials are heated and compressed in the reaction chamber and the curing material is extruded out, it was suspected that there would be some directional variability of the properties in the material. Therefore, compression tests were performed in three axial directions, *x*, *y*, and z, as shown in the schematic in Figure 42. Direction *x* coincides with the longitudinal direction, which is the pulling direction of the beam out of the molding die; *y* is the major transverse direction of the rectangular section; and z is the minor direction. Specimens with *x* direction had a designated letter L, in *y* direction T, and z direction TT. The dry groups were designated with the letter D and the wet group with letter W as shown in Table 7a. For compression testing in the *x*-direction, the sides of the sample were not machined; rather they were left with the rounding corners of the general 152- × 203-mm (6-× 8-in.) cross section, as they were received. The nominal dimensions of the specimens and their moisture contents before tests are given in Table 7a.

The properties were determined for both wet and dry conditions at

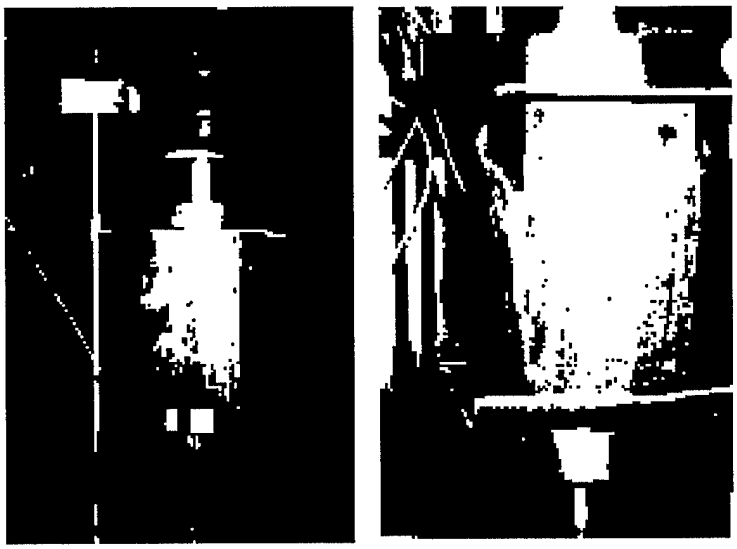

a. Before failure. *b. After failure.*

Figure 43. Axial compression testing of the full-sized (152 × 203 mm, 6 × 8 in.) guardrail post beam.

Table 7. Compression testing of RPC specimens.

a. Specimen sizes and moisture ingression data.

Specimen group (grain orient.)		*Nominal size (in.)*	*Avg. dry density (lb/in.^{3})*	*Immersion time (hr)*	*Avg. wet density (lb/in.^{3})*	*Moisture absorbed (%)*
DL	(*x*)	6 × 8 × 12	0.0315	0.00		
WL	(*x*)	6 × 8 × 12	0.0317	139.00	0.0318	2.203
WCL	(*x*)	6 × 8 × 12	0.0312	47.50	0.0314	0.641
DT	(*y*)	4.5 × 5.5 × 6.5	0.0326	0.00		
WT	(*y*)	4.5 × 5.5 × 6.5	0.0324	41.00	0.0330	2.240
WCT	(*y*)	4.5 × 5.5 × 6.5	0.0322	47.50	0.0328	1.862
DTT	(z)	3 × 3.5 × 4.5	0.0321	0.00		
WTT	(z)	3 × 3.5 × 4.5	0.0327	41.00	0.0330	2.690
WCTT	(z)	3 × 3.5 × 4.5	0.0321	47.50	0.0331	3.115

Table 7 (cont'd). Compression testing of RPC specimens.

b. Results of the RPC at room temperature (21°C, 70°F).

Specimen	Peak stress (psi)	Strain at peak stress	Secant modulus (psi)
1DL	1461.46	0.1146	12,749
2DL	1400.69	0.0521	26,861
3DL	1283.53	0.0628	20,423
4DL	1375.01	0.10824	12,703
5DL	1378.44	0.1139	12,102
6DL	1459.84	0.0502	29,067
7DL	1402.15	0.0708	19,810
Average	1394.45	0.0818	19,102
Std. dev.	60.28	0.0294	6,977
1WL	1571.48	0.0609	25,625
2WL	1686.93	0.0722	23,378
3WL	1295.29	0.0609	22,288
4WL	1597.52	0.0691	23,115
5WL	1738.62	0.0805	21,608
6WL	1281.59	0.0665	19,258
7WL	1696.23	0.0793	21,825
Average	1552.52	0.0699	22,471
Std. dev.	189.43	0.0080	2,000
1DT	1895.62	0.0642	29,516
2DT	1593.26	0.0630	25,286
3DT	1720.40	0.0545	31,528
4DT	1893.09	0.0648	29,219
5DT	1696.46	0.0543	31,250
6DT	1711.33	0.0525	32,619
7DT	1862.01	0.0605	30,782
Average	1767.415	0.0591	30,028
Std. dev.	116.83	0.0052	2,395
1WT	1922.94	0.0621	30,991
2WT	2006.44	0.0680	29,514
3WT	1739.41	0.0527	32,980
4WT	1715.00	0.0497	34,541
5WT	1657.62	0.0525	31,582
6WT	1985.66	0.0617	32,167
7WT	1977.83	0.0654	30,238
Average	1857.84	0.0589	31,716
Std. dev.	148.08	0.0072	1,701
1DTT	1754.84	0.0656	26,770
2DTT	1755.14	0.0746	23,625
3DTT	1830.36	0.0749	24,448
4DTT	1778.56	0.0663	26,846
5DTT	1710.68	0.0655	26,128
6DTT	1768.88	0.0741	23,872
7DTT	1818.33	0.0702	25,913
Average	1773.83	0.0701	25,372
Std. dev.	40.66	0.0043	1,363
1WTT	2031.60	0.0713	28,489
2WTT	2033.18	0.0787	25,824
3WTT	2058.90	0.0772	26,674
4WTT	2074.38	0.0822	25,241
5WTT	1986.51	0.0829	23,954
6WTT	2074.70	0.0812	25,587
7WTT	2087.09	0.0885	23,583
Average	2049.48	0.0800	25,622
Std. dev.	34.91	0.0050	1,656

c. Results of the RPC at low temperature (–30°C, –22°F).

Specimen	Peak stress (psi)	Strain at peak stress	Secant modulus (psi)
1CDL	3251.79	0.0439	74,140
2CDL	2882.96	0.0494	58,190
3CDL	2318.33	0.0301	76,918
4CDL	2220.51	0.0384	57,869
5CDL	3160.98	0.0471	67,126
6CDL	2490.11	0.0450	55,373
7CDL	2704.26	0.0409	64,176
Average	2717.99	0.04213	64,828
Std. dev.	401.62	0.0065	8,371
1WCL	2516.75	0.0394	63,953
2WCL	2435.011	0.0302	80,505
3WCL	2366.31	0.0288	82,157
4WCL	2310.07	0.0310	74,619
5WCL	2570.08	0.0285	90,076
6WCL	2547.10	0.0374	68,180
7WCL	2322.88	0.0264	87,941
Average	2438.31	0.0317	78,204
Std. dev.	108.26	0.0048	9,773
1CDT	2923.24	0.0445	65,658
2CDT	3107.87	0.0452	68,757
3CDT	3383.21	0.0404	83,771
4CDT	3062.94	0.0460	66,514
5CDT	3018.12	0.0463	65,239
6CDT	3577.07	0.0500	71,610
7CDT	3556.67	0.0470	75,697
Average	3232.73	0.0456	71,035
Std. dev.	268.457	0.0029	6,738
1WCT	3110.41	0.0446	69,696
2WCT	3183.20	0.0470	67,671
3WCT	3135.11	0.0421	74,421
4WCT	3652.15	0.0540	67,607
5WCT	3436.36	0.0478	71,835
6WCT	3213.35	0.0545	58,929
7WCT	3691.78	0.0491	75,208
Average	3346.05	0.0485	69,338
Std. dev.	246.82	0.0046	5,489
1CDTT	3738.73	0.0607	61,585
2CDTT	3695.97	0.0562	65,758
3CDTT	3649.45	0.0563	64,796
4CDTT	3715.04	0.0548	67,771
5CDTT	3838.96	0.0603	63,656
6CDTT	3879.02	0.0636	60,953
7CDTT	3712.03	0.0585	63,457
Average	3747.03	0.0586	63,997
Std. dev.	81.98	0.0031	2,362
1WCTT	3756.46	0.0695	54,057
2WCTT	3651.71	0.0646	56,560
3WCTT	3695.94	0.0574	64,422
4WCTT	3529.05	0.0577	61,110
5WCTT	3547.06	0.0626	56,673
6WCTT	3598.44	0.0570	63,161
7WCTT	3745.53	0.0582	64,377
Average	3646.31	0.0610	60,051
Std. dev.	91.62	0.0048	4,245

SI conversion factors: 1 in. = 25.4 mm, 1 lb = 0.454 kg, 1 psi = 6.89 kPa.
Legend: D = dry W = wet L = longitudinal (x direction) T = transverse (y direction) TT = transverse (z direction)

specimens, and Table 7c for the low-temperature specimens.

Figures 44a through f give the typical stress-strain curves from the room-temperature tests, and Figures 45a–f give the results from the low-temperature (–30°C, –22°F) tests. Figure 46 is the graphical representation of the compressive strength data for the three axes, and Figure 47 presents the same for the secant moduli. It is evident that there were significant differences in the

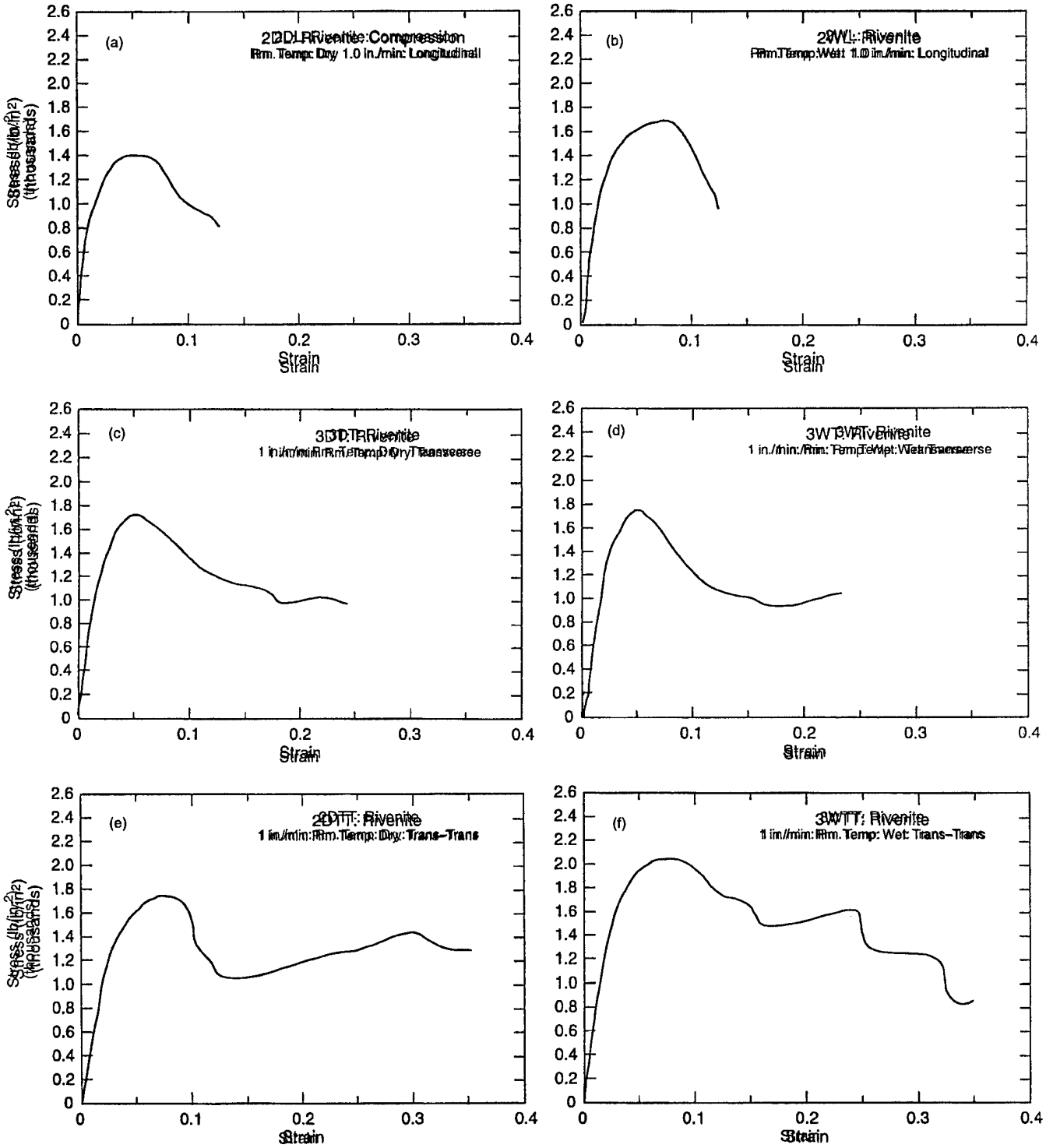

Figure 44. Stress-strain data of the RPC at room temperature.

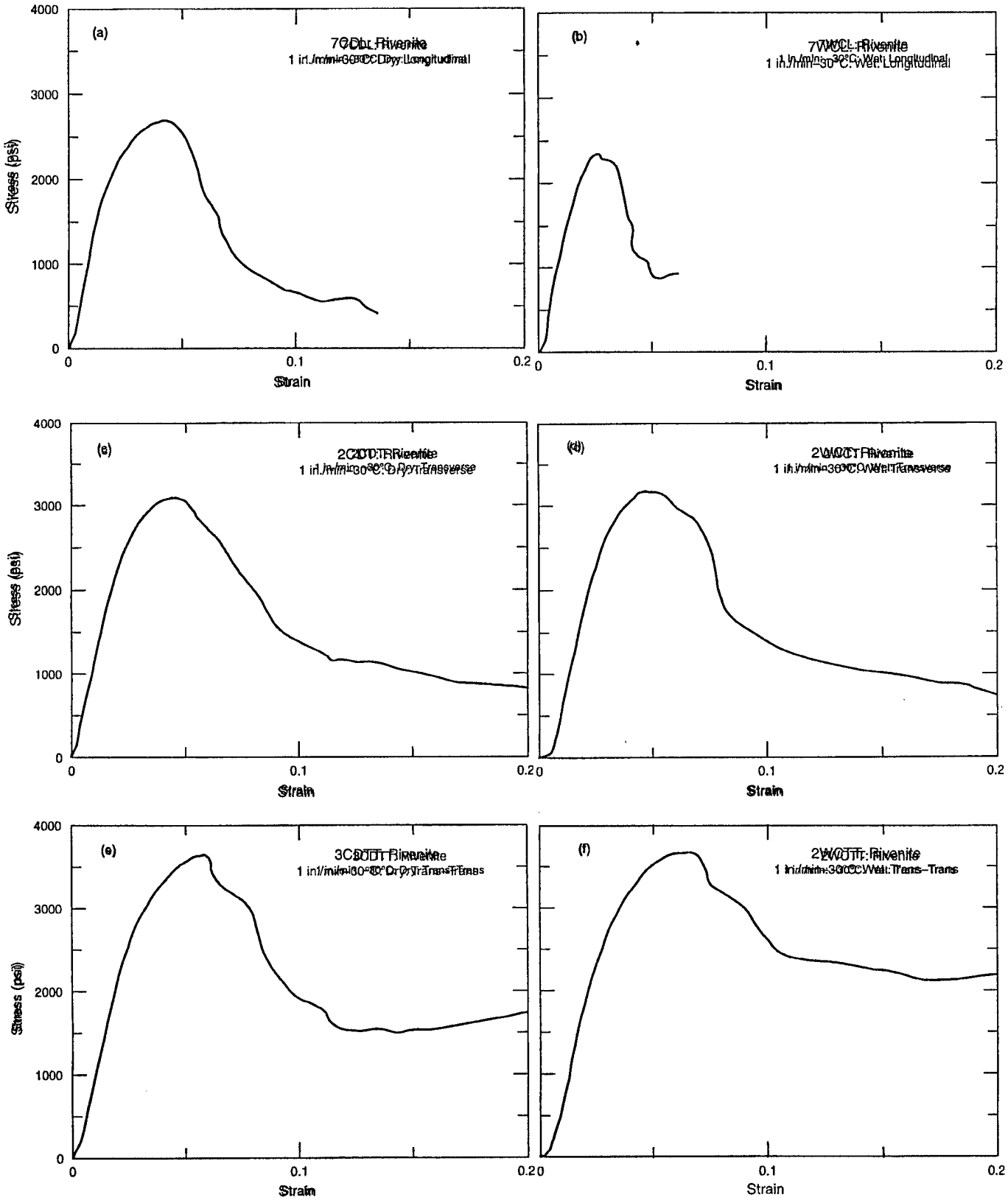

Figure 45. Stress-strain data of the RPC at low temperature (–30 ℃, –22 ℉).

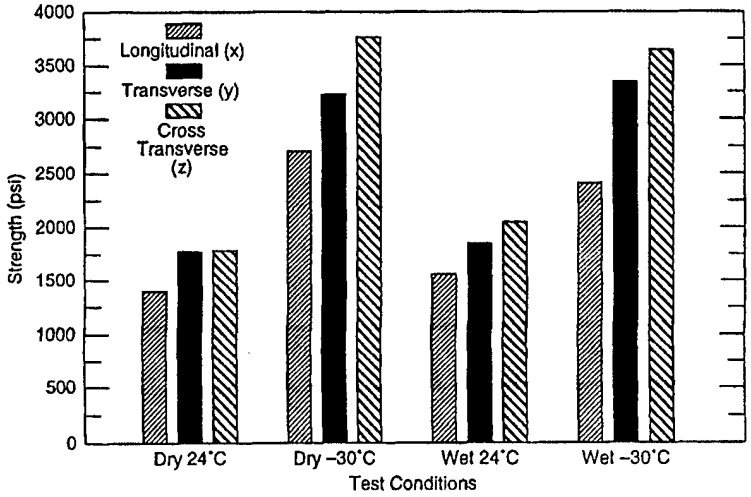

Figure 46. Compressive strength of the RPC in three axes and four conditions: dry, wet, dry and cold (–30°C, –22°F), and wet and cold (–30°C, –22°F).

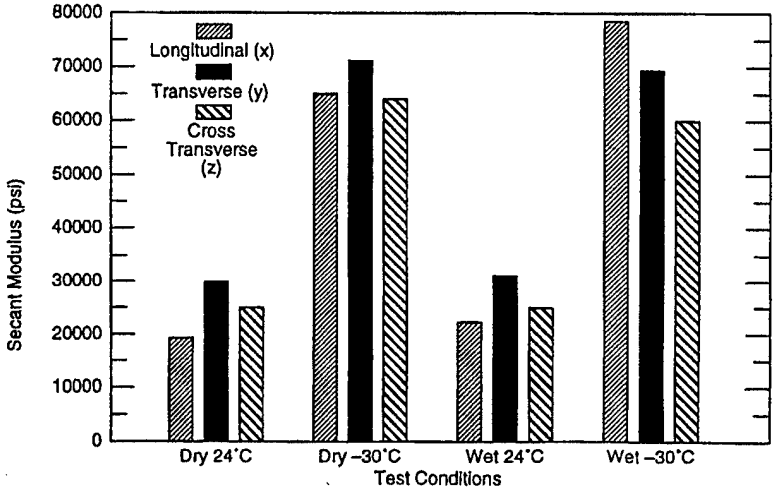

Figure 47. Secant moduli of the RPC in three axes and four conditions: dry, wet, dry and cold (–30°C, –22°F), and wet and cold (–30°C, –22°F).

material properties between the longitudinal and the two transverse directions. However, the differences in the properties between the two transverse directions were much smaller than those in the longitudinal direction.

The tests also showed that the material properties are highly temperature sensitive. Temperature has a significant effect on the compressive strength of the material, regardless of the orientation and moisture content. Low temperature caused a dramatic increase in the secant modulus. Moisture and orientation effects were secondary.

Tension testing

Since the RPCs under study were new materials, no standard test procedures were available for any of the mechanical tests undertaken. For tension tests, it is necessary to establish that the test specimen fails in the uniformly tensioned area, and that the effects of gripping and other stress concentration factors are absolutely minimized. Following a considerable amount of investigation, an optimum configuration for the test specimens was determined, as shown in Figure 48a. Figure 48b shows the specimens. A special gripping fix

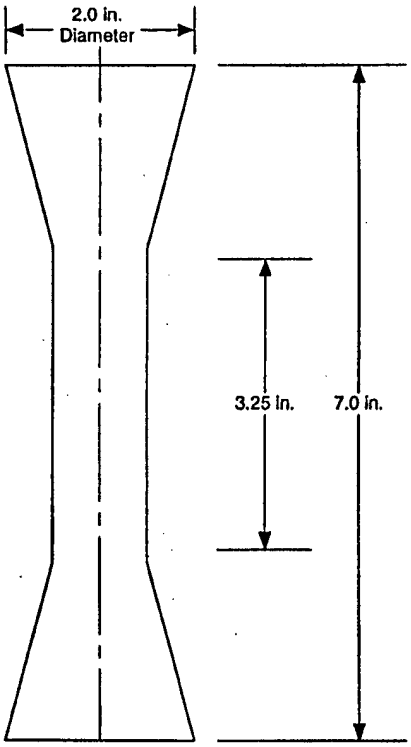

a. Tensile test specimen dimensions for the RPC material.

b. Some RPC tensile test specimens machined from the 152- × 203-mm (6- × 8-in.) beams.

Figure 48. Tensile test specimens for the RPC material.

ture for testing these specimens was also designed, as shown in Figure 49. Figure 49a shows the fixture cover plate removed, and Figure 49b shows the cover plate closed. Again, the tension tests were conducted in the servohydraulic machine with a cross-head displacement rate of 2.54 mm (0.1 in.) per min. An electrical data acquisition system was used to record the test data. From the 152 × 203-mm (6 × 8-in.) beams supplied by the manufacturer, six specimens, W1 through W6, were machined from the longitudinal direction (x), and six specimens, A1 through A6, were machined from the major transverse (y) direction. Figures 50a and b show the typical stress-strain curves for the tensile loading in the x and y directions. The properties were determined only in the longitudinal (x) and the major transverse (y) directions at room temperature The results of the tension tests are summarized in Table 8.

These results are graphically presented in Figure 51. Figure 51a gives the tensile strength data, and Figure 51b give the elastic modulus for the x direction specimens. Figures 51c and d give the

Table 8. Tensile test data of RPC.

Specimen	*Peak load (lbf)*	*Area (in.²)*	*Strength (psi)*	*Modulus (psi)*
x direction specimens				
W1	372.0	0.7933	468.93	23,628
W2	290.5	0.7838	370.63	19,383
W3	N/A	0.8028	N/A	14,290
W4	332.5	0.7948	418.34	28,432
W5	400.0	0.7933	504.22	31,570
W6	240.0	0.7933	302.53	19,637
Average			412.92	22,823.33
Std. dev.			79.81	6,378.33
y direction specimens				
A1	512	0.8075	634.06	27,820
A2	487.5	0.7917	615.76	23,046
A3	332	0.7964	416.88	29,116
A4	321.5	0.7948	404.50	25,502
A5	334	0.7933	421.03	26,307
A6	413.5	0.8028	515.07	35,130
Average			501.22	27,820.17
Std. dev.			103.78	4,136.88

SI conversion factors: 1 lbf = 4.45 N, 1 in.^{2} = 645 mm^2, 1 psi = 6.89 kPa.

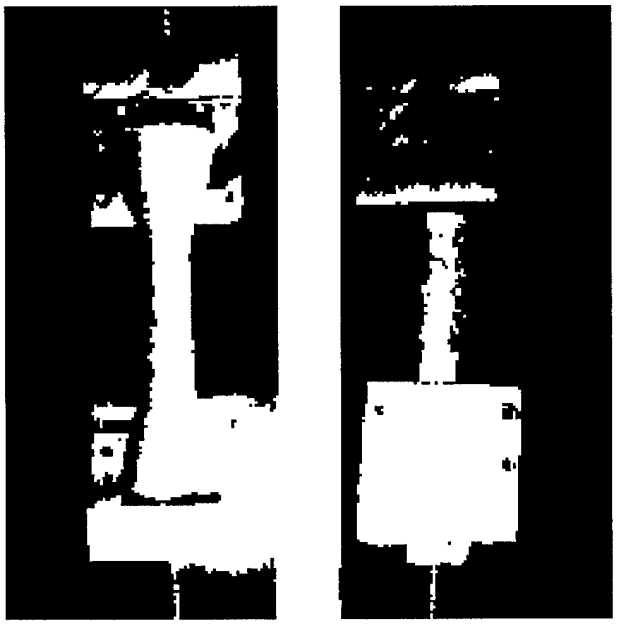

a. Open. *b. Closed.*

Figure 49. RPC tensile test specimen mounted in the special test fixture. Note the crack in the specimen in the gage section following a test.

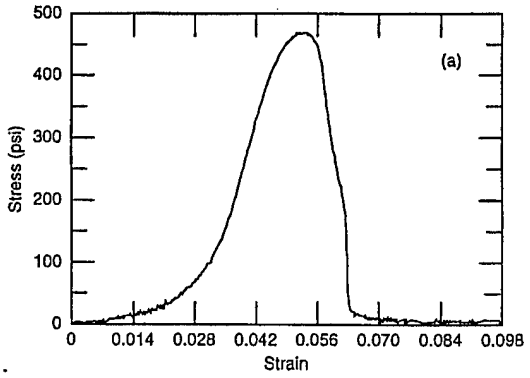

a. x directional specimens.

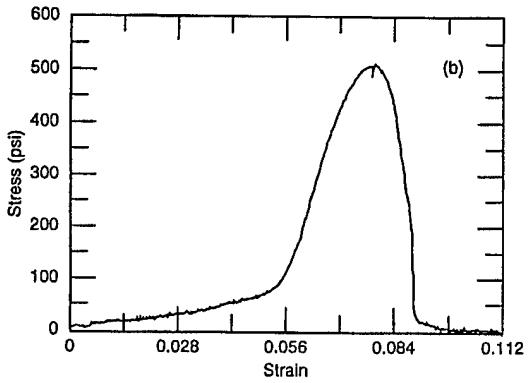

b. y directional specimens.

Figure 50. Stress–strain records of the tensile specimens.

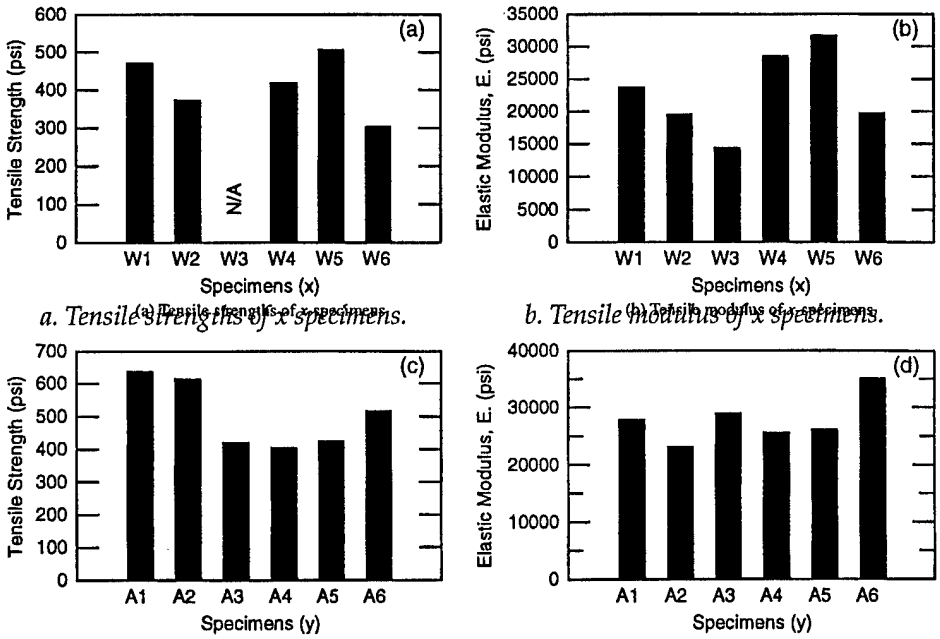

a. Tensile strengths of x specimens. *b. Tensile modulus of x specimens.*

c. Tensile strengths of y specimens. *d.Tensile modulus of y specimens.*

Figure 51. Results of tensile tests of the RPC.

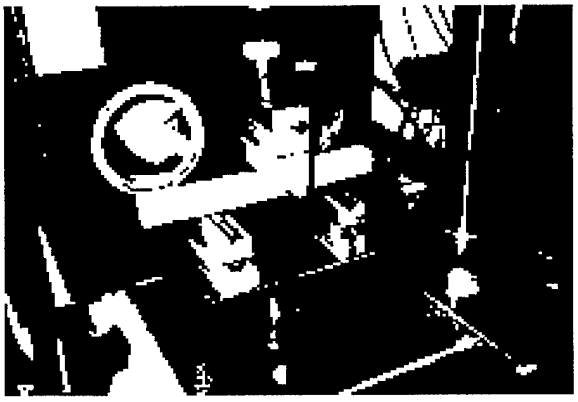

Figure 52. Flexural testing of the RPC.

same for the y direction specimens, respectively. The material clearly shows a significant amount of variability in properties between the specimens. However, the y direction specimens are stronger and stiffer overall than the x direction specimens. It is possible that transverse pressure and compacting of the materials at the time of forming in the die impart a higher strength to the material.

Flexural testing

As in compression, flexural testing of the RPC was performed at room temperature and low (–30°C) temperature for both dry and wet conditions, using the servohydraulic machine and a three-point bending fixture (Fig. 52). The data were recorded by the electrical data acquisition system. The flexural strength (S) and the flexural modulus (E_f) were calculated using the following equations for three-point bending of thin elastic solids:

$$S = (3PL)/(2bd^2)$$

where P = load on the beam
b = width of the beam
d = depth of the beam
L = span between the support points
δ = deflection of the beam.

All specimens were cut to the nominal size of 38.1 × 38.1 × 406.4 mm (1.5 × 1.5 × 16 in.). The span (L) for all tests was 203.2 mm (8 in.). Results from these tests are given in Table 9.

For the purpose of comparison, wood specimens of Douglas fir of the same dimensions (38.1 × 38.1 × 406.4 mm, 1.5 × 1.5 × 16 in.) were prepared and tested in flexure, both at room temperature (21°C, 70°F) and at low temperature (–30°C, –22°F) under wet and dry conditions. Results of the Douglas fir flexural tests are summarized in Table 10.

The moisture percentages of the wet specimens of both the RPC and the Douglas fir were determined immediately before the flexure tests by the weight gain (difference between wet density and dry density) of each specimen after water immersion. The moisture gain varied with time. A summary of the results is presented in Table 11. The data in Table 11 show that for a given size of specimen, moisture ingression was greater in the Douglas fir than in the RPC.

The influence of temperature and moisture ingression on the flexural behavior of the RPC is represented in Figure 53. Figure 53a shows the flexural strength (S) and Figure 53b the flexural modulus (E_f). They show that low temperature influenced the flexural behavior of the RPC significantly—in fact, much more significantly than moisture. The average values from all tests are summarized in Table 12. The flexural strength for the dry RPC specimens (specimens DCD) increased approximately 63% at –30°C (–22°F), and the flexural modulus by approximately

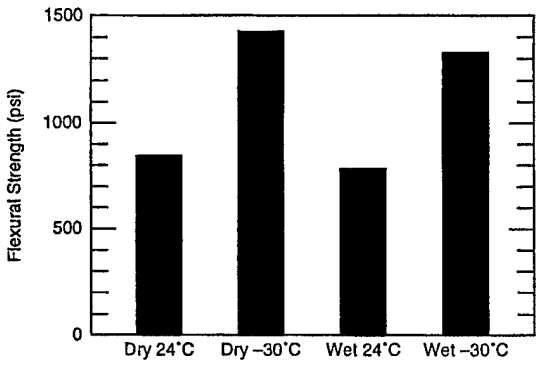

a. Flexural strength.

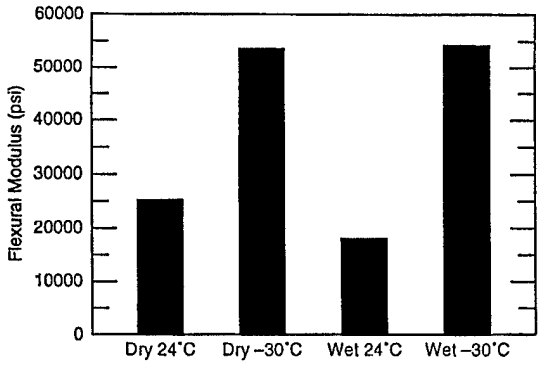

b. Flexural modulus.

Figure 53. Results of flexural testing of the RPC.

Table 9. Three-point flexural test results of the RPC.

Sample	Peak force (lb)	Deflection (in.)	Flexural strength (psi)	Flexural modulus (psi)
1DD	129.8	0.185	458.667	17,638.430
2DD	251.1	0.307	892.800	20,680.130
3DD	304.2	0.199	1081.608	38,747.495
4DD	255.7	0.258	989.156	25,107.208
5DD	237.4	0.233	844.089	25,816.817
6DD	251.3	0.222	893.511	28,685.584
7DD	236.9	0.304	842.311	19,735.644
8DD	236.7	0.178	912.711	26,267.096
9DD	297.3	0.268	1057.067	27,999.231
10DD	223.2	0.209	793.608	27,156.104
11DD	301.2	0.283	1070.933	26,889.201
12DD	179.5	0.225	638.222	20,170.974
13DD	250.2	0.208	889.608	30,390.846
14DD	261.1	0.248	928.356	26,663.191
Average	245.3	0.237	872.330	26,574.282
Std. dev.	45.0	0.048	160.017	5,799.107
1WD	145.1	0.192	515.911	19,107.819
2WD	263.8	—	—	—
3WD	277.6	0.342	987.022	20,552.927
4WD	239.0	0.286	849.778	21,165.899
5WD	335.6	0.465	1193.244	18,267.586
6WD	347.0	0.346	1233.778	25,393.722
7WD	197.5	0.245	702.222	20,381.960
Average	257.9	0.268	783.137	17,838.559
Std. dev.	66.7	0.135	397.948	7,578.142
1DCD	333.500	0.148	1165.778	56,974.308
2DCD	395.000	0.195	1404.444	51,216.208
3DCD	341.700	0.156	1214.933	55,381.576
4DCD	475.800	0.195	1691.733	61,851.433
5DCD	376.700	0.198	1339.376	48,225.135
6DCD	431.800	0.221	1535.289	49,512.970
7DCD	450.000	0.225	1600.000	50,567.901
Average	400.643	0.191	1424.508	53,389.933
Std. Dev.	50.204	0.027	178.503	4,516.735
1WCD	349.800	0.139	1243.733	63,628.244
2WCD	378.200	0.181	1344.711	52,977.231
3WCD	371.000	0.176	1319.111	53,449.263
4WCD	325.400	0.154	1156.978	53,598.601
5WCD	351.600	0.207	1250.133	42,946.073
6WCD	566.600	0.208	2014.578	68,874.454
7WCD	261.600	0.152	930.133	43,515.010
Average	372.029	0.174	1322.768	54,141.279
Std. Dev.	87.159	.025	309.00	8,843.460

SI conversion factors: 1 lbf = 4.45 N, 1 in. = 25.4 mm, 1 psi = 6.89 kPa.

Table 10. Three-point flexural test data of Douglas fir specimens.

Sample	Peak force (lb)	Deflection (in.)	Flexural strength (psi)	Flexural modulus (psi)
1DD	1750.0	0.444	6222.222	99,599.130
2DD	1715.0	0.462	6097.778	93,907.905
3DD	1800.0	0.483	6400.000	94,201.524
4DD	1610.0	0.525	5724.444	77,574.389
5DD	1585.0	0.527	5635.556	76,025.728
6DD	1935.0	0.377	6880.000	129,708.552
7DD	1530.0	0.382	5440.000	101,384.293
Average	1703.6	0.457	6057.143	96,057.360
Std. dev.	129.9	0.057	461.803	16,579.996
1WD	1325.0	0.518	4711.111	64,627.412
2WD	1405.0	0.616	4995.556	57,657.051
3WD	1170.0	0.407	4160.000	72,605.546
4WD	1575.0	0.605	5600.000	65,849.065
5WD	1540.0	0.626	5475.556	62,200.134
6WD	1420.0	0.520	5048.889	69,094.462
7WD	1380.0	0.434	4906.667	80,338.125
Average	1402.1	0.532	4985.397	67,481.685
Std. dev.	125.1	0.082	444.785	6,859.546
1DCD	1795	0.500	6382.222	90,769.383
2DCD	2245	0.461	7982.222	123,129.000
3DCD	2415	0.482	8586.667	126,616.362
4DCD	2185	0.512	7768.889	107,822.263
5DCD	2185	0.544	7768.889	101,589.118
6DCD	1900	0.384	6755.556	125,102.881
7DCD	2025	0.414	7200.000	123,596.862
Average	2107	0.471	7492.063	114,089.410
Std. Dev.	197	0.052	702.157	13,036.679
1WCD	1760	0.442	6257.778	100,592.830
2WCD	2010	0.478	7146.667	106,375.177
3WCD	1188	0.594	8568.889	102,604.624
4WCD	2230	0.645	7928.889	87373.497
5WCD	2150	0.513	7644.444	106,017.540
6WCD	1995	0.645	7093.333	78,249.341
7WCD	1750	0.546	6222.222	81,038.303
Average	2091	0.570	7266.032	94,607.330
Std. Dev.	207	0.063	795.541	11,164.284

SI conversion factors: 1 lbf = 4.45 N, 1 in. = 25.4 mm, 1 psi = 6.89 kPa.

100.1%. Because of this dramatic increase of E_f, deflections for cold RPC specimens decreased by approximately 20–35%, as seen in Table 9. When wet (specimens WD), both S and E_f decreased; S by approximately 10%, and E_f by 33%. However, (see WCD data) at low temperature (–30°C, –22°F), both S and E_f increased, by 51.6% and 103.7%, respectively, with much less moisture content (3.1%), as opposed to 15.6% moisture content for the WDs.

The Douglas fir wood showed a pattern of behavior with cold and moisture similar to the RPC, although the failure mechanism seems to be different (Fig. 54). The failure of the Douglas fir appeared to occur with the cracks propagating primarily in the grain or longitudinal

Table 11. Moisture content of the wet flexural specimens of RPC and Douglas fir (DF).

(Nominal dimensions of all specimens: 38.1 × 38.1 × 406.4 mm, 1.5 × 1.5 × 16 in.)

Specimen type	*No. of specimens*	*No. of hours in water*	*Average dry density (lb/in.^{3})*	*Average wet density (lb/in.^{3})*	*Moisture absorbed (%)*	*Avg. moisture absorption/hr*
RPC-WD	7	383	0.032	0.037	15.6	0.0407
RPC-WCD	7	48	0.032	0.033	3.1	0.0646
DF-WD	7	265	0.018	0.022	22.2	0.0838
DF-WCD	7	219	0.018	0.0198	8.2	0.0374

SI conversion factors: 1 lb = 0.454 kg, 1 in. = 25.4 mm.

Figure 54. Fracture and crack orientations from flexural tests. (Top is RPC material, and bottom is Douglas fir.)

direction of the specimen. Evidently, mode II failure dominated the mechanism. In the RPC the crack nucleated by exceeding the tensile strength at the bottom layer of the beam and then propagated virtually through the thickness, indicating the dominance of mode I failure. The flexural strength difference between these two materials is thus obvious. As shown in Table 12, the Douglas fir flexural strength is about seven times that of the RPC, and the E_f is about 3.6 times. However, as stated before, like the RPC, the S and E_f of Douglas fir also decreased with moisture ingression (22.2%). The flexural strength decreased approximately 17.7%, and the flexural modulus approximately 29.7%. Like RPC, the low temperature (–30°C, –22°F) increased the S and E_f values, S by approximately 23.7%, and E_f by 18.8%. When wet and cold, the value of S still increased, about 20%, the E_f did not; rather it shows a very minor decrease (1.5%).

Discussion

The RPC material investigated here is a new material. Its mechanical properties were largely unknown before these tests. In fact, the material was produced in large size beams (152.4 × 203.2 mm, 6 × 8 in.) for the first time only when this project was underway. After the manufacturer addressed the issue of large sized wood chip contamination, the material looked homogeneous. Because of the limited scope of this investigation, no major microstructural analysis was undertaken, but it was suspected that the pultrusion type manufacturing process would introduce a degree of variation with grain orientation and densification. The results of the compression, tension, and flexure tests are compiled in Table 13.

The compression tests showed that the major

Table 12. Comparison of flexural properties from test data for RPC and Douglas fir.

Type of specimen and test condition	*Flexural strength S (psi)*		*Flexural modulus E_f (psi)*	
RPC dry, room temp. DD	872.3		26,574.3	
RPC wet, room temp. WD	783.1	(10.2% decrease)*	17,838.6	(32.8% decrease)*
RPC dry, at –30°C. DCD	1424.5	(63.3% increase)*	53,389.9	(100.9% increase)*
RPC wet, at –30°C. WCD	1322.8	(51.6% increase)*	54,141.3	(103.7% increase)*
Doug fir dry, room temp. DD	6057.1		96,057.4	
Doug fir wet, room temp. WD	4985.4	(17.7% decrease)	67,481.7	(29.7% decrease)
Doug fir dry, –30°C. DCD	7492.1	(23.7% increase)	114,089.4	(18.8% increase)
Doug fir wet, –30°C. WCD	7266.1	(20.0% increase)	94,607.3	(1.5% decrease)

* Relative to dry room temperature (baseline) data.
SI conversion factors: 1 psi = 6.89 kPa, (–30°C = –22°F)

Table 13. Summary of all RPC test data.

Tests	Specimens	Size (in.)	Grain orientation	Temperature (°C)	Moisture (%)	Strength (psi)	Std. dev. as % of avg. strength	Modulus (psi)	Std. dev. as % of avg. modulus
Compression	DL	6 × 8 × 12	x	21	dry	1394	4.3	19,102	36.5
	DT	4.5 × 5.5 × 6.5	y	21	dry	1767	6.6	30,028	8.0
	DTT	3 × 3.5 × 4.5	z	21	dry	1774	2.3	25,372	5.3
	CDL	6 × 8 × 12	x	–30	dry	2718	14.8	64,828	12.9
	CDT	4.5 × 5.5 × 6.5	y	–30	dry	3233	8.3	71,035	9.5
	CDTT	3 × 3.5 × 4.5	z	–30	dry	3747	2.2	63,997	3.7
	WL	6 × 8 × 12	x	21	2.203	1553	12.2	22,471	8.9
	WT	4.5 × 5.5 × 6.5	y	21	2.240	1858	8.0	31,716	5.4
	WTT	3 × 3.5 × 4.5	z	21	2.690	2049	1.7	25,622	6.5
	WCL	6 × 8 × 12	x	–30	0.641	2438	4.4	78,204	12.5
	WCT	4.5 × 5.5 × 6.5	y	–30	1.862	3346	7.4	69,338	7.9
	WCTT	3 × 3.5 × 4.5	z	–30	3.115	3646	2.5	60,051	9.0
Tension	W	1 × 3.25 *	x	21	dry	413	19.3	22,823	27.9
	A	1 × 3.25	y	21	dry	501	20.3	27,820	14.9
Flexure	DD	1.5 × 1.5 × 16	x	21	dry	872	18.3	26,574	21.8
	DCD	1.5 × 1.5 × 16	x	–30	dry	1425	12.5	53,390	8.5
	WD	1.5 × 1.5 × 16	x	21	15.6	783	50.8	17,839	42.5
	WCD	1.5 × 1.5 × 16	x	–30	3.1	1323	23.3	54,141	16.3

* Gage length

SI conversion factors: 1 in. = 25.4 mm, 1 psi = 6.89 kPa, (21°C = 70°F, –30°C = –22°F)

variation occurs in the between longitudinal and transverse directions. In the transverse *y* direction the room-temperature compressive strength is higher by about 27%, and the modulus by about 57%. In the z direction, the compressive strength is also higher by 27%, and the modulus by about 33%. Of course, the modulus value showed a high variation in results, the standard deviation being 36.5% of the average. It is arguable, however, that this variation in directional properties is due to the variation of the test specimen sizes, the *y* and z specimens being much smaller than the *x* specimens. This question could not be resolved without further investigation and tests. However, in tension tests, when same-sized specimens were tested, selecting one batch (W) from the *x* direction specimens and the other (A) from the *y* direction, the differences in both strength and modulus between them were again significant. The strength and modulus in the *y* direction specimens were much higher than those in the *x* direction, which establishes that the RPC material is essentially anisotropic.

It is also interesting to note that the variability of results increases with the reduction of the size of specimens. In general, the variability is much lower in large sized compression specimens than in small tension and flexural specimens.

About 2 to 3% of the moisture present in the compressive test specimens WL, WT, and WTT caused a small increase (5 to 15%) in the compressive properties, as can be seen by comparing them with the test results of the DL, DT, and DTT groups of specimens (see Table 13). However, the presence of moisture seems to have an opposite effect on the flexural properties, possibly because the failures in these cases were initiated by tension, rather than compression. Comparing the results of the WD specimens, which were kept in water for a prolonged time (383 hr), with those of the DD (dry) specimens, it is clear that with the 15.6% moisture, the strength decreased about 10%, and the modulus about 33%. High moisture ingression has a softening effect on the material. A strength and modulus decrease in flexure is also observed in the Douglas fir study. For the same sized specimens (38.1 × 38.1 × 406.4 mm, 1.5 × 1.5 × 16 in.), Douglas fir appeared to absorb moisture at about the same rate as the RPC (see Table 11). Its room-temperature flexural strength decreased about 18%, and modulus 30%, with a moisture ingression of about 22%.

Low temperature had the most significant effect on both compression and flexural behavior. A comparison of compression strain at failure (peak stress), given in Table 7b for room temperature and Table 7c for low temperature (–30°C, –22°F), shows that the strain at failure decreased significantly at low temperature. The decrease ranged from the lowest, 17% for the DTT speci

mens, to 55% for the WL specimens. Correspondingly, the material became stiffer in cold. The compressive moduli for the cold and dry CDL, CDT, and CDTT specimens show about a 239%, 136%, and 152% increase, respectively. The compressive moduli increase of cold and frozen WCL, WCT, and WCTT specimens are equally dramatic, at 148%, 119%, and 134%, respectively. At –30°C the flexural strength of the dry DCD specimens increased 63%, and their modulus 101% (see Table 12). For the wet flexural specimens, WCD, the strength and modulus increase were 52% and 104%, respectively. A significant increase in both strength and modulus at low temperature were also observed for the Douglas fir specimens. Douglas fir DCD specimens showed a 24% increase in strength, and about a 19% increase in modulus.

Relating mechanical properties, such as those determined for the RPC, to the design of guardrail posts or blockouts is not straightforward. The analytical design is too complex, as it depends not only on the material properties and structural response of the rails and the posts, but also on the soil bearing capacity as the primary source of generating restraining forces (USDOT 1988). Such an analysis includes dynamic effects, large displacements, stiffness, yield strength, and the inelastic behavior of the materials in the system. The final goal is to redirect errant vehicles to allow the occupants to survive the impact, and to ensure that the redirected vehicle presents a minimum hazard to following and adjacent traffic. Experience and knowledge are the key factors in designing the system; therefore, highway engineers rely on trial and error of candidate systems, and they evaluate such systems by crash testing. Therefore, following the above laboratory tests, further investigations on the applicability of the RPC using crash testing was conducted by the FHWA at the Federal Outdoor Impact Laboratory (FOIL) at TFHRC in McLean, Virginia. The results of this test have been summarized by McDevitt and Dutta (1993) and are reproduced in part in Appendix B.

Figure 55. Use of RPC as a blockout material in a highway.

After the FOIL test, the FHWA continued the field crash tests. Guardrail blockouts made of RPC are considered as separate products that could replace the wood blockouts. The RPC blockouts performed satisfactorily in the FOIL test and several other crash tests, and were subsequently approved by the FHWA for use by state highway authorities. Figure 55 shows an example of its use.

The general mechanical properties of RPC indicate that it has a potential for use as supports for small signs. One of the evaluation criteria for crash tests of small signs is that after the full-scale test, the height of the stub section will be not higher than 102 mm (4 in.) above ground (AASHTO 1985). At the FOIL test, the RPC posts broke off cleanly at the ground line, indicating that this type of material may have potential for such applications. However, since the RPC materials were found to be stronger and stiffer at lower temperatures than at room temperature (before their application), some crash tests at a low temperature may be necessary.

Because some state legislatures have mandated recycling, interest in RPC is expected to grow in the future. Its potential applications will probably include noise barriers, blockouts, guardrail posts, fence posts, sign supports, delineator posts, etc. These applications will necessitate further assessment of the RPC's performance under prolonged stress, wider ranges of temperature, toxicity (if any), damage by insects, and cyclic periods of heat, cold, and dampness. The applications themselves should have some baseline specifications, subject to local conditions. Also, the RPC material must be available in consistent composition and properties, with an assured quality. Finally, the RPC materials will have to be economically competitive with the products they are intended to replace.

CHAPTER 5: CREEP STUDY OF FRP COMPOSITE REBARS FOR CONCRETE

Background

FRP reinforcing bars are receiving increased attention as the tension element in reinforced concrete (Roll 1991). This is primarily because the corrosion of steel reinforcement in concrete by chloride ions has been determined to be the major cause of premature deterioration of concrete structures (ACI Committee 208 1958). Available as long rods in the market, these rebars are made of very fine continuous glass fiber strands which are bound together with a thermosetting polymer. Wu et al. (1990) reported that E-glass reinforced composite rods, from which these rebars are made, may have a tensile strength in excess of 689 MPa (100×10^3 psi) and a longitudinal elastic modulus of about 51.7 GPa (7.5×10^6 psi). In tensile tests, the bars fail without any significant yield (brittle failure). The rods are produced by a pultrusion process. Since glass is commonly used as the reinforcing fibers in these rebars, they are also designated as GFRP (G for glass). Currently, there are several FRP rebar companies actively marketing their products in the U.S. Most FRP rebars contain about 55% E-glass fiber by volume and about 45% thermoset resin. The sizes (diameter) of the rebars follow the size designations of steel rebars (e.g., no. 3, 4, or 7 rebars). Faza (1995) reported a number of successful applications of rebars in the USA, including applications in sea walls, hospital MRIs, reactor pads, compass calibration pads, mill roofs, laser test facilities, highway barriers, residential foundations, and bridge decks. Table 14 gives a comparison of the mechanical properties of steel rebars and FRP rebars.

The light-weight, corrosion-resistant and nonmagnetic properties make FRP rebars an improved alternative to steel. One of the most critical problems to be overcome in large-scale applications of FRP rebars is the development of improved bond strength with the concrete. Some available designs provide a helically convex surface made with a strand spirally wound and cured on the surface. Other designs suggest the use of a sand or grit coating on the rebars. A recent design includes a pultruded ribbed surface. A comparative survey of the bond quality of these surface modifications is still not available. The bond strength of composite rebars and the bending response for carrying concrete strengths have been investigated by many, including GangaRao and Faza (1992), Pleimann (1991), Daniali (1992), Larralde and Siva (1990), Iyer and Anigol (1991), Tao et al. (1992), Challal and Benmokrane (1993), Challal and Benmokrane (1992), and Malavar (1994).

There are several major barriers to FRP rebar applications. These include a lack of sufficient data on: durability or performance under extreme environments (Dutta 1995b, GangaRao et al. 1995), creep, fatigue, and corrosion from the alkaline environment of concrete. Unlike steel, the FRP rebar is viewed as a viscoelastic material. As such, many of its properties are suspected to be time-dependent. Creep refers to the slow deformation with time under a constant stress that is less than the yield stress. When a constant load is applied (except for a short initial duration when the strain may increase quite rapidly) to a viscoelastic material, the strain increases steadily. This increase of strain is creep. If creep increases beyond a certain limit, the effective stress owing to a decrease in the cross-sectional area increases. The increased stress results in further deformation, which in turn increases the stress even more. Thus, the deformation suddenly accelerates, leading to the failure of the material.

At the microstructural level, creep occurs due to the presence of mobile defects, such as dislocations that move (enlarge) primarily at increased stress and temperatures. Thus, the general mathematical formulation of creep rate takes the form

Table 14. Comparison of mechanical properties of steel and FRP rebars (Faza 1995).

Properties	*Steel rebar*	*FRP rebar*
Specific gravity	7.9	1.5–2.0
Tensile strength, MPa (psi $\times 10^3$)	483–690 (70–100)	517–1207 (75–175)
Yield strength, MPa (psi $\times 10^3$)	276–414 (40–60)	—
Compressive strength, MPa (psi $\times 10^3$)	276–414 (40–60)	310–482 (45–70)
Tensile modulus, GPa (psi $\times 10^6$)	200 (29)	41–55 (5.9–8.0)
Coeff. of thermal expansion 10^{-6}/°C (°F)	11.7 (6.5)	9.9 (5.5)

$$d\varepsilon/dt = F(\sigma,T) \quad (11)$$

where ε = strain
t = time
$F(\sigma,T)$ = function of stress σ and temperature T.

In the case of composites, F is a function of the stresses produced in all the components, since the net creep resistance will depend on the creep resistance of each of the components. If the two components have two different creep resistances, the creep of the low-resistance component will be checked by the high-resistance material, owing to adhesion between them. Thus, with a higher bond strength between the components, a creep resistance even greater than that of its components should result.

Creep in polymeric composites has been the subject of investigation for a long time (Glaster et al. 1983, 1984). Tunik and Tomashevskii (1974) discussed creep and the long-time strength of glass FRP in interlaminar shear. Weidmann and Ogorkiewicz (1974) studied the tensile creep of a unidirectional glass fiber epoxy laminate. The creep strength of discontinuous fiber composite has also been studied by Bocker-Pedersen (1974). The power law approach to modeling the creep behavior of plastics and FRP is primarily due to the original work by Findley (1960), which he again updated in 1987. Numerous other projects about creep behavior of FRP in general have also been reported in composites literature. These include the work on creep in FRP beams by Holmes and Rahman (1980). Brinson et al. (1980), Hiel and Brinson (1983), and Dillard and Brinson (1983) used numerical methods of predicting creep and delayed failures. Transverse creep and the tensile behavior of composite laminates were studied by Eggleston (1994), and Huang and Gibson (1990) performed both theoretical and experimental studies on sandwich beams with linear viscoelastic cores. The creep behavior of Kevlar/epoxy composites was studied by Beckwith (1984), who concluded that the creep behavior in the laminate composites was primarily "fiber-dominated" and independent of resin modulus. Krishnaswamy (1991) presented the results of a finite-element model of the ductile behavior of polymers. The creep effects in composite columns were studied by Chen and Lottman (1991), Ueng (1991), and Vinogradov (1989). Slattery (1994) developed the procedure for predicting the accelerated failure rate by extrapolating short-term data and by taking into consideration the "progression of fundamental damage" mechanism. Recently, Mossalam and Bank (1991), and Mossalam and Chambers (1995) presented a simplified and efficient design procedure to predict the deflection of pultruded composites under sustained load, and a laboratory procedure for determining the creep coefficients. Thus, while a large volume of information is available on the creep characteristics of FRP materials in general, the specific information on whether FRP rebars will creep under sustained loading is very scant.

In this investigation, the scope of the creep study was limited to determining whether the commercially available FRP rebars would creep under a sustained tensile load over a wide range of temperatures: low temperature (–23°C, –10°F), room temperature (21°C, 70°F), and high temperature (49°C, 120°F). Because these rebars had fibers generally oriented in the longitudinal direction, the load was carried primarily by the fibers.

Test description

Commercially available fiberglass composite rebars (Fig. 56) made with 5- to 10-μm E-glass fibers in a polyester resin matrix were selected for this creep study. The mechanical characteris

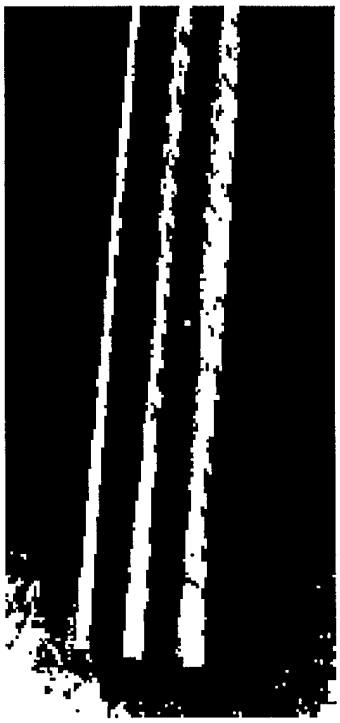

Figure 56. Examples of commercially available glass fiber reinforced composite rebars.

Table 15. Mechanical characteristics of composite rebars.

Density	1.85 g/cm^3 (0.067 lb/in.^{3})
Ultimate tensile strength	117.9 MPa (17,098 psi)
Tensile modulus	54.206 GPa (7.86 × 10^6 psi)
Coef. of thermal expansion	9.9 × 10^{-6} mm/mm °C (5.5 × 10^{-6} in./in. °F)
Matrix	Derakane 411-45 polyester resin
Fiber	E-glass
Spiral fiber pitch	190.5 mm (0.75 in.)

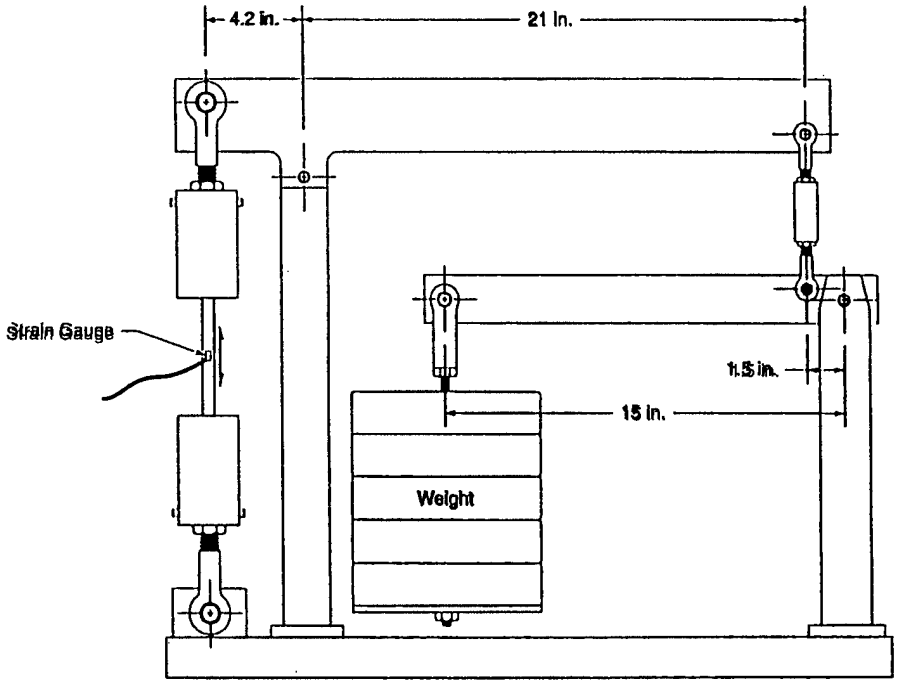

Figure 57. Deadweight creep test fixture.

tics of these bars, as provided by the manufacturer, are given in Table 15.

To conduct the creep tests, the deadweight creep test fixture shown in Figure 57 was designed and fabricated. The gripping mechanism is shown in Figure 58. The fixture provided a mechanical advantage of approximately 50 to 1. Six of these creep test fixtures were mounted on a common base frame (Fig. 59).

Initially, six fiberglass composite rebars made by a single vendor were selected for the tests. The rebars were obtained in 12.70, 15.88, and 19.05 mm (0.5, 0.625, and 0.75 in.) nominal diameters, with a spirally wrapped glass fiber strand, wound with an approximately 19.05 mm (0.75 in.) pitch. The entire rod was redipped in resin and then cured to obtain an irregular wavy but drip, surface to promote adhesion to the concrete. For fixing on the test jigs, the 19.05-mm- (0.75-in.-) diam. rebar specimen proved to be the most difficult to be gripped and was finally rejected from the test batch. Only 12.70-mm- and 15.88-mm- (0.5-in.- and 0.625-in.-) diam. bars were finally tested.

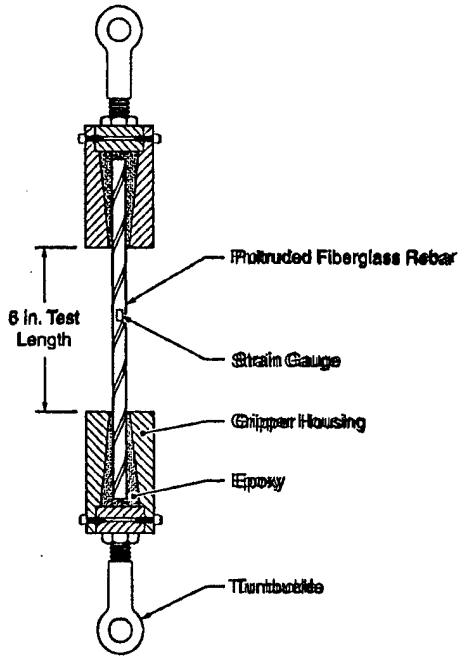

Figure 58. Details of the gripping mechanism of the creep test fixture.

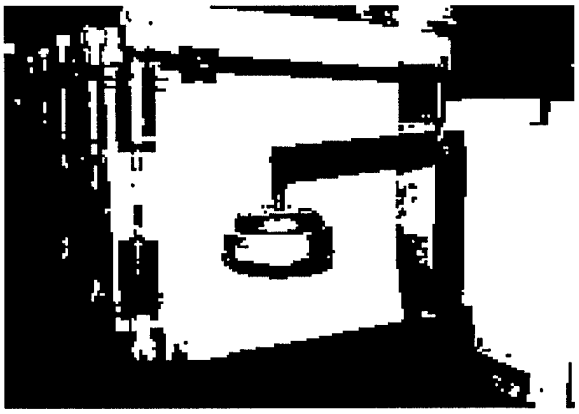

Figure 59. Creep test platform with six creep test fixtures.

Each composite rebar was instrumented with electrical foil strain gages to measure both the longitudinal and diametrical strains (Fig. 60). Even though only longitudinal strains were of interest in this creep study. The gages were centrally located along the length of each specimen and diametrically opposite to each other. Each longitudinal gage was axially aligned with the fiber direction and positioned so as not to interfere with the spiral wrapping of the rebar. The gages had an effective length of 1.58 mm (0.062 in.), 350-ohm resistance, and were temperature compensated for steel. The gages were bonded to the rebar surface according to the manufacturer's recommended procedure. To avoid modifying the rebar specimen resin, as per the gage manufacturer's instructions, the gages were cured overnight at room temperature. No elevated temperature curing was attempted. For measuring strain, each gage was put in a full-bridge configuration and initially balanced in a switching and balancing unit. All subsequent readings were referenced to this initial balance.

Figure 60. Strain gage instrumentation on the test specimens. Test specimens shown removed from the test fixture after the test was over.

The deadweights were adjusted to tension each of these rebars to about 50% of its ultimate strength, as specified by the rebar manufacturer. In order to monitor temperatures, a thermocouple was attached to each rebar. Once the tension for the rebar was fixed, the apparatus was not disturbed. For the room-temperature tests, temperature and strain readings were taken once a day for 1800 hours (75 days). The strain data are shown in Figures 61a and b for the 12.70-mm (0.5-in.) and 15.88-mm (0.625-in.) bars, respec

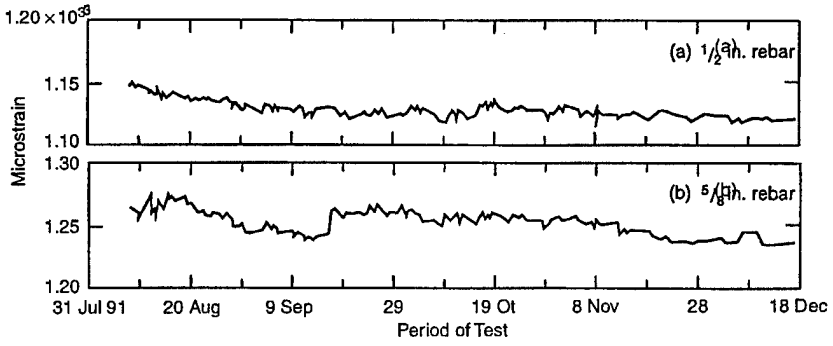

Figure 61. Records of room-temperature creep strain for (a) 12.70-mm (0.5-in.) diam. rebar, and (b) 15.88-mm (0.625-in.-) diam. rebar.

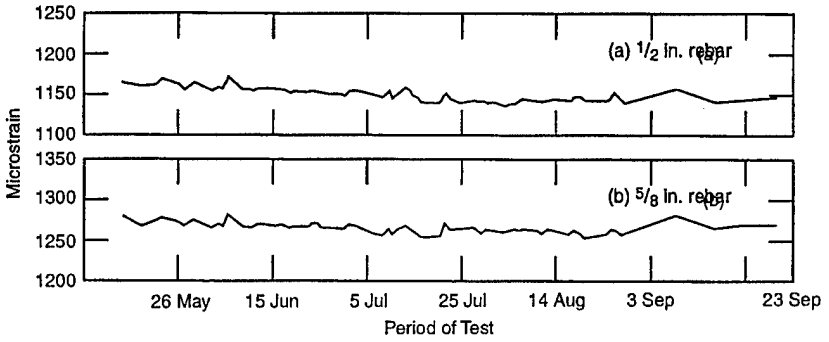

Figure 62. Records of low-temperature (–10°F, –23°C) creep strain for (a) 12.70-mm- (0.5-in.-) diam. rebar., and (b) 15.88-mm- (0.625-in.-) diam. rebar.

tively. If any creep occurred, the strain readings would continue to increase. However, the results showed that over this period, the strain did not tend to increase. The temperature variation of the room in which the test fixture was placed caused the daily variation of the strain, as seen by the zigzag lines of the record, but the general trend did not reveal the development of any creep under the test conditions.

Since no creep could be detected at room temperature, we expected no creep to occur at low temperature (–23°C, –10°F). However, creep might have resulted if the low temperature induced any microcracking or degradation of the interface bond by the induced thermal stresses from the thermal expansion coefficient mismatch between fibers and matrix. A relatively longer period of test was necessary to develop these effects. Accordingly, the deadweight test fixture was placed in a refrigerated coldroom, where the temperature was constantly maintained at approximately –10°C (–23°F). This test was continued for 3,552 hours (148 days). The strain records of the 12.70-mm (0.5-in.) and 15.88-mm (0.625-in.) rebars are shown in Figures 62a and b, respectively. Again, no discernible trend of increasing strain was observed.

For the high-temperature (120°F, 49°C) creep test, a special environment chamber of 1.22 × 1.22 × 2.44 m (4 × 4 × 8 ft) was built with a thermostatically controlled hot-air blowing system that would control the temperature of the chamber to between 50°C (122°F) and 47.2°C (117°F). At the end of the coldroom test, the strain gages on the 15.88-mm (0.625-in.) rebars were damaged and the bars themselves were unsuitable for further testing. Accordingly only two 12.70-mm- (0.5-in.-) diam. rebars were tested in the high-temperature chamber. Each specimen was instrumented with a thermocouple sensor, and a third thermocouple measured the air temperature of the chamber near the specimens. The specimens were again subjected to a long test period, from 25 April to 30 September, a total of 3,792 hours (158 days). The strain readings taken approximately once a week were remarkably steady over this period. The numerical data recorded for this test are shown in Table 16. Figure 63 gives the plotted data.

Table 16. FRP rebar creep test data at 49°C (120°F).

Date	*Chamber temp. (°F)*	*Microstrain* in rebar no. 5*	*Microstrain* in rebar no. 6*
04/25/94	120	1209	1281
05/02/94	120	1209	1273
05/09/94	119	1220	1279
05/16/94	119	1221	1274
05/23/94	120	1216	1273
06/01/94	120	1218	1276
06/07/94	120	1220	1270
06/15/94	119	1222	1276
06/22/94	121	1211	1268
07/01/94	119	1215	1269
07/05/94	121	1220	1272
07/06/94	122	1220	1272
07/07/94	121	1215	1272
07/15/94	121	1218	1275
07/21/94	118	1213	1273
08/01/94	119	1217	1268
08/08/94	118	1216	1272
08/15/94	121	1221	1276
08/22/94	121	1223	1277
09/01/94	122	1219	1276
09/07/94	122	1221	1276
09/15/94	120	1221	1271
09/20/94	121	1221	1271
09/30/94	118	1216	1262

* Microstrain = strain × 10^{-6}

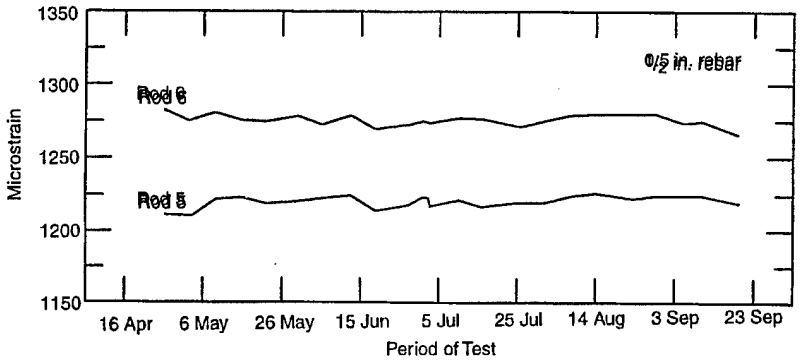

Figure 63. Records of high-temperature (49°C, 120°F) creep strain for two 70-mm- (0. 5-in.-) diameter rebars.

Analysis and discussion

Findley's general theory of creep behavior of viscoelastic polymer (1960) is represented by

$$\varepsilon = \varepsilon_0 + p\,(t/t_0)^q \qquad (12)$$

where ε = the total strain
ε_0 = stress dependent strain
p = the coefficient of time dependent term, which is dependent on stress level
t = duration of loading (hours)
t_0 = unit time (hour)
q = a material constant, independent of stress.

Parameters p and q are known as creep parameters. To obtain the particular values of p and q, eq 12 can be rearranged and written in the following form:

$$\log (e - e_0) = \log (p) + q \log (t/t_0) \qquad (13)$$

Equation 13 represents a straight line of slope n and intercept m at unit time, if log $(\varepsilon - \varepsilon_0)$ is plotted against log (t/t_0). Using the creep data of Table 16, in which a very small trend of increasing strain could be observed, the values of m and n were determined as $p = 9.45$ and $q = 0.297$. These values closely match Mosallam and Chamber's (1995) published values for commercially available pultruded FRP WF beams: $p = 9.72$ and $q = 0.298$. Findley's equation, when plotted over the Table 16 data points is shown in Figure 64, but the match is not very clear because of the scatter in the data. If the tests had been continued over a longer time, a more discernible creep strain might have developed. The data at room temperature and low temperature had not shown any trend of increasing; therefore, they were not analyzed with Findley's equation. It must be noted that Findley's theory applies very well to viscoelastic polymers, but in FRC composites rebars, when the stress is applied in the fiber direction, the behavior is not totally viscoelastic. In fact, with a higher volume fraction of glass fibers oriented in the loading direction, creep in FRP composites is not expected to be a problem.

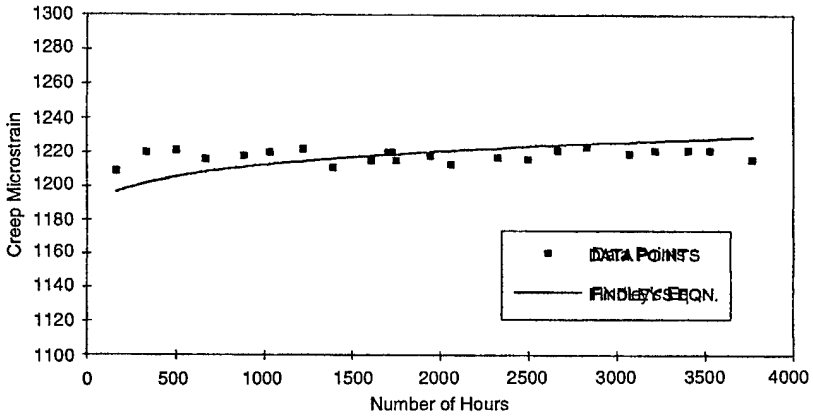

Figure 64. Comparison of high-temperature creep data with Findley's equation.

CHAPTER 6: FRP COMPOSITE BREAKAWAY COUPLERS

Background

Each year numerous injuries and fatalities occur as a result of vehicles hitting signposts, utility poles, and light poles. Even as early as 1976, Graf et al. (1976) noted that 1600 deaths and 100,000 injuries occurred annually as a result of collision with timber utility posts (Ivey and Morgan 1986). In 1985, to minimize injury to occupants and damage to the impacting vehicles, the American Association of State Highway Transport Officers (AASHTO), in "Standard Specifications for Structural Supports for Highway Signs, Luminaries, and Traffic Signals," stipulated that all light poles or ground-mounted signposts within 9.15 m (30 ft) of a highway shall be placed on breakaway supports. The AASHTO (1985) required that for a standard 816.5-kg (1800-lb) vehicle striking a breakaway support at a speed between 32.2 and 96.6 km/hr (20 to 60 mi/hr), the velocity change must not exceed 4.88 m/s (16 ft/s). A higher change of velocity results in more severe occupant injury. As a result, designs of many pre-1985 breakaway couplings were reevaluated and new design approaches developed. In 1989, Ross et al. (1989) in NCHRP Report 318, documented the evaluation of the impact performance of roadside safety elements for 680.5 kg (1500 lb) and identified several potential modifications of existing hardware that would accommodate vehicles weighing as little as 567.2 kg (1250 lb). From their test results on the breakaway sign supports with slip-base design, which were impacted at 32.2 km/hr (20 mi/hr) and 96.6 km/hr (60 mi/hr) and which produced only a 3.05 m/s (10 ft/s) and a 3.36 m/s (11 ft/s) change in velocity, respectively, they concluded that, in general, slip-base supports will pose no serious damage to vehicles in the 680.5-kg (1500-lb) weight range. However, cast aluminum transfer bases widely used as breakaway devices for roadside luminaries supports would not satisfy either the NCHRP Report 230 (1981) evaluation criteria (Michie 1981), or the AASHTO (1985) standards. The Ross et al. (1989) study provided the impetus to research and redesign of the breakaway supports for light poles, sign posts, and utility poles.

The impact dynamics between an errant vehicle and a pole depend on numerous variables, such as: the size, weight, and crush characteristics of the vehicle; the impact velocity; and the geometry and strength characteristics of the pole. A built-in breakaway mechanism in the pole reduces the amount of energy required to fracture the pole in a plane near the vehicle bumper. The essential criteria developed for the breakaway design were that the breakaway pole must (1) provide an acceptable momentum change (change of velocity below 5 m/s (16 fps), (2) provide sufficient structural integrity of the pole to withstand ice- and wind-induced loads, (3) minimize post-breakaway hazards to the vehicle and the occupants, and (4) have low implementation cost. In 1978, Dinitz and Chisholm (1978) described an innovative design of longitudinally grooved coupling bolts for ground-mounted sign supports. Later designs included notched coupling bolts for connecting the base plate to the anchor bolts for ground-mounted supports.

Breakaway mechanisms

As stated before, a breakaway mechanism should reduce the amount of energy required to fracture the pole. Under normal conditions, it is the environmental loads, like wind and ice, that provide bending stress at the base of the pole. During vehicular impact, shearing is the primary mechanism. Therefore, the ideal breakaway configuration would be the one that weakens the pole's shear strength without affecting its bending strength significantly. Theoretically, this provides a situation in which an anisotropic material like FRP composite, which is very strong in the fiber direction and weak in the cross-fiber (90°) direction (see Chap. 2), would be a desirable material. Besides, this material has the other advantages of lighter weight and high durability. In this study, the application of FRP material for designing a breakaway mechanism was explored.

FRP design approach

The FRP breakaway coupling design was aimed at providing both a high tensile load capacity and a low breakaway force requirement. This could be achieved by the composite material having the fibers carry the major tensile load, while the shear force acts at 90°to the fibers. Commercially available pultruded glass-fiber-reinforced FRP bars were considered as the basic raw material for the breakaway coupler. A discussion with an industrial expert* on breakaway coupler design resulted in the decision to develop a design based on the

* T. Husain, Transpo Industries, New Rochelle, New York, personal communication, 1995.

necked-down (notched) version of the couplers, similar to the design currently made with steel. Commercially available, unidirectional, pultruded FRP composites would be used as the basic raw material from which the couplers would be machined. Three major problems for making the prototype for the tests were to be resolved: (1) machining of the FRP, (2) an assessment of the mode of failure and energy absorption of the notched FRP under impact and the relationship with temperature, and (3) the development of a technique for cutting threads in the bar stock.

Notched bar impact test

In order to check if the pultruded FRP could be machined, we attempted to turn down the rough surface diameter of the FRP rebar stocks from 19.05 mm (0.75 in.) to 12.7 mm (0.5 in.). Except for dust production, which was handled by a suitable vacuum extraction technique, no major problem was encountered in machining the diameter down when sharp diamond-tipped tools were used (see Fig. 65). It was of concern whether the unidirectional notched (or necked-down) FRP composite would, in fact, shear off clean at the root of the notch, like metals. Transverse cracks in composites are usually blunted by the fibers and such cracks propagate in the fiber direction. A preliminary test was therefore conducted using the 12.7-mm (0.5-in.) round FRP bars with 2.54-mm (0.1-in.) deep notches cut into them. These notched bars were held in the anvil of a swing pendulum Charpy testing machine (Fig. 66), and were impacted with the pendulum hammer directly on the side of the notch, so that the crack developed at the root of the notch and propagated through the cross section of the bar.

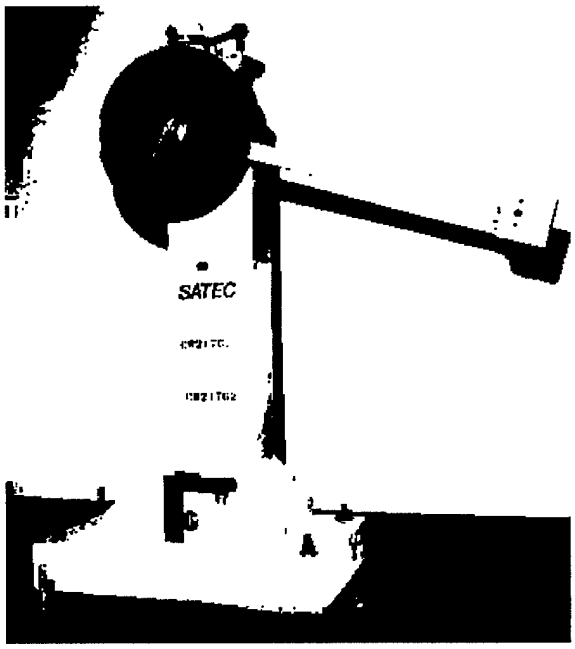

Figure 66. Charpy impact testing machine.

The energy absorbed was recorded directly from the Charpy testing machine dial recorder. Figure 67 illustrates the bars in three conditions. One before the notch was cut, the second with the notch, and the third after the test. As expected for composites, the cracks at the notch root did not propagate through the section. On the other hand, because of bending, longitudinal shear cracks developed at the free surface at the top of the bar and propagated downward to the plane of the notch where the bar was clamped in the vise. Nevertheless, the energy absorbed in the process over a range of low temperatures was recorded and is illustrated in Figure 68. Energy absorption tended

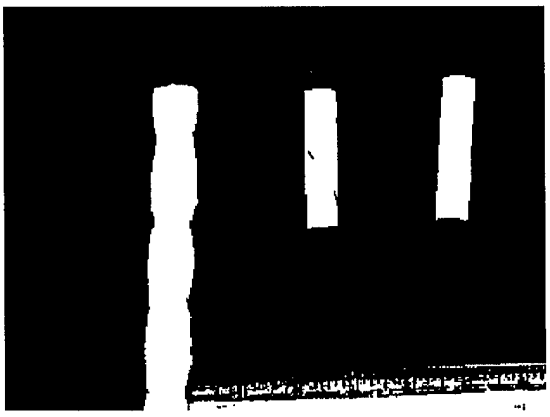

Figure 65. Preparation of the notched bar impact test specimen from the FRP rebar sample.

Figure 67. Unnotched, notched, and notch-impact-tested specimens.

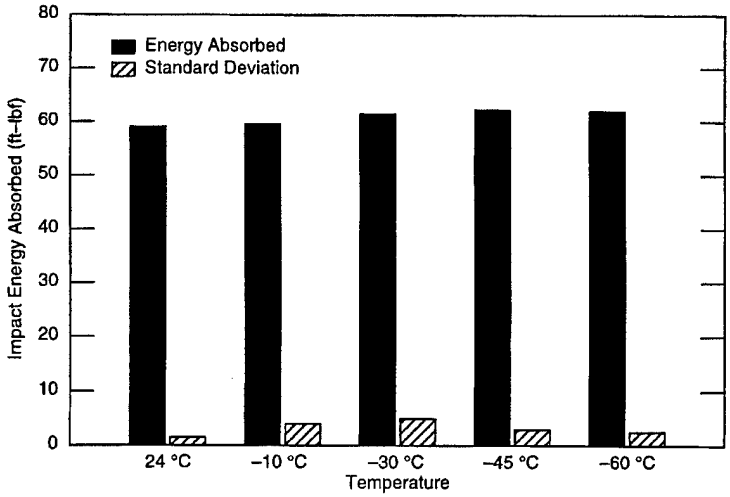

Figure 68. Influence of temperature on the energy absorption in notched bar impact tests.

to increase at lower temperatures. This is related to the mode of failure. Instead of across-the-section fiber fracture, the failure happened by shear debonding along the fiber. For composites, bonding strength tends to increase at low temperatures, which explains an increasing trend of energy absorption at lower temperatures, as observed in the test (Fig. 68).

Thread cutting and fabrication

A major problem that became apparent concerned the machining of threads in the commercial FRP composite stock materials. In this case, the longitudinal glass fibers in the thread area repeatedly came under tool attack and tended to shear off near the crests of the thread profile. However, FRP studs and nuts, even for 25.4-mm-(1-in.-) diam. sizes, were found to be commercially available (IMCO 1995, MMFG Co. 1994) (Fig. 69). Therefore, detailed instructions were obtained from the manufacturer of these commercial FRP bolts about the thread cutting technique on FRP bars.

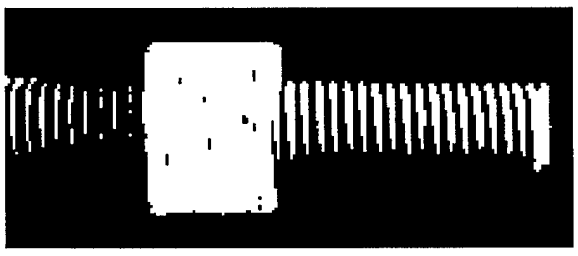

Figure 69. Commercially available FRP nuts and studs.

Considering that the stock of pultruded FRP round bars would be used, we developed the design drawings of the two prototype couplers shown in Figures 70a and b. Figure 70a shows the prototype design with male threads and Figure 70b with female threads. Two specimens of male-threaded and two specimens of female-threaded couplers were then fabricated by machining the diameter of the raw FRP bar down to a neck profile and cutting threads on the stems. As feared, the thread cutting was found to be extremely difficult; however, following the manufacturer's detailed instruction, threads could finally be cut, although many of the crests were lost. According to the manufacturer's literature, the FRP bar material would be made up of glass fiber and vinyl ester resin. A comparison of this material's mechanical properties with steel is shown in Table 17.

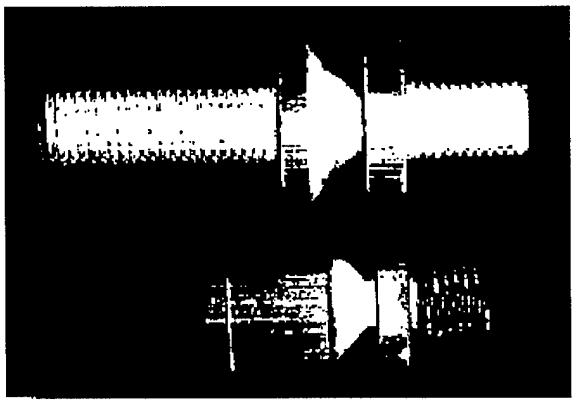

Figure 70. FRP composite breakaway coupler designs with (top) male and (bottom) female threads.

Table 17. Comparison of FRP breakaway coupler material and steel (MMFG Co. 1994).

Properties	*Carbon steel (M1020)*	*Coupler material (MMFG Co. 1994)*
• Tensile strength (psi)	35,000	30,000
Fiber direction		
90° to fiber direction	35,000	7,000
• Tensile modulus (psi × 10^6)	30	2.6
Fiber direction		
90° to fiber direction	30	1.0
• Izod impact (ft-lb/in.)		
Fiber direction	N/A	25
90° to fiber direction		4

SI conversion factors: 1 ft = 0.305 m, 1 in. = 25.4 mm, 1 lbf = 4.45 N, 1 psi = 6.89 kPa.

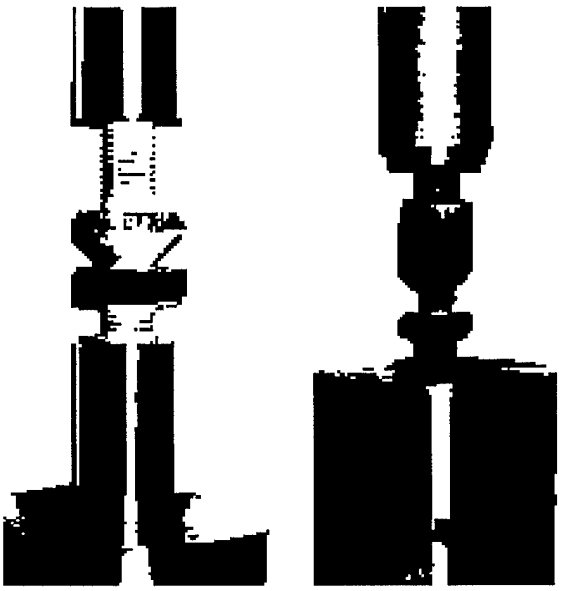

Figure 71. Tension testing of the male- (left) and female-threaded FRP breakaway coupler.

Tension tests of the breakaway couplers

One each of male- and female-threaded breakaway couplers were tested in a testing machine by applying a load to them. If these FRP couplers had been made of steel, we would have expected them to yield at about 111.25 MPa (25,000 lbf), and the failure would have occurred with a fracture through the entire cross section of the necked-down portion of the bolt. However, the FRP composite breakaway coupler–bolt failure mode, as suspected, was completely different from the steel failure. In the case of the FRP female-threaded coupler, the failure was initiated by interfacial shear bond failure, so that as the tensile load continued to be applied, a plug of material, roughly equal to the cross sectional area of the turned-down section of the stud, was pulled out (see Fig. 71 [left]). For the male-threaded coupler, the failure occurred by thread shearing at the thread roots (Fig. 71 [right]), when an approximately 31.7-mm (1.25-in.) length of threads at each end was engaged to the loading column of the testing machine. The tensile loads at which these couplers failed are given in Table 18.

Discussion

The above experimental effort clearly shows that the one-to-one replacement of steel breakaway couplers by FRP material cannot succeed. Fiber-reinforced composites properties are strongly direction oriented, and the failure mechanism is controlled by the fiber architecture. In order to have a clean transverse shear break in a necked-down breakaway coupler made with FRP composites, the fiber architecture has to be designed and developed such that the failure can be induced by interlaminar or interfacial bond failure in the transverse direction to the bolt. At the same time, sufficient longitudinal strength has to be available to withstand the tensile load occurring from bending under wind and ice loads. Theoretically, this could be accomplished by a microstructural analysis of load sharing between fibers and matrix, determining the optimum fiber volume fraction and the optimum orientations of the fibers. The composite breakaway coupler in this case would possibly have to be precast rather than machined from the commercially available bar stocks. Because of the limited scope of this study, no such attempts were made.

Table 18. FRP composite breakaway coupler test results.

FRP breakaway coupler type	*Rate of loading (mm/min, in./min)*	*Tensile breaking load (kN, lbf)*	*Mode of failure*
Male-threaded type	2.54 (0.1)	24.373 (1800)	Thread shear
Female-threaded type	2.54 (0.1)	6.675 (1500)	Fiber shear bond failure

CHAPTER 7: FRP COMPOSITES FOR CRUSHABLE CUSHIONS

Background

Every year, side impact collisions with roadside fixed objects involve approximately 225,000 people, of which 1 in 3 is injured and 1 in 100 is killed. This level of injury represents a societal cost of more than $3 billion (Troxel et al. 1991). Trees, utility poles, and light supports form the majority of the fixed objects (77%) in these accidents.

The objective of this study was to explore the feasibility of making a crushable plastic cushion (CPC) that could be used on wooden utility poles to reduce the severity of side impact collisions of vehicles. It was conceived that the plastic cushions could be designed such that they could accommodate shrinkage of the wooden utility pole. Possible future applications on trees could also accommodate some increase in the diameter of the tree due to growth. Thus, the plastic cushions would not be attached directly to the wooden utility pole with nails, staples, or screws. Other desirable features would be that the cushion's covering should be made of a reflective material or glass-beads coating to provide delineation. It must also be vandal-resistant, and its top cover should be such that rainwater or melted snow water could easily drip down.

Materials and design approach

A design of the crushable plastic cushion (CPC) would basically have three essential elements: (1) a pair of stiff plastic composite skins, one for the interior facing, and the other for the exterior facing, (2) a thick, lightweight, crushable core to separate the two facings and carry crushing loads from one facing to the other, and (3) an attachment or bonding of the facings to the core so that not only the direct normal loads, but also the shear loads, are transmitted to the core. Thus the material system that would be suitable for this design could be a structural "sandwich." A sandwich construction would also be lightweight, but stiff, strong, and durable. A fourth requirement would be an arrangement of deformable spring inserts to the interior facing, which would essentially clamp the crash cushion to the pole or tree trunk under an active force.

The primary functions of the facing material would be to (1) provide the bending and in-plane shear stiffness, and (2) carry the axial, bending, and in-plane shear loading. The facing material must also be impact resistant and tough. It must have a mode of fracture that would not let the cracks to propagate easily throughout the facing, and finally, it must be weather resistant and durable. A number of materials initially considered as facing materials were investigated. Their mechanical properties are briefly summarized in Table 19. The list includes a few materials, e.g., plywood, which could hardly be considered for the crushable cushion surface, but they were included for the convenience of comparison with the composites and metals from which the selec

Table 19. Mechanical properties of a number of facing materials for the crushable plastic (Marshall 1982).

Facing material	*Yield strength (psi)*	*Modulus of elasticity (psi)*	*Weight of 1-mil thickness (lb/ft²)*	*Comments*
Composites				
Glass/polyethylene	14,000	0.92×10^6	0.0070	
Glass/epoxy	62,000	3.50×10^6	0.0088	
Glass/phenolic	48,000	3.50×10^6	0.0094	High temp resist.
Glass/polyester	48,000	3.50×10^6	0.0100	
Glass/polyimide	60,000	3.50×10^6	0.0095	High temp resist.
Graphite/epoxy	80,000	10.0×10^6	0.0080	Woven graphite
Kevlar/epoxy	60,000	4.4×10^6	0.0070	Very tough
Metals				
Aluminum 7075-T6	66,000	10.0×10^6	0.014	High strength
Mild steel	50,000	30.0×10^6	0.040	Low cost, heavy
Stainless steel 316	60,000			
Nonmetals				
Plywood (Douglas fir)	2,650	1.80×10^6	0.003	
Southern pine	2,650	1.80×10^6	0.003	

SI conversion factors: 1 psi = 6.89 kPa, 1 lb = 0.454 kg, 1 ft = 0.305 m.

Table 20. Mechanical properties of several foam materials (Marshall 1982).

Foam material	*Density (lb/ft³)*	*Tensile strength (psi)*	*Compressive strength (psi)*	*Shear strength (psi)*	*Shear modulus (psi)*	*Max. service temp. (°F)*
ABS*	40–56	2000–4000	2300–3700	—	—	176–180
Cellulois acetate rigid	6–8	170	125	—	—	350
Epoxy closed cell rigid	5	51	90	—	—	350
Phenolics foam-in-place	0.5–1.5	3–17	2–15	—	—	—
Polycarbonate	50	5500	7500	—	—	270
HD polypropylene foam	35	1600	2100	—	—	—
Polyurethane rigid c. cell	1.3–3.0	15–96	15–60	20	226	180–250
Polyvinyl chloride rigid	3	1000	95	65	1200	—

* Acrylonitrile-butadiene-styrene
SI conversion factors: 1 lb = 0.454 kg, 1 psi = 6.89 kPa, 1°C = 0.56(°F–32)

tion would be made. Since the facing material will have to wrap around the luminaries supports or the trees, they must be deformable for fabrication.

Normally, the primary function of the core material is to stabilize the facings and transfer the shear loads, but at crush impact, the core material has to respond to most of the crushing load. Thus, the selection and design of the core material must be based on energy management during vehicular collision with the cushion and the fixed object. For a vehicle weight (m) of 908 kg (2,000 lb) and an impact speed (v) of 48.3 km/hr (30 mi/hr) or 13.42 m/s (44 ft/s), we have

$$U \text{ (kinetic energy)} = (mv^2)/(2g) = 81.528 \text{ kJ (60,124 ft-lbf)}. \quad (14)$$

Therefore, 81.528 kJ (60,124 ft-lbf) of energy would have to be dissipated in the impact by crush deformation of the plastic crash cushion. The core must possess the sacrificial and energy dissipating mechanisms for this purpose.

The use of foam as a structural, as well as a controlled energy dissipating material, has been and is now extensive. Because of the single-step injection molding process, foam is lower in cost too. It also has the potential to form the CPC with the two facing plates in a single operation by careful adjustment of the curing reaction and the heat-sink effect of the mold. This process forms a part in which the facings are simply the higher density form of the foam and are common in many applications in the automotive industries. The mechanical properties of several candidate foam materials for the CPC are listed in Table 20.

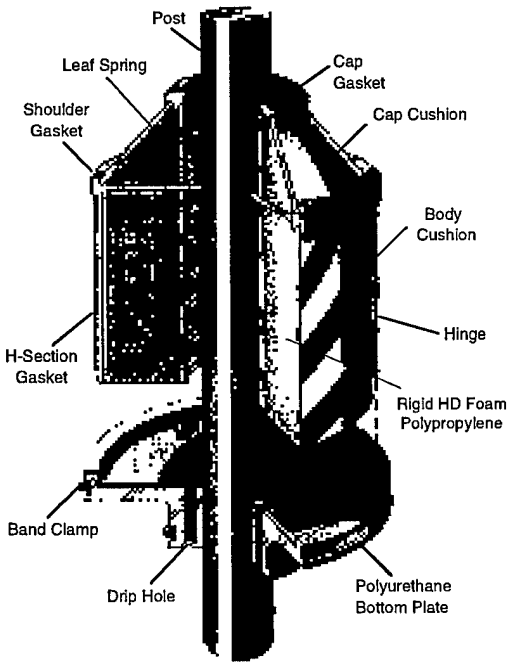

Figure 72. Cutout view of the conceptual crushable plastic cushion.

Conceptual design

A cutout view of the conceptual CPC is illustrated in Figure 72. The CPC would be mounted on a pole or a tree about 203.2 mm (8 in.) above the ground with the functional height extending to about 812.8 mm (32 in.) above the ground. This would give a crush length of about 610 mm (24 in.). Including the cap cushion, the overall length of the CPC would be approximately 1.02 m (40 in.), as shown in Figure 73. It has been designed to produce a potentially lightweight, compact, and radially symmetrical configuration that can be easily constructed. The body will consist of two

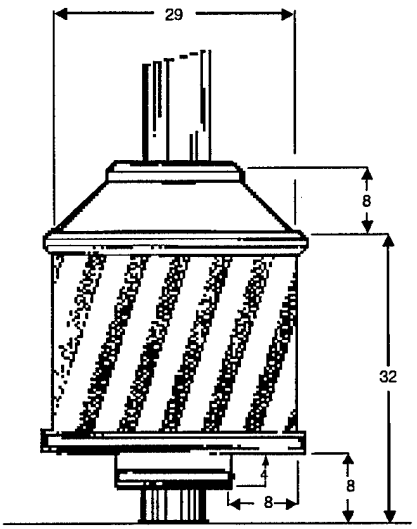

Figure 73. Overall view of the conceptual crushable plastic cushion. (Dimensions are in inches.)

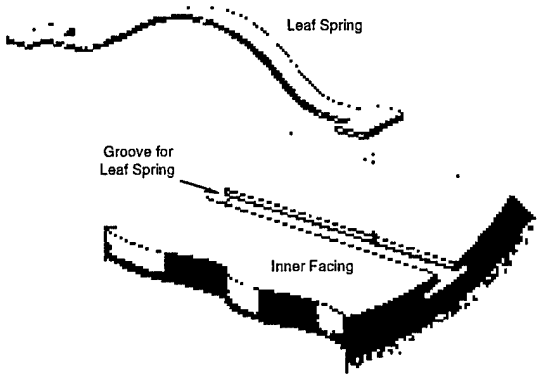

Figure 75. Details of the leaf spring and its T-groove on the inner facing.

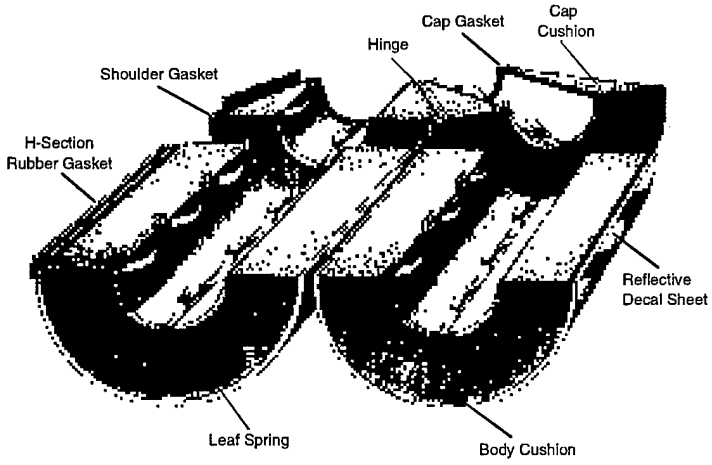

Figure 74. Illustration of the two halves of the crushable plastic cushion split open.

hubs of rigid high-density closed-cell polypropylene foam sandwiched between two FRP facings (Fig. 74). Both the outer facing and inner facing will be made of vinyl-ester-impregnated, chopped-glass-reinforced molded product. The outer facings of the two hubs will be joined with a full-length hinge to allow the two hubs to close around the rigid pole. A longitudinal groove in the foam on each hub will allow an H-section rubber gasket to seal the longitudinal open joint of the outer facings. Along the length of the inner facing, longitudinal T-grooves, molded in during casting, will receive a series of three stainless-steel leaf springs (Fig. 75). The leaf springs in four such slots, spaced at 90° apart, will hold the cushion in place against the pole. A conical cap cushion (Fig. 74) mounted directly above the cylindrical body cushion will allow excessive snow and water to drain, and will protect the crushable foam from excessive moisture and dirt. The cap cushion would be made of two hubs joined by a hinge. The cutout grooves in the foam surface of both the body cushion and the cap cushion will allow a specially profiled shoulder gasket to seal the cap cushion onto the body cushion (Fig. 72). The annulus between the inner facing and the pole will provide the dripping path for melted snow or rainwater. A specially molded polyurethane cap gasket configured with appropriate grooves and lips, and slit from the center, will serve as the top end-cap of the conical cap cushion. The bottom end-cap (Fig. 76) will also be made of molded polyurethane in two halves. The outer facing of the body cushion will fit into the recess of the bottom end-cap, which will be clamped together with a stainless-steel band clamp. Another stainless-steel band clamp of smaller diameter will tightly clamp the neck portion of the bottom end-cap onto the pole. The bottom end-cap will provide openings between the radial ribs through which water dripping from the pole can pass down. The outer surface of the outer FRP facing will have a bonded reflective decal sheet for easy recognition of the crush cushion at night or low lighting. Special care has been taken in this design to make it adaptable not only to fixed posts, but also to small or

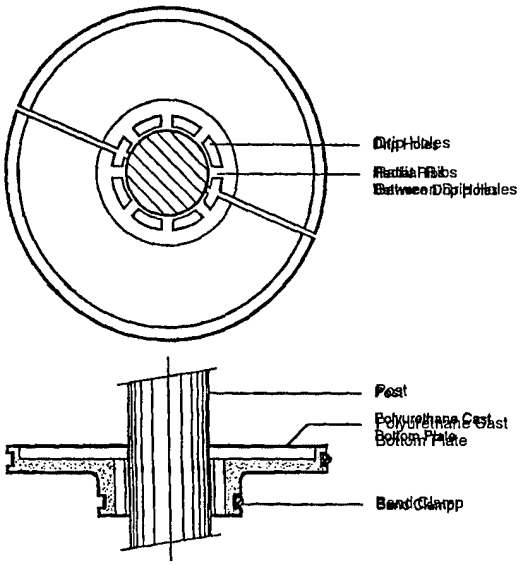

Figure 76. Details of the bottom end-cap.

medium roadside trees [approximately 20 cm (8 in.) in diam.]. Since the tree diameter grows, the inclusion of leaf springs can accommodate such growth. Dripping water would also not pose any problems. The crush cushion would be located and secured on the pole under the pressure of the leaf springs and by the two stainless-steel band clamps on the bottom end-cap. The slightly protruding cap gasket, shoulder gasket, and bottom end-cap will protect the decal surface from inadvertent damage by any large object. All gaskets, including the H-gasket that will hold the two halves of the body cushion together, are demountable. When required the entire crush cushion can be disassembled, cleaned or repaired, and then reassembled. Based on this conceptual design, a series of crush cushions can be developed for a range of pole or tree diameters. The inside diameter and outside diameter can be varied, depending on the requirements of crush attenuation. Because of the use of noncorrosive materials in all components, no corrosion problems are foreseen with this design.

Discussion

Because of safety hazards to errant motorists, the need for a feasible design for a crushable cushion for roadside fixed objects or structures cannot be overemphasized. The cushion concept developed above is purely exploratory. The scope of the current investigation did not allow any rigorous engineering analysis and design development for the concept. However, materials, shapes, and components that would provide a feasible preliminary design have been considered. Attempts were also made to cast some components out of polymeric materials, but as with most molding operations, the cost of tooling to mold or cast initial design parts became prohibitive. If this design is to be pursued, considerable capital investment will be needed for developing the tooling. Once all tooling is available for large-scale production, the cost of each unit would be very low. There are three rubber gaskets and one end-cap that require molding with either rubber or polyurethane. The inner FRP facing must be cast or machined with a slot to accept the leaf springs. In making the sandwich hubs for the body and cap cushions, additional machining for groove cutting in the foams would be needed. Assembling the crush cushion at the site would be very easy with the help of gaskets and band clamps.

CHAPTER 8: GENERAL REMARKS AND RECOMMENDATIONS

Composites are not being used in any large scale for highway safety structures. Yet, over the decade from 1984–1993, composites production grew about 40% in the U.S., from 0.79 to 1.11 million Mg (0.87 to 1.22 million tons) (Phelps 1994). This growth, although slow, happened only because of many significant advantages of composites in civil engineering applications over traditional materials. The present studies have shown how composites could be incorporated into components of highway safety structures. The definition of composites in this case included both the fiber-reinforced plastics (FRP) and the composites of recycled plastics with other fibrous additives like sawdust. The safety structures for which composites were considered included W-beam guardrails, guardrail posts and blockouts, rebars for concrete reinforcement, breakaway couplers for the luminaries and sign supports, and crushable cushions for roadside fixed objects like poles and trees.

The design study of FRP composite W-beam guardrail was limited to a small batch fabrication process, such as hand layup with vacuum bag technology. The scope did not allow developing commercial fabrication technology like tooling and dies for pultrusion processes. However, the batches were made in sufficient quantities and in three different thickness to test them for comparative mechanical performance.

The designing and manufacturing of the FRP W-beam profile showed that the process is more an art than a science. The vendor used the laminate theory as a first approximation to produce the first batch (RL) of laminates, but the desired tensile strength of 482.3 MPa (70,000 psi) was not developed. Subsequently, a series of batches was produced through trial and error (see Table 3), where the knowledge and experience of the vendor contributed to achieving the final and optimum strength of 447.9 MPa (65,000 psi). The vacuum process did not lead to sufficient squeezing pressure for improving the fiber volume fraction, as did the pultrusion process. The pultrusion process also produced a higher tensile strength.

The stiffness of the 6.1-m- (20-ft-) long FRP W-beams was sufficient for transportation and handling purposes, but was about one-third of steel W-beam's stiffness (see Table 5). This may not be a major disadvantage in its application as a guardrail. In flexural tests, it was observed that even a fractured FRP W-beam bounced back to a linear shape after the load was removed. Thus, in installations of FRP W-beam, the post-damage replacements could perhaps be delayed. Another major difference with steel is in the energy absorption characteristics. The drop impact tests showed that the fracture initiation energy of the FRP is higher than steel's, because FRP's brittle behavior in post-fracture energy absorption is lower. However, for composites, the properties of fibers and resins and the geometrical arrangement of the fibers can be controlled so that progressive crushing occurs.

The study showed that it is feasible to produce a W-beam of the same profile but of a different thickness than the standard AASHTO steel W-beams. The laminate designs could be customized and optimized to obtain the desired strength, stiffness, and impact characteristics. However, the splicing and jointing techniques are yet to be developed. In the standard 19.05-mm (0.75-in.) bolt pullout tests, the joint failed at only about 14% of the laminate strength. This is an area of future research.

In this effort, we tried to mimic the shape of the steel W-beam and then look at the performance. In a wider scope of research, a more desirable goal would possibly be to reinvestigate what mechanical performance and functional goals are needed for a guardrail, and then review whether the current W-beam profile is also ideal for composite guardrails. In future studies, different profiles may emerge that would have better failure characteristics and, consequently, better energy management in overall structure and interaction with posts and blockouts.

The study of the applications of composites for posts and blockouts focused totally on recycled plastic composites (RPC). This was an attractive goal from the perspective of improving the environment by first developing an increased opportunity for the use of plastic wastes, and then reducing timber consumption and the associated groundwater contamination from timber preservatives as creosote. The commercially available RPC materials were examined and a selected RPC was thoroughly tested for mechanical properties. No standard test methods were available for these materials, and the compression, tension, and flexural test methods needed to be developed. The results of the compression tests, in which relatively larger sized specimens were used, showed much less variability than the tension and flex

ure tests, where specimen sizes were relatively small (see Table 13). Thus, the variability of the properties appeared to be size dependent, with larger sizes having less variability. The results also showed directional variability (anisotropy) both in the compression and tension tests.

The presence of a small amount of moisture in RPC tends to increase the compressive strength and decrease the flexural strength (see Table 13). The exact mechanism of this phenomenon is not clear, but is possibly related to nonhomogeneity in the moisture distribution and the resulting stresses through the cross section of the specimens.

A comparison of Tables 7b and 7c shows that for the RPC, low temperature has the most significant effect on its mechanical properties. The strain at failure decreased significantly, as expected, indicating a tendency toward more brittleness. Simultaneously, the stiffness (modulus) and strength increased dramatically.

Relating the mechanical properties of the RPC to the design of guardrail posts or blockouts is not straightforward, because the analytical design is too complex. The relationship depends not only on the material properties and structural response of the rails and posts, but also on the restraining forces of the soil. It also includes dynamic effects, large displacements, stiffness, yield strength, and the inelastic behavior of all materials in the system, the final goal of which is to redirect errant vehicles and other traffic to safety. Experience and knowledge are the key factors in designing the system; therefore, highway engineers rely on trial and error in evaluating candidate systems by crash testing.

For a large-scale application of RPC in highway structures or in civil engineering, two things are needed: (1) nationally acceptable, standardized test methods to ensure consistency in quality from the suppliers, and (2) additional research and tests to assess performance under prolonged stress, wider ranges of temperature, and cyclic periods of heat, cold, and dampness. The FHWA approved RPC blockouts, which when used by some State DOTs, can provide valuable field data for such assessments and evaluations.

The quickest implementation of FRP composites in civil engineering is FRP rebars for concrete reinforcement. The present study evaluated with the creep behavior of FRP rebar at low-temperature, room-temperature, and high-temperature conditions using a deadweight loading system. Only a very small trend of increasing strain was observed at high-temperature testing, from which the creep parameter results match Mosallam and Chamber's (1995) published values for commercially available, pultruded FRP WF beams: $p = 9.72$ and $q = 0.298$. These results, however, did not follow Findley's classical creep equation, possibly because of the scatter in the data. If the tests had been continued over a longer time, a more discernible creep strain might have developed. The data at room temperature and low temperature did not show any trend of increasing; therefore, they were not analyzed with Findley's equation. It must be noted that Findley's theory applies very well to viscoelastic polymers, but in composites, when the stress is applied in the fiber direction, the behavior is not totally viscoelastic. In fact, with a higher volume fraction of glass fibers oriented in the load direction, the creep in FRP composites is not expected to be a problem.

The application of FRP in breakaway couplers, although attractive at first, actually presents serious problems if the design is a "one-to-one" replacement of steel couplers. The FRP coupler failures (Fig. 71a and b) in fiber-reinforced composites are strongly direction oriented, and the failure mechanism is controlled by the fiber architecture. In order to have a clean, transverse, shear break in a necked-down breakaway coupler made with FRP composites, the fiber architecture has to be developed and designed properly. The design must force the failure to be induced by interlaminar or interfacial bond failure in the transverse direction to the bolt, without reducing the longitudinal strength to withstand wind and ice loads. Further research and design development through microstructural analysis of composites are needed to accomplish this. The composite breakaway coupler in this case would have to be precast rather than machined from the commercially available bar stocks.

Crushable plastic cushions to protect vehicle occupants from side impacts with roadside fixed objects is another potential application for FRP composites and plastics for highway safety structures. This investigation was confined only to a conceptual design, shown in Figure 74. The design requires three rubber gaskets, and one endcap to be molded with either rubber or polyurethane. The inner FRP facing would be cast or machined with a slot to accept the leaf springs. In making the sandwich hubs for the body and cap cushions, additional machining for groove cutting in the foams would be needed. Assembling

of the crush cushion at the site would be very easy with the help of gaskets and band clamps. Once all tooling is available for large-scale production, the cost of each unit would be very low. However, like most FRP components, the initial cost of tooling and die making is daunting.

In this study, we focused on several highway safety structures where FRP composites could be suitable, due to their corrosion resistance, light weight, high strength, design flexibility, low maintenance, and parts consolidation. These are tremendous advantages. However, the development of FRP composite materials and fabrication processes to provide parts that are at once cost effective, functional, and aesthetically appealing presents a significant challenge. The key to successful application probably lies in an approach that allows the new designs to outperform competitive products on the basis of cost and performance. Research has to be committed to bringing these FRP composite structures and components from the concept stage to the marketplace. The focus has to be to optimize the design and standardize the materials and processes, so that the FRP composites can be used where their particular cost is minimal and the physical, mechanical, and durability performance is maximized.

The introduction of any new material or innovative design does not guarantee automatic acceptance by the highway community. Those interested in the promotion of new products or concepts must appreciate the necessity of assuring that what is supplied will perform the necessary function, that quality control will ensure acceptable performance, and that production capability is adequate to satisfy demand.

LITERATURE CITED

AASHTO (1977) *Guide for Selecting, Locating and Designing Traffic Barriers*. American Association of State Highway and Transportation Officials, Washington, D.C.

AASHTO (1985) *Standard Specifications for Structural Supports for Highway Signs, Luminaries and Traffic Signals*. American Association of State Highway and Transportation Officials Subcommittee on Bridges and Structures, Washington, D.C., p. 40, 68.

AASHTO (1989) *Roadside Design Guide*. American Association of State Highway and Transportation Officials, Task Force for Roadside Safety, Washington, D.C., p. 5–11.

ACI (1958) Test procedure to determine relative bond value of reinforcing bars. American Concrete Institute, Committee 208. *ACI Journal*, 5: 1–16.

Anderson, R.G., E. Munley, and L.C. Bank (1994) Durability of concrete reinforced with pultruded fiber-reinforced plastic grating. *Plastics in Building Construction*, Vol. XVII, No. 9, Lancaster, Penn.: Technomic Publishing Co., p. 6–12.

Auchey, F.L., and P.K. Dutta (1996) The use of recycled high density polyethylene fibers as secondary reinforcement in concrete subjected to severe environment. In *Proceedings of the Sixth International Offshore and Polar Engineering Conference (1996)*, Los Angeles, California, 26–31 May, p. 287–291.

Ballinger, C. (1991) Development of composites for civil engineering. In *Proceedings, ASCE Advanced Composites Materials in Civil Engineering Structures, Las Vegas, Nevada* (S.L. Iyer and R. Sen, Ed.), p. 288–301.

Beckwith, S.W. (1984) Creep behavior of Kevlar/epoxy composites. In *Proceedings of the 29th SAMPE Symposium*, p. 578–591.

Bloomquist, D., G. Diamond, M. Ogden, B. Ruth, and M. Tia (1993) Engineering and environmental aspects of recycled materials for highway construction. FHWA Report No. FHWA-RD-93-088.

Bocker-Pedersen, O. (1974) *Journal of Materials Science*, 9: 948.

Brinson, H.F., W.I. Griffith, and D.H. Morris (1980) Creep rupture of polymer-matrix composites. *Fourth SESA International Congress on Experimental Mechanics*, Boston Massachusetts, p. 329–335.

Busel, J.P. (1995) *FRP Composites in Construction Applications*. New York, NY: Market Development Alliance, SPI Institute.

Cao, L., S.G. Byun, D.W. Baugh, C.L. Beatty, and R. Ramer (1991) Mechanical properties of recycled commingled post materials. In *Proceedings of Polymer Technology Conference, American Chemical Society*, Philadelphia, Pennsylvania, Vol. 32, No. 2, June, p. 129–130.

Challal, O., and B. Benmokrane (1992) Glass-fiber reinforcing rod: Characterization and application to concrete structures and grouted anchors, materials performance and prevention of deficiencies and failures. In *Proceedings of the Materials Engineering Congress, ASCE*, Atlanta, Georgia, p. 606–617.

Challal, O., and B. Benmokrane (1993) Pullout and bond of glass-fiber rods embedded in concrete and cement grout. *Materials and Structures*, **26**: 167–175.

Chamis, C.C. (1974) Mechanics of load transfer at the interface. *Composite Materials*, (Edwin P. Plueddemann, Ed.) Vol. 6, p. 31–77. New York: Academic Press.

Chen, S., and R.P. Lottman (1991) Buckling loads of columns made of viscoelastic materials. In *Proceedings, ASCE Mechanics, Computing in 1960's and Beyond* (H. Adeli, and R.L. Sierakowski, Ed.), p. 691–695.

Daniali, S. (1992) Development length of fiber reinforced plastic bars. *Advanced Composite Materials in Bridges and Structures*. First International Conference, Sherbrooke, Quebec, Canada, p. 179–188.

Dewimille, B., and A.R. Burnsell (1983) Accelerated aging of a glass fiber reinforced epoxy resin in water. *Composites*, **14**: 35.

Dillard, D.A., and H.F. Brinsonson (1983) *A Numerical Procedure for Predicting Creep and Delayed Failures in Laminated Composites*. ASTM STP 813 (T.K. O'Brien, Ed.), ASTM, Philadelphia, Pennsylvania, p. 23–37.

Dinitz, A.M., and D.B. Chisholm (1978) Development and testing of a breakaway support coupling for light poles. *Roadside Safety Appurtenances*, Transportation Research Record 679, National Academy of Sciences, Washington, D.C., p. 26–28.

Dutta, P.K. (1992) Tensile strength of unidirectional fiber composites at low temperatures. In *Proceedings of the Sixth Japan-U.S. Conference on Composite Materials*, 22–24 June, Orlando, Florida, p. 782–792.

Dutta, P.K. (1994) Low-temperature compressive strength of glass-fiber-reinforced polymer composites. *Journal of Offshore Mechanics and Arctic Engineering*, **116**: 167–172.

Dutta, P.K. (1995a) Durability of FRP composites in fiber reinforced structural plastics in civil engineering. In *Proceedings of the International Conference on Fiber Reinforced Structural Plastics in Civil*

Engineering, Indian Institute of Technology, Madras, 18–20 Dec., p. 360–370.

Dutta, P.K. (1995b) Durability of FRP composites in extreme environment. In *Proceedings of the Fifth International Offshore and Polar Engineering Conference*, The Hague, The Netherlands, 11–16 June, p. 271–276.

Dutta, P.K., and C.F. McDevitt (1994) Application of advanced composites crashworthy designs for highway guardrails. In *Proceedings of the International Conference on Composites Engineering, ICCE/1* (D. Hui, Ed.), 28–31 August, New Orleans, Louisiana, p. 337–338.

Eggleston, M.R. (1994) The transverse creep and tensile behavior of SCS-6/Ti-6AL-4V metal-matrix composites at 482°C. *Journal of Mechanics of Composite Materials and Structures*, **1**(1): 53–73.

English, L.K. (1987) Fabricating the future with composite materials. *Materials Engineering*, September, p. 20–21.

Faza, S.S. (1995) Properties of FRP reinforcing bars. *Fiber Reinforced Plastics Workshop*, Office of Technology Applications, FHWA, Washington, D.C.

Findley, W.N. (1960) Mechanism and mechanics of creep in plastics. *SPE Journal*, **16**(1): 57–65.

Findley, W.N. (1987) 26-year creep and recovery of polyvinyl chloride and polyethylene. *Polymeric Engineering and Science*, **27**(8): 582–585.

GangaRao, H. (1995) Mckinleyville jointless bridge with FRP bars in concrete deck. *Fiber Reinforced Plastics Workshop*, Office of Technology Applications, FHWA, Washington, D.C.

GangaRao, H. and S.S. Faza (1992) Bending and bond behavior and design of concrete beams reinforced with fiber-reinforced plastic rebars. Report on Phase I of West Virginia Department of Highways Project No. RP 83, 1992.

GangaRao, H.V.S., P.V. Vijay, and P.K. Dutta (1995) Durability of Composites in Infrastructure. The National Association of Corrosion Engineers (NACE) International 50th Annual Conference, *Corrosion 95*, Paper No. 550, NACE Publications Division, Houston, Texas.

Glaster, R.E., R.L. Moore, and T.T. Chiao (1983) Life estimation of an S glass/epoxy composite under sustained tensile loading. *Composites Technology Review*, **5**(21).

Glaster, R.E., R.L. Moore, and T.T. Chiao (1984) Life estimation of an S glass/epoxy composite under sustained tensile loading. *Composites Technology Review*, **6**(26).

Graf, N.L., J.B. Boos, and J.A. Wentworth (1976) *Single-Vehicle Accidents Involving Utility Poles.* Transportation Research Record 571, Transportation, Research Board, National Research Council, Washington, D.C., p. 36–43.

Hahn, H.T., and R.Y. Kim (1978) Swelling of composite laminates. In *Advanced Composite Materials-Environmental Effects* (J.R. Vinson, Ed.), ASTM-STP 658, American Society for Testing of Materials, Philadelphia, Pennsylvania, p. 98–130.

Heger, F.J. (Ed.) (1981) *Structural Plastics Design Manual*, Section 10.6. American Society of Civil Engineers.

Heil, C.C., and H.F. Brinson (1983) The nonlinear viscoelastic response of resin matrix composites. Composites structure 2. In *Proceedings of the Second International Conference on Composites Structures*, Paisley, Scotland, p. 271–281.

Hinch, J.A., R.P. Owings, and G.A. Manhard (1984) *Safety Modifications of Turned-Down Guardrail Terminals.* Volume II—Technical Report, Federal Highway Administration Report No. FHWA/RD-84/035, June.

Holmes, M., and T.A. Rahman (1980) Creep behavior of plastic box beams. *Composites*, p. 79–85.

Huang, J.S., and I.J. Gibson (1990) Creep of sandwich beams with polymer foam composites, *ASCE Journal of Materials in Civil Engineering*, **2**(3): 171–182.

Hull, D. (1983) Axial crushing of fiber reinforced composite tubes. *Structural Crashworthiness* (N. Jones and T. Wierzbicki, Ed.), London: Butterworths, p. 118–135.

IMCO Reinforced Plastics, Inc. (1995) *FIBERBOLT Fiberglass Studs and Nuts.* Commercial literature.

Ivey, D.L., and J.R. Morgan (1986) *Timber Pole Safety by Design.* Transportation Research Record 1065, Transportation, Research Board, National Research Council, Washington, D.C., p. 1–11.

Iyer, S., and M. Anigol (1991) Testing and evaluating fiberglass, graphite, and steel prestressing cables for pretensioned beams. In *Proceedings, ASCE Advanced Composites Materials in Civil Engineering Structures, Las Vegas, Nevada* (S.L. Iyer and R. Sen, Ed.), p. 44–56.

Karbhari, V.M. (1995) Civil infrastructure and composite materials: Issues in materials and manufacturing, in fiber reinforced structural plastics in civil engineering. In *Proceedings of the International Conference on Fiber Reinforced Structural Plastics in Civil Engineering*, Indian Institute of Technology, Madras, 18–20 December, p. 17–26.

Kim, P., and U. Meier (1991) CFRP cables for large structures. In *Proceedings, ASCE Advanced Composites Materials in Civil Engineering Structures, Las Vegas, Nevada* (S.L. Iyer and R. Sen, Ed.), p. 233–244.

Kimball, C.E., M.E. Bronstad, and L.C. Meczkowski (1982) Evaluation of guardrail breakaway cable terminals. Federal Highway Administration Report No. FHWA/RD-82/057.

Krisnaswamy, P., M.E. Tuttle, A.F. Emery, and J. Ahmad (1991) Finite element modeling of time dependent behavior of nonlinear ductile polymers. *Plastics and Plastic Composites*, MD-Vol. 29, p. 77–99. New York: American Society of Mechanical Engineers.

Larralde, J., and R. Siva (1990) Bond stress-slip relationships of FRP rebars in concrete, serviceability and durability in construction materials. In *Proceedings of the First Materials Engineering Congress*, Denver, Colorado, August 1990, p. 1134–1141.

Larsson, F. (1988) The effect of ultraviolet light on mechanical properties of Kevlar 49 composites. *Environmental Effects on Composite Materials* (G. Springer, Ed.), Vol. 3, p. 132–135. Lancaster, Penn.: Technomic Publishing Co.

Lord H.W., and P.K. Dutta (1988) On the design of polymeric composite structures for cold regions applications. *Journal of Reinforced Plastics and Composites*, 7: 435–450.

Lorenzo, L., and H.T. Hahn (1986) Fatigue failure mechanisms in unidirectional composites. *Composite Materials—Fatigue and Fracture*, ASTM STP 907, p. 210.

Malavar, L.J. (1994) Bond stress-slip characteristics of FRP rebars. Naval Facilities Engineering Service Center, Port Hueneme, California, Technical Report TR-2013-SHR.

Mallick, P.K. (1988) *Fiber Reinforced Composites.* New York: Marcel Dekker, Inc., p. 215–248.

Marshall, A. (1982) Sandwich construction. *Handbook of Composites* (G. Lubin, Ed.), p. 557–601. New York: Van Nostrand Reinhold Co.

McDevitt, C.F., and P.K. Dutta (1993) New and recycled plastic composites for roadside safety hardware. *Plastics in Building Construction*, XVIII(2): 6–12.

Meier, U., and H. Kaiser (1991) Strengthening of structures with CFRP laminates. In *Proceedings, ASCE Advanced Composites Materials in Civil Engineering Structures, Las Vegas, Nevada* (S.L. Iyer and R. Sen, Ed.), p. 224–232.

Michie, J.D. (1981) *Recommended Procedures for the Safety Evaluation of Highway Appurtenances.* Transportation Research Board, Washington, D.C., National Cooperative Highway Research Program Report No. 230, March 1981.

Middleton, L.B., J.Y. Huntley, and J.J. Burgiel (1991) *U.S. Navy Shipboard-Generated Plastic Waste Pilot Recycling Program, March 1991.* The Council for Solid Waste Solutions (A Program of the Society of the Plastic Industry Inc.), Washington, D.C.

Miller, W.L., and J.B. Johnson (1989) A review of environmental thermoplastic degradation. University of Florida, Report No. 89-2.

Monaghan, M.R., and L.C. Brinson (1994) Analysis of variable stress history on polymeric composite materials with physical aging. To be published in *Composites Engineering.*

Morrison Molded Fiber Glass Company (MMFG) (1994) *Extren Fiberglass Structural Shapes Design Manual.* Section 12, Bristol, Virginia.

Mosallam, A.S., and L.C. Bank (1991) Creep and recovery of pultruded FRP frame. In *Proceedings, ASCE Advanced Composite Materials in Civil Engineering Structures, Las Vegas, Nevada* (S.L. Iyer and R. Sen, Ed.), p. 24–35.

Mosallam, A.S., and R.E. Chambers (1995) Design procedure for predicting creep and recovery of pultruded composites. In *Proceedings of the 50th Annual Conference, Composites Institute,* The Society of Plastic Industry, p. 6C/1–13.

Phelps, E.F. (1994) Challenges for the composites industry in the 1990's, a global concern. In *Proceedings of the 39th International SAMPE Symposium and Exhibition,* Vol. 39, p. 2361–2372 (K. Drake, J. Baur, T. Serafini, P. Cheng, Ed.), SAMPE, Covina, California.

Pleimann, L.G. (1991) Strength, modulus of elasticity, and bond of deformed FRP rods. In *Proceedings, ASCE Advanced Composites Materials in Civil Engineering Structures, Las Vegas, Nevada* (S.L. Iyer and R. Sen, Eds.), p. 99–110.

Rivenite (1990) *Technical Information TIS-1-90.* Philadelphia, Pennsylvania: Riverhead Milling Inc.

Rizkalla, S.H., and A.A. Abdelrehman (1995) FRP for the 21st century, in fiber reinforced structural plastics in civil engineering. In *Proceedings of the International Conference on Fiber Reinforced Structural Plastics in Civil Engineering* (S.L. Iyer and V. Kalyanraman, Ed.), p. 3–16. New Delhi: Tata McGraw-Hill Publishing Co.

Roll, R.D. (1991) Use of GFRP rebar in concrete structures. In *Proceedings, ASCE Advanced Composites Materials in Civil Engineering Structures, Las Vegas, Nevada* (S.L. Iyer and R. Sen, Ed.), p. 93–98.

Ross, H.E., H.S. Perera, D.L. Sicking, and R.P. Bligh (1989) *Roadside Safety Designs for Small Vehicles.* National Cooperative Highway Research Program Report 318.

Seible, F. (1996) Advanced composite materials

for bridge in the 21st century. In *Proceedings of the 2nd International Conference on Advanced Composite Materials in Bridges and Structures, Montreal, 11–14 August*, p. 17–30 (M.M. El-Badry, Ed.). The Canadian Society of Civil Engineering.

Slattery, K.T. (1994) Mechanistic model of creep-rupture process in filamentary composites. In *Proceedings of the 3rd Materials Engineering Conference, ASCE, Infrastructure, New Materials and Methods of Repair, San Diego, California*, p. 215–222 (K.D. Basham, Ed.).

Svenson, A.L., M.W. Hargrave, and L.C. Bank (1993) Impact behavior of pultruded composites. *48th Annual Conference, Composites Institute*, February 8–11. The Society of Plastic Industry, Cincinnati, Ohio, Session 21-D/1–6.

Tao, S., M.R. Eshani, and H. Sadatmanesh (1992) Bond strength of straight GFRP rebars, materials performance and prevention of deficiencies and failures. *Proceedings of the Materials Engineering Congress, ASCE*, Atlanta, Georgia, p. 598–605.

Troxel, L.A., M.H. Ray, and J.F. Carney, III (1991) Side impact collisions with roadside obstacles. Transportation Research Board, 70th Annual Meeting, Paper No. 910732, January 13–17, Washington, D.C.

Tunik, A.L., and V.T. Tomashevskii (1974) *Mekhanika Polimerov*, Vol. 7, p. 893.

Tutt, P.R., and J.F. Nixon (1970) Roadside design guidelines, highway safety. In *Proceedings of the 2nd Western Summer Meeting*, Highway Research Board, Special Report 107, National Research Council.

Ueng, C.S. (1991) The elastic stability of the laminated composite columns. In *Proceedings, ASCE Mechanics, Computing in 1960's and Beyond* (H. Adeli and R.L. Sierakowski, Ed.), p. 971–974.

USDOT (1988) Technical summary. *Force-Deflection Characteristics of Guardrail Posts*, Publication No. FHWA-RD-88-193, October 1988.

Vinogradov, A.M. (1989) Long-term buckling of composite columns. In *Proceedings, ASCE Structures Congress*, San Francisco, California, p. 536–545.

Weidmann, G.W., and R.M. Ogorkiewicz (1974) *Composites*, 5: 117.

Willet, T., and C. Bennett (1990) W-beam guardrail end terminals. Federal Highway Administration Memorandum.

Wu, W.P., H. GangaRao, and J.C. Prucz (1990) Mechanical properties of fiber reinforced plastic bars. Internal Report, Constructed Facilities Center, College of Engineering, West Virginia University.

MATERIALS PROPERTIES

(Room Temperature: 14° C +/- 10° C)

Material	Method	Tens. Str. ksi	Elong. atBreak %	Tens. Yld Str. ksi	Cmp. Str. ksi	Flex. Str. ksi	El.Md. Tens. msi	El.Md. Cmp. msi	Flex. Mod. msi	Imp. Str. (a) ft*lb/in	Hrdnss	Therm. Exp. Coeff. in/in/Fx10e-6	Density lb/cu.in x10e-2	H20 Abs, % (b) 24 hr /Sat.	Pois's Ratio	Ref.
Epoxy (Glass Fabric)		65.0			55.0		3.60			30.0	112.5 (d)		6.5		0.140	1
Epoxy (Glass Fiber Reinforced,	ASTM D638	12.5	4.0				3.00									15
Bisphenol Molding Compound)	ASTM D695				29.0											15
	ASTM D790					19.0			3.25							15
	ASTM D256A									5.2						15
	ASTM D785										M106 (d)					15
	ASTM D696											17.000				15
	ASTM D792												6.5			15
	ASTM D570													0.12/-		15
Epoxy (Glass Filled, High-Strength,	ASTM D638	22.5														15
Novolak Molding Compound)	ASTM D695				34.0											15
	ASTM D790					60.0			3.50							15
	ASTM D2583										67 (e)					15
	ASTM D792												6.6			15
Epoxy (S-Glass Unidirectional)		215.0			95.0		7.10					2.300	6.9			1
Epoxy (Unfilled, Casting Resin and Com-	ASTM D638	8.5	4.5				0.35									15
pound)	ASTM D695				20.0											15
	ASTM D790					17.0										15
	ASTM D256A									0.6						15
	ASTM D785										M95 (d)					15
	ASTM D696											31.000				15
	ASTM D792												4.5			15
	ASTM D570													0.115/-		15
Epoxy (60% Graphite Fiber-Reinforced,	ASTM D638	20.0	0.4				6.00									15
Novolak Molding Compound)	ASTM D695				28.0											15
	ASTM D790					40.0			5.50							15
	ASTM D256A									10.0						15
	ASTM D785										R110 (d)					15
	ASTM D696											0.600				15
	ASTM D792												5.3			15
	ASTM D570													0.4/0.8		15
Epoxy S2-Glass/Filament Wound															0.242	2
Fiberglass Epoxy	MIL-HDBK-17	100.5			61.8		4.20									3
Fiberglass Epoxy (26% Resin)	ASTM D790					94.1										3
Hexcel F-161/7781 (ECDE-1/0-550)	Short Beam															3
Fiberglass Epoxy (31% Resin)	ASTM D790					90.2										3
Hexcel F-161/7781 (ECDE-1/0-550)																
Fiberglass Epoxy (36% Resin)	ASTM D790					86.3										3
Hexcel F-161/7781 (ECDE-1/0-550)																

Material	Method	Tens. Str. ksi	Elong. atBreak %	Tens. Yld Str. ksi	Cmp. Str. ksi	Flex. Str. ksi	El.Md. Tens. msi	El.Md. Cmp. msi	Flex. Mod. msi	Imp. Str. (a) ft*lb/in	Hrdnss	Therm. Exp. Coeff. in/in/Fx10e-6	Density lb/cu.in x10e-2	H20 Abs, % (b) 24 hr /Sat.	Pois's Ratio	Ref.
Fiberglass Epoxy 3M XP251S	ASTM D790					164.2										3
0-90 Deg. Crossply	MIL-HDBK-17	141.4														3
	SEE TEXT				91.2		4.72	4.75								3
	Short Beam															3
Fiberglass Epoxy 3M XP251S	ASTM D790					219.6										3
100%-0 Deg. Direction	MIL-HDBK-17	276.0														3
	SEE TEXT				100.0		7.99	7.52								3
	Short Beam															3
Fiberglass Epoxy 3M XP251S	ASTM D790					133.4										3
Quasi-Isotropic	SEE TEXT	76.2			81.6		3.95	3.90								3
	Short Beam															3
Fiberglass Epoxy Bloomingdale	ASTM D638 Type 1						3.85									3
BP-911/7781 (ECDE-1/0-VOLAN)	ASTM D790					97.4										3
	MIL-HDBK-17	72.3			73.5			3.94								3
	Short Beam															3
Fiberglass Epoxy Bloomingdale	ASTM D638 Type 1						3.15									3
BP-915/7781 (ECDE-1/0-550)	ASTM D790					86.6										3
	MIL-HDBK-17	58.0			56.7			3.67								3
	Short Beam															3
Fiberglass Epoxy Cordo	ASTM D638						3.39									3
E-293/7781 (ECDE-1/0-550)	ASTM D790					92.2										3
	MIL-HDBK-17	68.6			67.0			4.11								3
	Short Beam															3
Fiberglass Epoxy Hexcel	ASTM D790					94.6										3
F-161/3405 (S1014-S24)	MIL-HDBK-17	85.6			68.4		3.96	3.97								3
	Short Beam															3
Fiberglass Epoxy Hexcel	ASTM D790					160.0										3
F-161/7743 (550)	MIL-HDBK-17	95.5			75.9		5.30	4.96								3
	Short Beam															3
Fiberglass Epoxy Hexcel	ASTM D790					103.9										3
F-161/81 (S994-904)	Short Beam															3
	MIL-HDBK-17	100.5			61.8		4.20	3.90								3
Fiberglass Epoxy Narmco	ASTM D638 Type 1						3.71									3
N-588/7781 (ECDE-1/0-550)	ASTM D790					90.4										3
	MIL-HDBK-17	58.4			74.0			4.18								3
	Short Beam															3
Fiberglass Epoxy US Polymeric	ASTM D790					91.7										3
E-720E/7781 (ECDE-1/0-550)	MIL-HDBK-17	60.4			64.8			3.25								3
	Short Beam															3
Fiberglass Epoxy US Polymeric	ASTM D790					108.1										3
E-779/7743 (VOLAN)	MIL-HDBK-17	93.6			50.4		4.66	4.17								3
	Short Beam															3
Fiberglass Modified DAP Plystr	FED-STD 406	64.4			50.7	76.6	3.38	3.57								3
Cordo IFRR/7781 (ECDE-1/0)																

Material	Method	Tens. Str. ksi	Elong. atBreak %	Tens. Yld Str. ksi	Cmp. Str. ksi	Flex. Str. ksi	El.Md. Tens. msi	El.Md. Cmp. msi	Flex. Mod. msi	Imp. Str. (a) ft*lb/in	Hrdnss	Therm. Exp. Coeff. in/in/Fx10e-6	Density lb/cu.in x10e-2	H20 Abs, % (b) 24 hr /Sat.	Pois's Ratio	Ref.
Fiberglass Modified DAP Plystr	FED-STD 406	64.4			66.5	85.5	3.74	4.21								3
US Polymer P-670A/7781 (ECDE-1/0)																
Fiberglass Polyester	MIL-HDBK-17	69.1			72.6											3
	N/A						3.34									3
Fiberglass Polyester Ferro	ASTM D790					95.4										3
CP1304/7781 (550)	MIL-HDBK-17	69.1			72.6		3.34	3.29								3
	Short Beam															3
Fiberglass Polyester	ASTM D790					107.5										3
Hexcel F-141/7781 (550)	MIL-HDBK-17	84.6			71.0		4.10	4.04								3
	Short Beam															3
Glass Epoxy (Scotchply 1002)	Long.	154.0			88.5		5.6					4.778			0.260	4
	Trans.	4.5			17.1		1.2									4
Glass Fiber (S2)	Long.	700.0					12.50					2.778				5
															0.220	5
Graphite Epoxy (AS-5/3501)		250.0					16.00									6,7
Graphite Epoxy (AS/3501)	Long.	209.9			209.9		20					neg. 0.167			0.300	4
	Trans.	7.5			29.9		1.23									4
Graphite Epoxy (AS/3501-5A) L1	Long.	83.0			83.0											8
	Trans.	84.9			68.7											8
Graphite Epoxy (AS/3501-5A) L2	Long.	142.5			138.2											8
	Trans	23.3			43.8											8
Graphite Epoxy (AS/3501-5A) U1	Trans.	3.7			34.8											8
	Long.	214.2														8
Graphite Epoxy (AS/3501-5A) U1	Long.				155.6											8
Unidirectional																
Graphite Epoxy (AS/3501-6)													5.8			9
Graphite Epoxy (Hercules 3002M)		94.0					0.28	22.00								6,7
Graphite Epoxy (High Modulus)	Long.	110.0			100.0		25.00					neg. 0.300	5.6		0.300	11
		160.0			96.0		38.50						5.8		0.199	1
Graphite Epoxy (High Strength)	Long.	180.0			180.0		21.00					neg. 0.210	5.6		0.210	11
Graphite Epoxy (Int. Modulus)		235.0			221.5		25.00			28.0			5.6		0.045	1
Graphite Epoxy (Int. Strength)	Long.	160.0			160.0		17.00					0.300	5.5		0.210	11
Graphite Epoxy (Narmco 5206)		174.0					25.00	19.00								6,7
Graphite Epoxy (T300/1034)													5.8			9
Graphite Epoxy (T300/5208)	0-Deg.	210.0			247.4											8
	90-Deg.				28.6											8
	Long.	218.0			218.0		26.3					0.011			0.280	4
	n/a												5.8			4
	Short Beam															8
	Trans.	5.8			35.7		1.49									4
Graphite Epoxy (T300/5208)		24.0					2.60									8
(+/- 45)-2S Lay Up																
Graphite Epoxy (T300/5208)		85.0					8.10									8
(+/- 45)-S Lay Up																

Material	Method	Tens. Str.	Elong. atBreak	Tens. Yld Str.	Cmp. Str.	Flex. Str.	El.Md. Tens.	El.Md. Cmp.	Flex. Mod.	Imp. Str. (a)	Hrdnss	Therm. Exp. Coeff.	Density lb/cu.in	H20 Abs, % (b)	Pois's Ratio	Ref.
		ksi	%	ksi	ksi	ksi	msi	msi	msi	ft*lb/in		in/in/Fx10e-6	x10e-2	24 hr /Sat.		
Graphite Epoxy (T300/5208)		219.0					18.10									8
(0)-6 Lay Up																
Graphite Epoxy (T300/5208)		78.0					0.01									8
(0/90/ +/- 45)-S Lay Up																
Graphite Epoxy (T300/5208)		6.0					1.60									8
(90)-15 Lay Up																
Graphite Epoxy (T300/5208)		27.0					3.70									8
(90/ +/- 45)-S Lay Up																
Graphite Epoxy (T300/5208) L1	Long.	76.4			70.6											8
	Trans.	77.8			58.2											8
Graphite Epoxy (T300/5208) L2	Long.	149.4			130.6											8
	Trans.	20.3			33.8											8
Graphite Epoxy (T300/5208) U1	Long.	196.7			143.4											8
	Trans.	4.0			30.0											8
Graphite Epoxy (T300/934)	0-Deg.				252.1											8
	90-Deg.				27.7											8
	Short Beam															8
Graphite Epoxy (Thornel 300)		219.0					28.00	17.00								6,7
Graphite Epoxy (Woven)		87.5			100.0		10.20						6.0		0.077	1
Graphite Epoxy ATS 2002 HMS TR		6.3			31.5											12
Graphite Epoxy ATS 2002 HMS		130.0					0.03									12
Unidirectional																
Graphite Epoxy Unidirectional		218.0			218.0		26.30									1
Graphite Epoxy Unidirectional		197.7			157.4		20.30									1
29-33% Resin 1.7-2.4% Void																
Graphite Fiber (Hercules AS)	Long.	450.0					32.00					neg. 0.200				5
															0.200	5
Graphite Fiber High Modulus		300.0					55.00						7.0			11
Graphite Fiber High Strength		400.0					38.00						6.5			11
Graphite Fiber Intermediate		360.0					27.00						6.3			11
Kevlar							18.10								0.170	13
Kevlar (Ionomer Resin) Random		17.3					0.73									1
Kevlar (Ionomer Resin) Unidirectional		22.9					1.29									1
Kevlar (Nylon 12 Resin) Random		15.5					0.61									1
Kevlar (Nylon 12 Resin) Unidirectional		22.0					1.24									1
Kevlar (PolyCarbonate Resin) Random		16.8					0.73									1
Kevlar (PolyCarbonate Resin) Unidir.		23.7					1.42									1
Kevlar (Polyethylene Resin) Random		10.7					0.75									1
Kevlar (Polyethylene Resin) Unidir.		19.1					1.54									1
Kevlar (Polymethyl Methacrylat.) Random		26.4					1.13									1
Kevlar (Polymethyl Methacrylat.) Unidir.		30.1					1.61									1
Kevlar Fabric (Epoxy BP-907)		75.0					4.50									1
Kevlar Fabric (Polyester) Altac		64.0					3.40									1
Kevlar Fabric (Polyester) Corezyn		60.0					3.50									1
Kevlar, Longitudinal												neg. 1.111				13

Material	Method	Tens. Str. ksi	Elong. atBreak %	Tens. Yld Str. ksi	Cmp. Str. ksi	Flex. Str. ksi	El.Md. Tens. msi	El.Md. Cmp. msi	Flex. Mod. msi	Imp. Str. (a) ft*lb/in	Hrdnss	Therm. Exp. Coeff. in/in/Fx10e-6	Density lb/cu.in x10e-2	H20 Abs, % (b) 24 hr /Sat.	Pois's Ratio	Ref.
Polyester (24.9% Glass)		10.5					1.20			9.7						1
2 Ply Mat. 2 Ply Cloth																
Polyester (28.2% Glass) 2 Ply Mat.		14.1					0.92			9.0						1
Polyester (28.4% Glass)		10.5					0.89			8.2						1
1 Ply Mat. 1 Ply Cloth																
Polyester (30% Glass)	D638	19.0					12.00									1
	D695				18.0											1
Polyester (30.1% Glass)		15.0					0.95			9.8						1
2 Ply Mat. 1 Ply Cloth																
Polyester (32% Glass)		13.9					1.10			9.8						1
2 Ply Mat. 1 Ply Cloth																
Polyester (32% Glass)		13.2					0.92			12.0						1
3 Ply Mat. 1 Ply Cloth																
Polyester (38.3% Glass)		17.1					1.25			31.5						1
1 Ply Cloth 1 Ply Woven 1 Ply Mat.																
Polyester (39.2% Glass)		30.3					1.59			31.2						1
1 Ply Mat. 3 Ply Fabmat																
Polyester (42.5% Glass)		18.5					0.78									1
2 Ply Cloth 1 Ply Woven																
Polyester (52.7% Glass)		39.0					1.85			36.3						1
2 Ply Woven																
Polyester (53.2% Glass)		29.0					2.20			45.8						1
1 Ply Mat 2 Ply Woven																
Polyester (EA-SMC-R30)		4.4					1.26								0.300	10
Polyester (Glass Fabric)		44.0			40.0		2.40			16.0	110.0 (d)	10.000	6.2		0.110	1
Polyester (MAT) 15-25% Glass		10.0			20.0		1.60			10.0	95.0(d)	10.000	5.5		0.115	1
Polyester (MAT) 30-40% Glass		22.5			26.5		1.80			14.0	105.0 (d)	12.000	6.2		0.110	1
Polyester (SMC-C20/R30)	Long.	41.9			44.4	93.5	3.10	2.96							0.300	10
	Trans.	12.2			24.1	0.1	1.80	1.77							0.180	10
Polyester (SMC-R25)	Short Beam															10
		11.9			26.5	31.9	1.93	1.70							0.250	10
Polyester (SMC-R50)	Short Beam															10
		23.8			32.6	45.5	2.29	0.002							0.310	10
Polyester (SMC-R57)		23.2					2.39									10
Polyester (SMC-R65)	Short Beam															10
		32.9			35.0	58.5	2.13	0.003							0.260	10

Material	Method	Tens. Str. ksi	Elong. atBreak %	Tens. Yld Str. ksi	Cmp. Str. ksi	Flex. Str. ksi	El.Md. Tens. msi	El.Md. Cmp. msi	Flex. Mod. msi	Imp. Str. (a) ft*lb/in	Hrdnss	Therm. Exp. Coeff. in/in/Fx10e-6	Density lb/cu.in x10e-2	H20 Abs, % (b) 24 hr /Sat.	Pois's Ratio	Ref.
Polyester (Thermoplastic)	D256															1
	D696									1.4						15
30% Glass Fiber-Reinforced, Polyester/	ASTM D638	12.7														15
Polycarbonate Blend	ASTM D695				11.2											15
	ASTM D790					20.0			0.82							15
	ASTM D256A									3.2						15
	ASTM D785										R109.5 (d)					15
	ASTM D696											14.000				15
	ASTM D792												5.3			15
	ASTM D570													0.095/ -		15
30% Glass Fiber-Reinforced, Wholly	ASTM D638	20.0	1.7				2.30									15
Aromatic (Liquid Crystal)	ASTM D695				9.9			0.47								15
	ASTM D790					23.3			1.94							15
	ASTM D256A									2.0						15
	ASTM D785										77 (d)					15
	ASTM D696											6.390				15
	ASTM D792												5.8			15
	ASTM D570													<0.1/ -		15
40% Glass Fiber-Filled, Wholly	ASTM D638	13.6	1.8				1.87									15
Aromatic (Liquid Crystal)	ASTM D695				10.4			0.42								15
	ASTM D790					20.5			1.32							15
	ASTM D256A									1.6						15
	ASTM D785										79 (d)					15
	ASTM D696											8.280				15
	ASTM D792												6.1			15
	ASTM D570													<0.1/ -		15
Polyester (Thermosetting and Alkyd)																
Alkyd Molding Compound																
Glass-Fiber Reinforced	ASTM D638	6.8					2.40									15
	ASTM D695				25.5											15
	ASTM D790					16.3			2.00							15
	ASTM D256A									8.3						15
	ASTM D785										E95 (d)					15
	ASTM D696											13.000				15
	ASTM D792												7.8			15
	ASTM D570													0.265/ -		15
Glass Fiber-Reinforced																
Preformed, Chopped Roving	ASTM D638	22.5	3.0				1.40									15
	ASTM D695				22.5											15
	ASTM D790					25.0			2.00							15
	ASTM D256A									11.0						15
	ASTM D2583										65 (e)					15
	ASTM D696											19.000				15
	ASTM D792												6.6			15
	ASTM D570													0.505/ -		15

Material	Method	Tens. Str. ksi	Elong. atBreak %	Tens. Yld Str. ksi	Cmp. Str. ksi	Flex. Str. ksi	El.Md. Tens. msi	El.Md. Cmp. msi	Flex. Mod. msi	Imp. Str. (a) ft*lb/in	Hrdnss	Therm. Exp. Coeff. in/in/Fx10e-6	Density lb/cu.in x10e-2	H20 Abs, % (b) 24 hr /Sat.	Pois's Ratio	Ref.
Polyester (Thermosetting and Alkyd)																
Glass Fiber-Reinforced																
Premix, Chopped Glass	ASTM D638	6.5	< 1.0				1.75									15
	ASTM D695				25.0											15
	ASTM D790					13.5			1.50							15
	ASTM D256A									8.8						15
	ASTM D2583										65 (e)					15
	ASTM D696											15.000				15
	ASTM D792												7.1			15
	ASTM D570													0.17/ -		15
SMC	ASTM D638	16.0	3.0				1.95									15
	ASTM D695				22.5											15
	ASTM D790					23.0			1.60							15
	ASTM D256A									14.5						15
	ASTM D2583										60 (e)					15
	ASTM D696											9.300				15
	ASTM D792												7.7			15
	ASTM D570													0.175/ -		15
SMC, Low-Shrink	ASTM D638	12.3	4.0				1.75									15
	ASTM D695				22.5											15
	ASTM D790					22.0			1.75							15
	ASTM D256A									8.8						15
	ASTM D2583										55 (e)					15
	ASTM D696											10.000				15
	ASTM D792												7.2			15
	ASTM D570													0.13/ -		15
Woven Cloth	ASTM D638	40.0	1.5				3.00									15
	ASTM D695				37.5											15
	ASTM D790					60.0			2.00							15
	ASTM D256A									17.5						15
	ASTM D2583										70 (e)					15
	ASTM D696											13.000				15
	ASTM D792												6.5			15
	ASTM D570													0.275/ -		15
Polyester (XMC-3)	Long.	81.4			69.6	141.0	5.18	5.40							0.310	10
	Short Beam															10
	Trans.	10.0			23.2	20.2	1.78	2.10							0.116	10
Polyester-Styrene (Poly-Con)		2.0			8.5						50.0 (e)	13.100				11

Material	Method	Tens. Str. ksi	Elong. atBreak %	Tens. Yld Str. ksi	Cmp. Str. ksi	Flex. Str. ksi	El.Md. Tens. msi	El.Md. Cmp. msi	Flex. Mod. msi	Imp. Str. (a) ft*lb/in	Hrdnss	Therm. Exp. Coeff. in/in/Fx10e-6	Density lb/cu.in x10e-2	H20 Abs, % (b) 24 hr /Sat.	Pois's Ratio	Ref.
Polyetheretherketone																
30% Carbon Fiber-Reinforced	ASTM D638	31.4	2.5				2.68									15
	ASTM D695				29.7											15
	ASTM D790					44.0			2.22							15
	ASTM D256A									1.8						15
	ASTM D696											10.000				15
	ASTM D792												5.2			15
	ASTM D570													0.09/0.06		15
30% Glass Fiber-Reinforced	ASTM D638	25.5	2.5				1.43									15
	ASTM D695				21.9											15
	ASTM D790					37.5			1.43							15
	ASTM D256A									2.4						15
	ASTM D696											9.000				15
	ASTM D792												5.5			15
	ASTM D570													0.09/0.115		15
Polyethylene HD												61.000	3.4			14
Polyethylene Homopolymer,	ASTM D638	3.9	0.6	4.3			0.16									15
High Density	ASTM D695				3.2											15
	ASTM D790								0.19							15
	ASTM D256A									2.2						15
	ASTM D2240										D69.5 (f)					15
	ASTM D696											47.000				15
	ASTM D792												3.5			15
	ASTM D570													<0.01/ -		15
Polyethylene and Ethylene Copolymer, HD																
High Molecular Weight Copolymer	ASTM D638	3.4	0.5	3.35			0.136									15
	ASTM D695															15
	ASTM D790								0.15							15
	ASTM D256A									3.9						15
	ASTM D2240										D64 (f)					15
	ASTM D696											50.000				15
	ASTM D792												3.5			15
Ultra High Molecular Weight	ASTM D638	5.6	0.5	3.55												15
	ASTM D695															15
	ASTM D790								0.14							15
	ASTM D256A									No Break						15
	ASTM D785										R50 (d)					15
	ASTM D696											72.000				15
	ASTM D792												3.4			15
	ASTM D570													< 0.01		15

Material	Method	Tens. Str. ksi	Elong. atBreak %	Tens. Yld Str. ksi	Cmp. Str. ksi	Flex. Str. ksi	El.Md. Tens. msi	El.Md. Cmp. msi	Flex. Mod. msi	Imp. Str. (a) ft*lb/in	Hrdnss	Therm. Exp. Coeff. in/in/Fx10e-6	Density lb/cu.in x10e-2	H20 Abs, % (b) 24 hr /Sat.	Pois's Ratio	Ref.
Polyethylene and Ethylene Copolymer, HD																
30% Glass Fiber-Reinforced	ASTM D638	8.25	2.0				0.8									15
	ASTM D695				6.5											15
	ASTM D790					11.5			0.75							15
	ASTM D256A									1.3						15
	ASTM D785										R82.5 (d)					15
	ASTM D696											27.000				15
	ASTM D792												4.4			15
	ASTM D570													0.04/ -		15
20-30% Long Glass Fiber-Reinforced	ASTM D638	7.75	2.3				0.85									15
	ASTM D695				5.5											15
	ASTM D790					8.75			0.70							15
	ASTM D256A									3.0						15
	ASTM D785										R82.5 (d)					15
	ASTM D792												4.1			15
	ASTM D570													0.055/ -		15
PVC Molding Compound, 20% Glass	ASTM D638	10.7	3.5				0.825									15
Fiber-Reinforced	ASTM D695															15
	ASTM D790					18.35			0.83							15
	ASTM D256A									1.5						15
	ASTM D785										R113.5 (d)					15
	ASTM D2240										D87 (f)					15
	ASTM D696											17.000				15
	ASTM D792												5.3			15
	ASTM D570													0.01/ -		15

(a) Izod Impact, ft -lb /in of notch (1/8-in thick specimen)	(d) Units = Rockwell
(b) 1/8-in thick specimen	(e) Units = Barcol
	(f) Method = Shore

1. Lubin, G., editor. Handbook of Composites. Van Nostrand Reinhold Co., New York, New York., 1982.
2. Recent Advances in Composites in the United States and Japan. American Society for Testing and Materials, Philadelphia, PA, 1985.
3. Military Handbook: Plastics For Aerospace Vehicles. Department of Defense, Washington, D. C., 1971.
4. Tsai, Stephen W., Hahn, H. Thomas. Introduction to Composite Materials. Technomic Publishing Co., Lancaster, PA, 1980.
5. Cairns, D. S., Adams, D. F. "Moisture and Thermal Expansion Properties of Unidirectional Composite Materials and the Epoxy Matrix," Environmental Effects on Composite Materials, Vol. 2, Technomic Publishing Co., Lancaster, PA, 1984.
6. Shen, Chi-hung, Springer, George S. "Effects of Moisture and Temperature on the Tensile Strength of Composite Materials," Environmental Effects on Composite Materials, Vol. 1, Technomic Publishing Co., Lancaster, PA, 1984.
7. Shen, Chi-hung, Springer, George S. "Environmental Effects in the Elastic Moduli of Composite Materials, "Environmental Effects on Compostie Materials, Vol. 1. Technomic Publishing Co., Lancaster, PA, 1984.
8. Springer, G. S. "Moisture and Temperature Induced Degradation of Graphite Epoxy Composites," Environmental Effects on Composite materials, Vol. 2, Technomic Publishing Co., Lancaster, PA, 1984.
9. Pering, Gregory A., Farrell, Patrick V., Springer, George S. "Degradation of Tensile and Shear Properties of Composites Exposed to Fire or High Temperatures," Environmental Effects on Composite Materials, Vol. 1, Technomic Publishing Co., Lancaster, PA, 1984.
10. Springer, G. S. "Effects of Temperature and Moisture on Sheet Molding Compounds," Environmental Effects on Composite Materials, Vol. 2, Technomic Publishing Co., Lancaster, PA, 1984.
11. Heger, F. J., Chambers, R. and Dietz, A. G. H, "Structural Plastics Materials," Structural Plastics Design Manual. American Society of Civil Engineers, Washington, D. C., 1978.
12. Hartwig, G. and Evans, D. Nonmetallic Materials and Composites at Low Temperatures 2. International Cryogenics Materials Conference Board, Boulder, Colorado, 1982.
13. Takao, Y. "Thermal Expansion Coefficients of Misoriented Short-Fiber Reinforced Composites," Recent Advances in Composites in the United States and Japan. J. R. Vinson and M. Taya, editors., American Society for Testing and Materials, Philadelphia, PA, 1985.
14. Heger, F. J., Chambers, R. and Dietz, A. G. H, "Overall Considerations in Structural Design with Plastics," Structural Plastics Design Manual. American Society of Civil Engineers, Washington, D. C., 1978
15. Juran, Rosalind, Editor, "Modern Plastics Encyclopedia," McGraw-Hill, 1221 Avenue of the Americas, New York, New York, NY 10020 (Publishing Off.), Vol. 66, No. 11, October 1989.

APPENDIX B: CRASH TESTING OF RPC POSTS AND BLOCKOUTS

Report on the crash testing of RPC posts and blockouts at the
Federal Outdoor Impact Laboratory (FOIL) at TFHRC in McLean, Virginia.
Extract from reference McDevitt and Dutta (1993)

"In order to investigate the suitability of Rivenite posts and blockouts for guardrails, a 100-ft- (30.5-m-) long test section of guardrail was constructed at the Federal Outdoor Impact Laboratory (FOIL) at TFHRC in McLean, Virginia. The upstream end of the guardrail was anchored with a 37.5-ft- (11.4-m-) long BCT. A cable anchorage was used on the downstream end. The 6-in × 8-in. (152-mm × 203-mm) Rivenite posts were driven into the ground by a subcontractor that specializes in constructing guardrails. It was found that the Rivenite posts could readily be driven, but they required about twice as many hammer blows as wood posts. This was due to the greater energy absorption of the Rivenite material. When driven, the posts retained their shape and did not mushroom out on the bottom end. In appearance, this guardrail looked very much like the G4 (2w) W-beam on strong wood post guardrail used by many states (AASHTO, 1977 and 1989).

In October 1991, this guardrail was crash-tested with an 1,800-lb (816 kg) car at 60 mi/h (96.5 km/h) at an impact angle of 20°. The test vehicle was redirected parallel to the guardrail. Several Rivenite posts were broken in the impact zone and flew away from the back of the guardrail. This was expected because wood posts also break under these test conditions. However, since the Rivenite posts are nonfibrous, they broke cleanly in a horizontal plane at groundline. The test data met all of the evaluation criteria in National Cooperative Highway Research Program Report No. 230 (Michie 1981). The maximum lateral deflection of the guardrail was two ft (609 mm). Under the same test conditions, a guardrail with wood posts and blockouts deflected ten in (254 mm) (AASHTO, 1977). This test indicates that the Rivenite posts are not a one-for-one substitute for either the Douglas fir or the Southern Yellow Pine wood posts that are used in this guardrail system (AASHTO, 1977).

Each guardrail system has its own characteristic design deflection. For example, the G1 3-cable guardrail has a design deflection of 11 ft (3.4 m) (AASHTO, 1977). This guardrail with Rivenite posts and blockouts can be thought of as a new guardrail system that will have its own unique design deflection. However, since the FOIL facility does not have the capability to conduct tests with full-size sedans, the crash test needed to investigate the strength of this guardrail and establish its design deflection has not yet been conducted."

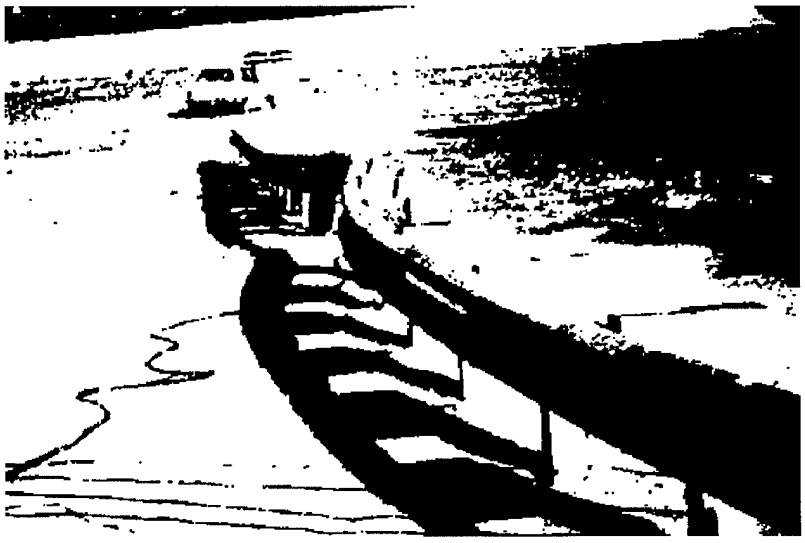

Figure B1. Crash testing of RPC posts and blockouts at the FHWA FOIL Laboratory.

REPORT DOCUMENTATION PAGE

Form Approved
OMB No. 0704-0188

1. AGENCY USE ONLY (Leave blank)	2. REPORT DATE	3. REPORT TYPE AND DATES COVERED
	August 1998	

4. TITLE AND SUBTITLE

Investigations of Plastic Composite Materials for Highway Safety Structures

5. FUNDING NUMBERS

DTFH61-90-Y-00035

6. AUTHORS

Piyush K. Dutta

7. PERFORMING ORGANIZATION NAME(S) AND ADDRESS(ES)

U.S. Army Cold Regions Research and Engineering Laboratory
72 Lyme Road
Hanover, New Hampshire 03755-1290

8. PERFORMING ORGANIZATION REPORT NUMBER

CRREL Report 98-7

9. SPONSORING/MONITORING AGENCY NAME(S) AND ADDRESS(ES)

Federal Highway Administration
6300 Georgetown Pike
McLean, Virginia 22101

10. SPONSORING/MONITORING AGENCY REPORT NUMBER

FHWA-RD-98-060

11. SUPPLEMENTARY NOTES

For conversion of SI units to non-SI units of measurement, consult ASTM Standard E380-93, *Standard Practice for Use of the International System of Units*, published by the American Society for Testing and Materials, 100 Barr Harbor Drive., West Conshohocken, Pennsylvania 19428-2959.

12a. DISTRIBUTION/AVAILABILITY STATEMENT

Approved for public release; distribution is unlimited.

Available from NTIS, Springfield, Virginia 22161

12b. DISTRIBUTION CODE

13. ABSTRACT (*Maximum 200 words*)

This report presents a basic overview and assessment of different concepts and technologies of using polymer composites in structures generally used for highway safety. The structural systems included a highway barrier guardrail with its posts and blockouts, sign posts, concrete reinforcing rebars, breakaway couplers, and crushable plastic cushions to protect errant drivers from roadside sign and utility posts, and small trees. The composites included fiber reinforced plastics (FRP) in laminated and bar forms, and commercially available recycled and reconstituted structural plastic composites. Commercially available FRP composites, recycled plastic composites, and several conceptual designs and prototype components were assessed and tested. The results showed many potential advantages of using composites in almost all the structures considered, but one-to-one replacement of conventional materials was not always found attractive. For deriving maximum benefits from fiber composites, the basic performance of the given structures should be reassessed and then composites should be designed at the materials level using innovative fiber architecture and appropriate manufacturing technologies that can meet those performance requirements.

14. SUBJECT TERMS

Breakaway supports, Composites, Crush cushions, Guardrails, FRP, Highway barriers
Highway safety structures, New materials, Rebars, Recycled plastics, Roadside safety

15. NUMBER OF PAGES

85

16. PRICE CODE

17. SECURITY CLASSIFICATION OF REPORT	18. SECURITY CLASSIFICATION OF THIS PAGE	19. SECURITY CLASSIFICATION OF ABSTRACT	20. LIMITATION OF ABSTRACT
UNCLASSIFIED	UNCLASSIFIED	UNCLASSIFIED	UL